FCP Report No. 10

FATIGUE DAMAGE ANALYSIS FOR IRREGULAR SHAPED STRUCTURES SUBJECTED TO REPRESENTATIVE LOADS

by

J. F. Martin
Department of Theoretical and Applied Mechanics

ABSTRACT

A fatigue damage analysis is presented that is capable of analyzing structures subjected to representative service load histories. After theoretically or experimentally determining the nominal stresses or strains, a mechanics analysis combined with a model of uniaxial stress-strain behavior calculates the stress-strain response at the critical location. Based on the stress-strain response at the highly strained region, a cumulative damage procedure that sums damage over small increments of the local stress-strain curve and corrects for the effect of mean stress, estimates the total number of reversals to crack initiation.

This procedure is applied to a box-beam structure and an automotive fan blade. Analyses were made for both constant and variable types of loading patterns.

A Report of the
FRACTURE CONTROL PROGRAM

College of Engineering, University of Illinois
Urbana, Illinois 61801
December, 1973

This report was prepared especially for distribution to Sponsors of the Fracture Control Program of the College Engineering at the University of Illinois. The Program encompasses a cooperative research effort to contribute and disseminate better knowledge and procedures for the development and manufacture of safe, reliable, structural or mechanical products.

The industrial sponsors cooperating in this Program are:

CATERPILLAR TRACTOR COMPANY
CLARK EQUIPMENT COMPANY
DEERE and COMPANY
GENERAL MOTORS
INTERNATIONAL HARVESTER COMPANY
MARION POWER SHOVEL COMPANY
REXNORD
ROCKWELL INTERNATIONAL
A.O. SMITH CORPORATION

ACKNOWLEDGMENT

This investigation was conducted in the Department of Theoretical and Applied Mechanics, University of Illinois, with Professor R. T. Shield as Department Head. The author is indebted to his adviser, Professor JoDean Morrow, for providing the necessary technical environment that made this research possible. Messrs. J. R. Wiley, R. Isaacson and T. M. Johnson, of General Motors Proving Grounds, supplied the automotive fan blade data and were involved in useful discussions concerning the analysis of the blades. Messrs. F. F. Borriello, M. S. Rosenfeld and R. E. Vining, of the Naval Air Development Center, provided data and technical guidance concerning the box-beam analysis. Special acknowledgment must be given to Professor T. H. Topper, of the University of Waterloo, who originally formulated the model of uniaxial stress-strain behavior and who provided many useful suggestions concerning its development.

The author wishes to thank his wife, Janet, for her patience and varied stimuli during this interim. Also, appreciation is extended to his son, Jason, whose appearance accelerated final culmination of this thesis.

Mrs. R. A. Mathine typed the manuscript, and Mr. H. T. James drafted the figures. Mr. D. F. Dittmer reduced much of the data and generated the test results for the bar steel.

TABLE OF CONTENTS

LIST OF TABLES

LIST OF FIGURES

LIST OF SYMBOLS

α	Material constant indicating sensitivity to mean stress
b	Fatigue strength exponent
b_n	Minimum width of a notched specimen
c	Fatigue ductility exponent
C	Constant increment of stress
D_i	Damage related to i^{th} element
E	Elastic modulus
E_i	Modulus constant for i^{th} element
E_i^*	Effective modulus of i^{th} segment of stress-strain curve
e, Δe	Nominal strain, range
d	Material constant
ϵ, $\Delta\epsilon$	True strain, range
$\Delta\epsilon_{cr}$	Equivalent completely reversed strain range
ϵ_f'	Fatigue ductility coefficient
ϵ_e, $\Delta\epsilon_e$	True elastic strain, range
ϵ_p, $\Delta\epsilon_p$	True plastic strain, range
ϵ_i^*	Maximum strain attained over the i^{th} segment of the stress-strain curve
$\delta\epsilon_i^*$	Change in strain over the i^{th} segment of the stress-strain curve
$\bar{\epsilon}_i$	Plastic strain related to i^{th} element
$\bar{\epsilon}_i^*$	Plastic strain at end of i^{th} segment of stress-strain curve
g	Reference load
h	Constant for hardening expression
K*	Transient strength coefficient
K_t	Theoretical elastic stress concentration factor

K_σ	Stress concentration factor
K_ϵ	Strain concentration factor
K_f	Fatigue notch factor
K_o	Constant for hardening expression
M	Constant in relaxing function
μ_e	Elastic Poisson's ratio
$2N_f$	Number of reversals to failure
$2N_t$	Transition fatigue life
n^*	Transient strain hardening exponent
P	Load
r	Notch radius
s	Constant for hardening expression
S, ΔS	Nominal stress, range
S_u	Ultimate tensile strength
σ, $\Delta\sigma$	True stress, range
σ_f'	Fatigue strength coefficient
σ_f	True fracture strength
$\Delta\sigma_{cr}$	Equivalent completely reversed stress range
σ_{max}	Maximum stress
σ_m	Mean stress
σ_o	Reference stress for mean stress damage
$\bar{\sigma}_i$	Frictional yield stress of i^{th} element
σ_i	Residual stress of i^{th} element
σ_f^*	Final stress attained for a particular reversal
σ_i^*	Maximum stress attained over i^{th} segment of stress-strain curve
$\delta\sigma_i^*$	Change in stress for i^{th} segment for stress-strain curve

t	Specimen thickness
V_n	Highly stressed volume for notched specimen
V_u	Highly stressed volume for unnotched specimen

INTRODUCTION

Developments in the areas of mechanics and materials have prompted fatigue damage procedures that base failure on the behavior of the metal at the highly strained regions where cracks initiate. Since local repeated plastic strain is responsible for crack nucleation (1,2)*, procedures that account for the damage due to this strain would be expected to result in more accurate fatigue life estimations than procedures based on nominal stresses that are removed from the most highly damaged area.

Fatigue procedures based on local stresses and strains have been discussed by several authors (3-18) and employed in analyses of laboratory notched specimens (8-16). Figures 1 and 2 depict the basic concepts for such approaches. Uniaxial test results provide data for both the stress-strain and fatigue analysis of the material at the critical location.

To establish the local stresses and strains, two expressions, one originated by Neuber (19) and the other by Stowell (20), have been expanded to include the type of structures and load histories encountered in fatigue environments. Neither expression independently yields a unique state of local stress and strain. However, uniaxial test results provide the necessary relationship between stress and strain for a unique solution.

Once the local stresses and strains have been determined, a variety of methods exist for estimating the number of reversals that can occur before the initiation of a crack. Linear summation of damage as proposed by Palmgren (21) and Miner (22) provides the simplest method of cumulating damage. Many of the errors once attributed to the means of summing damage using nominal stress-life data have been since traced to other sources such as not accounting for the effects of mean stress and cyclic overstrains.

---

*Numbers in parentheses refer to references.

References 8 through 16 successfully employed experimental stress-strain and fatigue test data to estimate the fatigue lives of notched laboratory specimens. Wetzel (14) and Stadnick and Morrow (15) directly controlled smooth specimens according to the relation originated by Neuber. In this manner the specimen directly simulates the local behavior at the notch root. All procedures that are presented in Refs. 8 through 16 depended on experimental data for establishing the relation of stress and strain. No attempts were made to establish a general model of stress-strain behavior of the metal from which the component is made.

Application of this type of procedure to large structures is discussed in Refs. 16 through 18. In many realistic situations, determining the nominal stresses or strains near the critical location can present the most difficult problem. Experimental techniques often provide the only solution. Finite element methods can determine stresses and strains throughout a structure that is geometrically complicated but for which the behavior is elastic. Direct application of the method to determine local behavior that experiences plastic strains is not practical at this time.

To expand these local stress-strain procedures for the analysis of structures subjected to long representative load histories, a model of uniaxial stress-strain behavior is needed. Martin et al. (23) developed a model that successfully simulated the uniaxial stress-strain behavior of 2024-T4 aluminum. This model, in conjunction with an expression relating nominal and local stress-strain response, was incorporated into a fatigue damage procedure. Accurate estimations of the fatigue lives of center notched plates were made. Later, Wetzel (24) modeled 2024-T351 aluminum and 1045 steel. Incorporating this model into a damage procedure, fatigue life estimations were made and compared to predictions based on nominal stresses. Superior life estimations were made with the local damage approach. Jhansale and Topper (25,26) modeled a mild steel and utilized this model to estimate the fatigue

lives of laboratory flexural members. All of these procedures were programmed for the digital computer. Consequently, the computational effort is transferred to high speed devices and the problem encountered in analyzing a large number of reversals is minimized.

Purpose and Scope

References 23 through 26 have shown the advantages of fatigue damage procedures that are based on local stresses and strains. Since computational problems are lessened, more direct and realistic methods of fatigue analysis can be made. The aim of this research is to produce a fatigue damage procedure that incorporates the latest developments in the fields of mechanics and materials.

Figure 3 expands on the basic concept of the procedure presented in Fig. 2. Initially, the local stresses, σ, and strains, ϵ, are determined from the nominal stresses, S, and strains, e. Determining the local behavior depends on the mechanics expression and the model of uniaxial behavior. Also involved is the fatigue notch factor, K_f. In certain cases this is determined by comparing long life fatigue data of the structure and smooth specimens, as indicated by the dashed line in Fig. 3. However, alternative analytical means exist. Fatigue damage is based on the local components of elastic strain, ϵ_e, and plastic strain, ϵ_p. Also, the effect of mean stress, σ_m, is included. For certain types of loading spectra, the method of cumulating damage is of extreme importance. For this procedure damage is summed over small segments of the local stress-strain curve. A mean stress correction is made at the end of each reversal and upon formation of a complete hysteresis loop. In summary the following four inputs to this fatigue damage procedure will be presented: (1) analysis for local stresses and strains, (2) model of uniaxial stress-strain behavior, (3) fatigue damage parameters, and (4) a procedure for fatigue cumulative damage analysis.

All stress-strain and fatigue data were generated from uniaxial specimens. Figure 4 defines the stress and strain ranges for a hysteresis loop that might be encountered during cyclic loading. Most of the smooth specimen testing was performed on the mechanical testing system shown in Fig. 5. Figure 6 shows a smooth uniaxial specimen mounted in the load frame.

Five metals are cited throughout the text. The two aluminum alloys, 2024-T4 and 7075-T6, and 4340 steel are discussed in Refs. 10 through 12. Two mild structural steels, one supplied in the form of cylindrical bars and the other in thin plates, are discussed in Appendix C. The properties of the bar steel varied through the cross section, therefore this metal will be simply referred to as the bar steel. Similarly, the metal taken from the plates will be called the sheet steel. In the main text, the 2024-T4 aluminum and the 4340 steel are used for illustrations of materials behavior. Analysis of the box-beam structure involved the 7075-T6 aluminum. Both mild structural steels are discussed with regard to analysis of the fan blades.

This fatigue damage procedure is applied to two structural members. Fatigue lives are predicted for an automotive fan blade that is subjected to constant amplitude and representative loading spectra. Also analyzed is a box-beam structure that was subjected to constant amplitude loading with various mean loads. Equivalent flight spectra loading were also applied to the beams. These spectra are representative of the type of loading aircraft components undergo during service.

The main text presents a general formulation of the fatigue damage procedure. Appendix A gives details of the analysis. Specifics for the fatigue analyses of the box-beams and fan blades are presented in Appendices B and C. As a reference to further developments of fatigue procedures, Appendix D discusses the possibilities of the application of finite element methods.

A RELATION BETWEEN NOMINAL AND LOCAL STRESSES AND STRAINS

A necessary component of the fatigue damage procedure as presented in Fig. 3 is establishment of a relation between nominal and local stress-strain response. Assuming fatigue cracks initiate at the surface, the most complicated state of stress at the notch root is biaxial. However, for this analysis a uniaxial stress state will be assumed. Biaxial stress-strain and fatigue theories in most cases have little or no experimental verification. Therefore, basing all the analysis on uniaxial data, for which the stress-strain and fatigue behavior are comparatively well documented and verified, is a practical and realistic approach at this stage of development.

The expression used in this analysis is that originated by Neuber (19). For the special case of a "V" notched prismatic bar in shear, Neuber developed a relationship between the stress and strain concentration factors, K_σ and K_ϵ, respectively.

$$K_t = (K_\sigma K_\epsilon)^{\frac{1}{2}} \tag{1}$$

where K_t is the theoretical elastic stress concentration factor. Expressed in terms of the definitions of K_σ and K_ϵ,

$$\sigma \epsilon = K_t^2 (S e) \tag{2}$$

Equation 2 has been employed for fatigue analyses of other geometries and modes of loading (8,10-16). Since the elastic theoretical stress concentration factor predicts too severe a criteria for fatigue loading, K_t is replaced by the fatigue notch factor, K_f. Point values of stress and strain are replaced by ranges that are denoted by the symbol Δ.

$$\Delta\sigma \, \Delta\epsilon = K_f^2 (\Delta S \, \Delta e) \tag{3}$$

Once the fatigue notch factor is determined, Eq. 3 contains four variables. If the nominal behavior is assumed to be elastic, Eq. 3 can be simplified to one of the following forms.

$$\Delta\sigma\ \Delta\epsilon = \frac{(K_f\ \Delta S)^2}{E} \tag{4}$$

or

$$\Delta\sigma\ \Delta\epsilon = E\ (K_f\ \Delta e)^2 \tag{5}$$

The elastic modulus, E, can be obtained from monotonic tension test results. However, this still leaves three variables and one equation. It will be assumed that either the nominal value of stress or strain can be obtained by theoretical or experimental techniques. Equation 3 is then reduced to three independent variables and Eqs. 4 and 5 to two. For Eq. 3, if the nominal stress ranges can be related to the nominal strain ranges and a similar relationship obtained for the local behavior, a complete solution would be obtained. Similarly, for Eqs. 4 and 5 a relationship is needed for the local stress-strain behavior. This type of relation can be obtained by modeling the uniaxial behavior of the metal at both the nominal and local regions.

Few research efforts (9, 27-30) have been carried out that might be used to verify Eq. 1. Gowda and Topper (27) theoretically investigated an infinite plane with a circular hole. For nonlinear stress-strain relations, Eq. 1 was found to be valid for small strains. Experimental verification was also accomplished by Gowda and Topper (28). Equation 1 was found to be valid for mild steel plates with circular holes for strains less than 0.008. Although direct verification of Eq. 1 is limited, accurate fatigue estimations of notched plates have been made using this relation (8, 10-16).

MODEL OF UNIAXIAL STRESS-STRAIN BEHAVIOR

To utilize the mechanics analysis as expressed by Eq. 3, it is necessary to develop a model for the cyclic stress-strain response of the metal at both the nominal and local regions. As a general goal, this model should exhibit all the characteristics observed for cyclic behavior. However, the sophistication that might be obtained in modeling cyclic behavior may not always be fully utilized for fatigue predictions.

Characteristics of Uniaxial Stress-Strain Behavior

While observing the cyclic response of uniaxial specimens, several dominant features become apparent. If a specimen is loaded in a random manner and plastic deformation is present, its prior load history will influence its future behavior. This history dependence is the most important effect to be modeled for realistic fatigue analyses. Figure 7 shows the behavior of two steels and an aluminum alloy that were subjected to the same variable strain limits. Besides showing the effect of history dependence, cyclic hardening or softening or both are occurring. After cycling each specimen until a relatively stable condition was obtained, the same strain limits were imposed again. The stable response of the metals is shown in Fig. 8.

Cyclic hardening or softening is most easily observed while a sample is being cycled between completely reversed strain limits. Figure 9a shows an example of cyclic softening, in which case the stress amplitude decreased while the controlled strain amplitude remained constant. Cyclic hardening is demonstrated by the aluminum alloy, Fig. 9b. Many mild structural steels have been observed to either harden or soften, depending on the strain amplitude. For small strain amplitudes, the bar steel shown in Fig. 10 cyclically softens and for large strain amplitudes, it hardens. Figure 11 demonstrates a characteristic that has been observed for many metals that cyclically soften. Although the specimen is being strain cycled below the lower yield

stress, cyclic softening still occurs. For this specimen, the softened condition existed for the majority of the fatigue life. Since a relatively stable condition usually reached within ten percent of the life, the necessity for modeling the transient period is questionable.

Another observable phenomenon is that of cyclic relaxation of mean stress. If strain limits are chosen in such a manner so as to produce an initial mean stress, this mean stress will relax with cycles if sufficient plastic strain is present. Figure 12 shows the response of three metals that were subjected to zero to maximum strain limits. Both the phenomena of cyclic hardening or softening and cyclic relaxation of mean stress occurred simultaneously. Experimental isolation of these characteristics presents one of the problems in modeling a material. Cyclic relaxation is only obvious for the 4340 steel. The bar steel exhibited enough plastic strain on the first reversal to eliminate any subsequent mean stress. If the specimens had been precycled to obtain a stable condition, cyclic relaxation would have been more obvious. However, complete separation of hardening or softening and relaxation is nearly impossible.

Of the cyclic characteristics shown in Figs. 7 through 12, modeling of the history dependence of the metal is the most important. Extremely large errors arise if prior deformation is ignored and the metal assumed to behave as it would in its original state. Modeling cyclic hardening or softening is questionable, since a metal reaches a stable condition early in its fatigue life. Inclusion of cyclic relaxation of mean stress can be important for load histories that produce mean stresses that cyclically relax.

Model of Uniaxial Stress-Strain Behavior

The basic formulation of the model of uniaxial stress-strain behavior is based on expressions governing the mechanical model shown in Fig. 13. This model consists of series elements that are conceptually made up of springs and frictional sliders. Other models with different arrangements of components can simulate the same behavior.

Figure 13 shows the characteristics of each of the components. The element modulus constant, E_i, is linear with respect to the stress and strain of the element. Multiplication of E_i by a relaxing function, $f(|\sigma|)$, produces the modulus of the element. Positive and negative yield stress values, $\bar{\sigma}_i$, between which no deformation occurs bound the frictional sliders. Once the yield stress of the slider is exceeded, further resistance to strain is maintained at that yield stress. Residual stresses are associated with an element due to the parallel spring and frictional slider combination. These residual stresses produce the memory capabilities of the model.

Various combinations for the values of $\bar{\sigma}_i$ and E_i can be assigned to produce a desired behavior. Yield stresses are assigned stress values that will result in consecutive yielding of the elements. Since this type of model approximates a stress-strain curve with small linear segments, Fig. 14, the size of each segment depends on the values of the yield stresses. For each segment, the slope of the stress-strain curve is a function of all the elements that have been yielded. Excluding the relaxing function, $f(|\sigma|)$, Eq. 6 represents the relation of the total slope, E_i^*, for the i^{th} segment of the curve.

$$\frac{1}{E_i^*} = \frac{1}{E_1} + \frac{1}{E_2} + \frac{1}{E_3} + \ldots + \frac{1}{E_i} \tag{6}$$

The stress at which an element is activated is equal to the sum of the element yield stress and the residual stress.

One of the early references that utilized a mechanical model of this type to simulate stress-strain behavior is by Jenkin (31). Jenkin's main concern was with modeling the endurance limit in fatigue. He did, however, simulate the behavior of metals subjected to completely reversed loads. Koibuchi (32) gives a detailed discussion of this type of model with applications to cyclic loading. Iwan (33-35) describes the dynamic behavior of a model with a mass associated with each element.

He proposes a form of the model for three dimensions (34) and applies it to built-up structures (35).

Figure 15 shows the behavior of a three element model, with yield stresses of 60 and 100 ksi. All element moduli constants are assigned a value of 30,000 ksi. No relaxing function is included. Following the rules of the model, the response shown in Fig. 15 is obtained. Figure 15a shows the initial curve as generated by the model. Each break of the curve is at a yield stress. When cyclic limits are simulated, a response as shown in Fig. 15b or 15c is obtained. Figure 15b shows the response for completely reversed limits: A-A', B-B' and C-C'. The stress and strain range of each segment has doubled. If the tips of all the loops have a common origin, Fig. 15c, one side of all the loops are coincident. This type of behavior is reported (36) to be typical for many metals. Consequently, the mechanical model is capable of simulating the constant amplitude stress-strain behavior of metals.

Without any alterations, this model also behaves in a similar manner to metals with regard to memory. Figure 16a shows the response of the model to varying strain limits. For simulation of the transients of cyclic hardening and softening and cyclic relaxation mean stress, alterations of the model are necessary.

Hardening or softening can be accomplished by changing the element parameters, $\bar{\sigma}_i$ and E_i, at the end of a reversal during which hardening or softening has taken place. Figure 16b is an example of the response of the model when the element moduli are increased by a factor of 1.5 after each reversal. For this example the yield stresses remained constant.

Simulation of cyclic relaxation of mean stress is accomplished by multiplying E_i by a relaxing function, $f(|\sigma|)$. If $f(|\sigma|)$ is of such a form that it reduces the value of the element moduli with increasing $|\sigma|$, cyclic relaxation will occur.

Equation 7 shows the relaxing function that was chosen for this model.

$$f(|\sigma|) = 1 - \frac{|\sigma|}{M} \tag{7}$$

All values of E_i remain constant unless cyclic hardening or softening is occurring. Higher values of M result in slower rates of cyclic relaxation. Regardless of the choice of M, unless it is extremely small, the model can correctly simulate cyclic stress-strain behavior for which no mean stress is present. The form of Eq. 7 is such that only small changes of element moduli occur for different values of $|\sigma|$, so that basic loop shape is not appreciably distorted due to the relaxing function.

With the addition of the relaxing function, Eq. 6 is changed to the form of Eq. 8.

$$\frac{1}{E_i^*} = \frac{1}{E_1} + \left(\frac{1}{E_2} + \frac{1}{E_3} + \ldots + \frac{1}{E_i}\right)/\left(1 - \frac{|\sigma|}{M}\right) \tag{8}$$

Figure 16c shows the simulation of cyclic relaxation for a relaxing constant of 300. Although the other values of the constants for the model are of a realistic nature, a low value of M was chosen for illustration. To exclude cyclic relaxation from the examples shown in Figs. 16a and 16b, M was assigned a large value.

In summary, the general characteristics of memory, cyclic hardening or softening, and cyclic relaxation can be simulated by a mathematical model. Memory is accomplished by direct utilization of the rules that govern the mechanical model shown in Fig. 13a. To include cyclic hardening or softening, the constants of the model are changed at the end of each reversal in such a manner so as to reflect the new condition of the metal that is being modeled. Multiplication of the element moduli constants with the relaxing function enables the model to cyclically relax mean stress. Remaining is the problem of assigning the appropriate values of $\bar{\sigma}_i$ and E_i for simulation of the stress-strain response of a particular metal.

Fitting the Simulation Model to Material Behavior

Throughout the remainder of the text, reference will be frequently given to the mechanical model shown in Fig. 13a, however, it is only helpful in visualizing the behavior of the simulation. The modeling procedure simulates real material behavior rather than the response of this simple mechanical system.

To enable the model to simulate the behavior of a particular material, the values of $\bar{\sigma}_i$ and E_i must be properly assigned. Empirical expressions based on experimental test results provide the basis for determining $\bar{\sigma}_i$ and E_i. For most metals, Eq. 9 has been found to be an accurate relation for stress and plastic strain.

$$\sigma = K^*(\epsilon_p)^{n^*} \tag{9}$$

where K^* is the strength coefficient and n^* the strain hardening exponent. The (*) denotes the properties for any condition of the material and not necessarily for either the initial or stable cyclic conditions. Total strain is calculated by adding the components of elastic, σ/E, and plastic strain.

$$\epsilon = \frac{\sigma}{E} + \left(\frac{\sigma}{K^*}\right)^{1/n^*} \tag{10}$$

For cyclic loading, the properties K^* and n^* can be related to stress and strain ranges, Eqs. 11 and 12.

$$\frac{\Delta\sigma}{2} = K^*\left(\frac{\Delta\epsilon_p}{2}\right)^{n^*} \tag{11}$$

$$\frac{\Delta\epsilon}{2} = \frac{\Delta\sigma/2}{E} + \left(\frac{\Delta\sigma/2}{K^*}\right)^{1/n^*} \tag{12}$$

Equations 11 and 12 describe a hysteresis loop that might occur during any reversal of a load history. The values of K^* and n^* can be adjusted to best describe the shape of the loop. For the model, the values of $\bar{\sigma}_i$ and E_i are assigned to approximate the

curve described by Eq. 10. During cyclic loading, the model doubles its shape to simulate the desired stress-strain response. Figure 15a could represent the approximation of a curve described by Eq. 10. The portion of the curve from O-B produces the cyclic loop with tips at B and B'.

As an example of determining the values of K^* and n^*, the initial monotonic and stable cyclic stress-strain properties of a sheet steel are determined. No attempt is made to characterize continuous cyclic hardening or softening. The test results in terms of plastic strain and stress are shown in Fig. 17. A single accurate fit to all the data is not possible. Figure 17 shows two least squares approximations to the data. Each of the lines can be represented by Eq. 9. The initial line is a fit to all data with strains less than 0.02. Figure 18 shows the cyclic stress-strain data obtained from companion specimen test results. Each data point represents one specimen that was cycled under constant strain control until failure. At approximately half the life of each specimen, a hysteresis loop was taken for obtaining the data shown in Fig. 18. The line through these data is represented by Eq. 11.

Several alternative methods exist for determining the stable cyclic stress-strain curve (37). One of these techniques is the incremental step strain test. By this type of test, a specimen is strain cycled according to a spectrum similar to that shown in Fig. 19a. Figure 19b shows the stress-strain response of the sheet steel to this type of straining. Data taken from the hysteresis loops shown in Fig. 19b are presented in Fig. 20. Also included in Fig. 20 is the companion specimen data line. The two methods produced significantly different results. This is not the case for the higher strength steel and aluminum data reported in Ref. 37. Caution should be exercised while determining materials properties. For the example of the sheet steel, the incremental strain step test did not result in establishing steady state properties.

For the sheet steel, two conditions of the metal have been determined. From the data shown in Figs. 17 and 18, values of K^* and n^* are calculated for each condition of the steel. For particular values of K^* and n^*, $\bar{\sigma}_i$ and E_i are adjusted to approximate the smooth curve described by Eq. 10. An infinite variety of combinations of $\bar{\sigma}_i$ and E_i can be obtained. This procedure initially sets all $\bar{\sigma}_i$. With a large relaxing constant ($M > 10^{10}$) and ignoring any residual stresses, appropriate values of E_i are calculated to fit the curve described by Eq. 10. Details of the procedure are given in Appendix A.

Once the values of $\bar{\sigma}_i$ and E_i are assigned, the relaxing constant, M, is determined. To minimize the effects of cyclic hardening or softening, the metal is cycled until a stable condition is reached. Strain limits are imposed to produce an initial mean stress. With various values of M the model simulates the actual test data. The value of M that most accurately simulates the data is chosen. Examples of this procedure are given in Appendices B and C for the fan blade and box-beam metals.

Simulation of Stress-Strain Response by the Model

Simulation by the model occurs by activating each element in sequence until the desired limit is reached. At the end of the reversal, the residual stresses of all the elements that were activated during that reversal are reset and the signs of all the yield stresses reversed. If cyclic hardening or softening has occurred, the values of $\bar{\sigma}_i$ and E_i are reset. All values of the residual stresses, σ_i, are ignored and the new stress-strain curve is approximated by the model as shown in Fig. 14. Once again taking into account the residual stresses, the stress-strain response of the next reversal is simulated.

Accurate simulation by the model relies on empirical expressions of the stress-strain behavior of the metal. If sufficient information is not available for a particular metal, approximations of the necessary properties might be obtained from a similar

metal. The most important function of the model is to complete the solution for the local stress-strain behavior.

Application of the Model to 2024-T4 Aluminum and A 36 Steel

Extensive modeling of 2024-T4 aluminum (23) and A 36 Steel (38) has been accomplished. Examples of the simulation achieved by these models is shown in Figs. 21 through 24. Figures 21 and 23 demonstrate the ability of each model to simulate the initial behavior of the metals. During this initial loading sequence, both cyclic hardening and cyclic relaxation of mean stress are occurring. Figures 22 and 24 show actual and simulation results for the metals after a stable condition is reached. For all four load histories, the simulation is close to the actual test results.

Both simulations were based on the mechanical model shown in Fig. 13a. Cyclic relaxation was accomplished with the relaxing function given in Eq. 7. However, the method of simulating cyclic hardening is different for each procedure.

For the aluminum, cyclic hardening was based on the summation of plastic strain to the (-1/s) power, Eq. 13.

$$K^* = K_o \left[\Sigma \left(\frac{\Delta \epsilon_p}{2} \right)^{-1/s} \right]^h \tag{13}$$

where K_o, s and h are constants. The strain hardening exponent, n^*, is assumed to remain constant. After each reversal during which plastic strain occurred, a new value of K^* is calculated and the model parameters changed.

Plummer (38) obtained accurate simulation of cyclic hardening by assuming a common shape (constant K^* and n^*) and incrementing the elastic range ($\bar{\sigma}_2$) by means of a stress offset that is a function of total strain range of the previous reversal and the total number or reversals. Cyclic softening of the steel at small strains was ignored.

FATIGUE DAMAGE PARAMETERS

Once the stress-strain behavior at the critical location is determined, a cumulative damage analysis is made based on the calculated stresses and strains. Several procedures (7, 39-47) lend themselves to the simulation procedure just outlined. For accurate fatigue life estimations, the effects of mean stress and initial and periodic overstraining must be included.

Fatigue Properties

The fatigue properties are associated with the components of elastic and plastic strain. Figure 25 is representative of the strain-reversals to failure, $2N_f$, data for many engineering metals, in that a log-log linear fit approximates the data reasonably well. The fit was made by the least squares method. Equations 14 and 16 describe these lines. For elastic strain,

$$\frac{\Delta\epsilon_e}{2} = \frac{\sigma_f'}{E} (2N_f)^b \tag{14}$$

or in terms of stress

$$\frac{\Delta\sigma}{2} = \sigma_f' (2N_f)^b \tag{15}$$

For plastic strain,

$$\frac{\Delta\epsilon_p}{2} = \epsilon_f' (2N_f)^c \tag{16}$$

where:

σ_f' is the fatigue strength coefficient

ϵ_f' the fatigue ductility coefficient

b the fatigue strength exponent

c the fatigue ductility exponent.

At long lives the elastic line is dominant and at short lives the plastic line dominates. The transition fatigue life, $2N_t$, is the number of reversals where the elastic and plastic strain components are equal. Equations 14 and 16 can be combined into a single equation for total strain.

$$\frac{\Delta\epsilon}{2} = \frac{\Delta\epsilon_e}{2} + \frac{\Delta\epsilon_p}{2} = \left(\frac{\sigma_f'}{E}\right)\left(2N_f\right)^b + \epsilon_f'\left(2N_f\right)^c \qquad (17)$$

Either the elastic or plastic strain-life curve will be the basis for the fatigue damage analysis.

Effect of Cyclic Overstrains

Since many structures are subjected to some type of overstraining, the fatigue properties should also reflect this effect. Initial cyclic overstraining (39-43) has been shown to reduce the fatigue resistance of several metals to a higher degree than would be expected due to the amount of plastic strain for each reversal during the overstrain. Periodic cyclic overstraining has also been shown to affect fatigue lives (43). This type of overstrain is representative of many service histories.

An example of a cyclic overstrain is shown in Fig. 26. Figure 27 shows the large strain and initial overstrain data for the structural bar steel. Also included in the figure are the non-overstrained data lines from Fig. 25. Watson and Topper (41, 42) reported on the effect of an initial cyclic overstrain for five structural steels. Four of the steels demonstrated an effect due to the initial overstrain at intermediate and long lives. One steel with a yield strength of 84 ksi was not affected. Initial cyclic overstraining was also shown (39, 40, 43) to reduce the fatigue lives of a 4340 alloy steel and 2024-T4 aluminum.

Additional periodic overstrains every 2×10^5 reversals after the initial overstrain did not further reduce the fatigue resistance of the bar steel. However, the sheet steel did show an effect due to periodic overstraining. Figure 28 shows the

large strain and periodic overstrain data for the sheet steel. Also included in the figure are the non-overstrained data lines. Initial cyclic overstraining did not affect the sheet steel. This might be expected since the metal was initially strained during the rolling process.

Dowling (43) reported a reduction in fatigue life of a 4340 alloy steel due to periodic overstraining every 2×10^5 reversals. It was observed that the metal would harden slightly at small strain ranges. By periodically overstraining, a softer condition could be obtained and, therefore, more plastic strain would be present throughout a greater portion of the fatigue life. The opposite situation was observed for both the sheet and bar steels. After each overstrain, a very small degree of hardening was observed. Therefore, no explanation based on stress-strain behavior for the effect of periodic overstraining on the sheet steel can be given.

Effect of Mean Stress

The continuing presence of a mean stress at the highly strained region can have a pronounced effect on the fatigue life. If a tensile mean stress is present during cycling, the fatigue life will be shortened. A compressive mean stress will have the opposite effect. Large errors can be made in fatigue life calculations at intermediate and long lives if the effect of mean stress is not included.

Many mean stress equations involve an equivalent completely reversed strain amplitude (7, 39, 41, 44, 45). Smith et al. (46) proposed the fatigue damage parameter $[(\Delta\epsilon/2)\ \sigma_{max}\ E]^{\frac{1}{2}}$, where σ_{max} is the maximum stress for a reversal and $\Delta\epsilon/2$ the strain amplitude. This parameter versus reversals to failure was shown to produce a single curve for different levels of mean stress. Wetzel (24) used this parameter with 2024-T351 aluminum by dividing the data on a log-log plot into three segments and fitting a straight line through each segment.

Wilson (47) generated data on 2024-T4 aluminum that included mean stress. Based on constant amplitude stress data, which included mean stress, cumulative damage analyses were made for block loadings consisting of various mean stress levels. Most of the life estimations over-estimated the actual life of the specimens. Topper and Sandor (39) also studied the effect of mean stress for this aluminum and 4340 steel. For this study the effect of overstrain was also included. Completely reversed tensile and compressive mean stress test results were obtained for specimens that were cyclically prestrained. The following equation fit the completely reversed and mean stress data reasonably well.

$$\frac{\Delta\epsilon_{cr}}{2} = \frac{\Delta\epsilon}{2} + \frac{\sigma_m^{\alpha}}{E} \tag{18}$$

where $\Delta\epsilon_{cr}/2$ is the equivalent completely reversed strain amplitude. Equation 18 describes a fully reversed strain amplitude which would give the same life as a strain amplitude $\Delta\epsilon/2$, co-existing with a mean stress, σ_m. Equation 18 with the constant, α, assigned to fit the completely reversed prestrained data, was used to estimate the fatigue lives of the varying mean stress data from Wilson (47). Damage summations ranging from 1.3 to 0.55 were obtained. These improved estimations are due to the inclusion of prestrain in the damage procedure. During the change of mean stress levels, plastic strain occurred which was similar to the prestrain of the constant amplitude tests.

Dowling (40, 43) investigated the $[(\Delta\epsilon/2)\ \sigma_{max}\ E]^{\frac{1}{2}}$ parameter and the following mean stress parameters.

$$\frac{\Delta\sigma_{cr}}{2} = \frac{\Delta\sigma/2}{1 - \sigma_m/S_u} \qquad \text{Smith (44)} \tag{19}$$

$$\frac{\Delta\sigma_{cr}}{2} = \frac{\Delta\sigma/2}{1 - \sigma_m/\sigma_f'} \qquad \text{Morrow (7)} \tag{20}$$

$$\frac{\Delta\sigma_{cr}}{2} = \frac{\Delta\sigma}{2} + \frac{\sigma_m}{d} \qquad \text{Stulen (45)} \qquad (21)$$

where S_u is the ultimate strength, σ_f' the fatigue strength coefficient and d is a constant for a particular material. Equations 19 and 20 have constants that are determined from data without mean stress. To determine the constant, d, of Eq. 21, mean stress data are necessary. The parameter proposed by Smith et al. (46) does not rely on any experimentally derived constants. Dowling reported that Eq. 21 gave the best agreement for both the aluminum and 4340 alloy steel.

In another investigation of this nature (41), the effect of prestrain and mean stress was studied for SAE 1015 steel. Equation 20 and the parameter proposed by Smith et al. (46) were used. It was found that both equations agree reasonably well with the data.

Any of the mean stress parameters discussed might be included in a fatigue damage analysis. The accuracy of Eqs. 18 and 21 is due to the constants being fit to the actual mean stress data. Equation 19 depends on the monotonic tension property S_u. The fatigue strength coefficient, σ_f', can be approximated by the true fracture strength, σ_f (7). Equations 19 through 21 are equivalent stresses and therefore can be directly related to the elastic strain versus life data for completely reversed test results. It is necessary to obtain a relation between the right side of Eq. 18 or the Smith et al. parameter (46) and the reversals to failure. These mean stress parameters do not deviate appreciably from each other for small mean stresses. Since large mean stresses do not exist in many practical cases, the choice of the mean stress parameter is not critical. Equation 20 was used for this analysis.

PROCEDURE FOR CUMULATIVE FATIGUE DAMAGE ANALYSIS

Once the mechanics analysis and model of uniaxial stress-strain behavior is formulated and appropriate fatigue damage parameters determined, a procedure is needed to combine these individual analyses into an efficient method for estimating the fatigue lives of structures that are subjected to representative loads. The following discussion outlines the procedure and Appendix A presents more details. Figure 29 shows the general flow chart of the procedure.

Local Stress-Strain Response

Equation 3 and the model of uniaxial stress-strain behavior constitute the ingredients for the simulation of the stress-strain response of the metal at the highly strained region. Theoretical or experimental methods must determine the nominal stress, ΔS, or strain, Δe, ranges. Only one nominal variable must be supplied, either ΔS or Δe, the model of uniaxial behavior calculates the other. If nominal elastic behavior exists, either Eqs. 4 or 5 may be used. The value of K_f^2 (ΔS Δe) can now be calculated. This sets a constant for which the product $\Delta\sigma$ $\Delta\epsilon$ must satisfy. In a similar manner to the nominal response, increments of the local stress-strain curve are constructed until the product of $\Delta\sigma$ $\Delta\epsilon$ exceeds or exactly satisfies the condition K_f^2 (ΔS Δe).

Cumulative Fatigue Damage

Once the local stress-strain response has been determined, a cumulative damage procedure is employed. For this analysis the variables involved in the damage summation are elastic and plastic strain and mean stress. Damage due to either elastic or plastic strain is summed along each increment of the local stress-strain curve. Each increment of damage is determined by the element that is activated to form a segment of the stress-strain curve. This increment of damage is

the same as would be experienced if the model were simulating a completely reversed closed hysteresis loop.

Since the value of mean stress can not be determined during an increment of stress, it is corrected for at the end of a reversal or at the closure of a hysteresis loop. To correct for mean stress when only elastic behavior exists, the equivalent stress amplitude calculated by Eq. 20 is substituted for the stress range in Eq. 15. Thus the damage due to a stress amplitude of $\Delta\sigma/2$ with a mean stress of σ_m is given by Eq. 22.

$$\frac{1}{2N_f} = \left(\frac{\Delta\sigma/2}{\sigma_f' - \sigma_m}\right)^{-1/b} \tag{22}$$

To calculate damage due to mean stress based on the plastic strain fatigue properties, Eqs. 16 and 11 are combined.

$$\frac{1}{2N_f} = \left[\frac{\left(\frac{\Delta\sigma/2}{K^*}\right)^{1/n^*}}{\epsilon_f'}\right]^{-1/c} \tag{23}$$

The equivalent value of stress from Eq. 20 is substituted for the completely reversed stress amplitude.

$$\frac{1}{2N_{f\ cr}} = \left[\frac{\left(\frac{\Delta\sigma/2}{K^*(1 - \sigma_m/\sigma_f')}\right)^{1/n^*}}{\epsilon_f'}\right]^{-1/c} \tag{24}$$

The difference between Eqs. 24 and 23 produces the damage correction, D_m, for mean stress.

$$D_m = \left(\epsilon_f'\right)^{1/c}\left(\left(\frac{\Delta\sigma/2}{K^*}\right)^{-1/n^*c}\right)\left[\left(1 - \frac{\sigma_m}{\sigma_f'}\right)^{1/n^*c} - 1\right] \tag{25}$$

For each segment of the stress-strain curve damage will be summed without the effect of mean stress. For the first segment, damage is based on elastic strain. All other segments calculate damage from plastic strain. Each time a hysteresis loop is closed and at the end of each reversal the damage due to the mean stress for that closed loop or reversal is added.

At any portion of a load history, the model associates each segment with a closed hysteresis loop. The model can also determine the mean stress for that loop. To perform this function, additional information is obtained when determining the element moduli and yield stresses. Figure 30a defines a plastic strain, $\bar{\epsilon}_i$, associated with each element. The element damage, D_i, is the damage produced by $\bar{\epsilon}_i$.

Figure 30b shows a stress-strain history that illustrates the possibilities of the incremental damage procedure. This load history consists of five reversals: A-D, D-E, E-G, G-I and I-K. For the first segment of each reversal (A-B, D-E, E-D, G-H and I-J) damage is calculated from the elastic strain, Eq. 14 or 15. For all other segments (B-C, C-D, D-F, F-G, H-I, J-G and G-K) damage is based on the plastic strain. Mean stress corrections are added at the end of each reversal (D, E, G, I and K). At point D, the mean stress correction is for the segment A-D and at point G for the segment D-G. Each time the model encounters a hysteresis loop that has been completed (points D and G), a mean stress correction is also added. For this correction, at point D mean stress is for the segment E-D and at point G for the segment I-G.

Determination of Failure

The load spectrum could be repeated or continued until a total damage summation of one is reached. However, this is in many cases unnecessary. If a particular load history is to be repeated, it would be a waste of computational time to not extrapolate the failure. For the analyses of the fan blade and the box-beam each

time a block of loading was taken, a check of the change of damage for that block as opposed to the previous block is compared. Once an acceptable difference is obtained, the final failure point is extrapolated. The main factor producing differences in the damage per block is the relaxation of mean stress and cyclic hardening or softening.

APPLICATIONS OF THE FATIGUE DAMAGE ANALYSIS

The fatigue damage procedure was programmed for the digital computer. Life predictions were made for a box-beam structure and an automotive fan blade. More detailed explanations of the analysis are given in Appendix B for the box-beam and Appendix C for the fan blade.

Application to Box-Beam Structures

The computer based fatigue damage analysis was used to estimate the fatigue lives of some of the built-up box-beams that have been tested by the Navy (48-52). Fatigue lives were estimated for constant amplitude and flight test spectra. Figure 31 shows a photo of the beam that was supported in unidirectional bending.

The box-beams are built-up structures. General design, fabrication techniques and materials are representative of components used in aircraft structures. An aluminum alloy, 7075-T6, made up the top and bottom plates. All failures were reported on the top tension plate.

Stress-strain properties consisted only of the stable cyclic strength coefficient and strain hardening exponent. A relaxing constant, M, of 3×10^3 was determined. Reference 53 reported an elastic stress concentration factor, K_t, of 2.9. The fatigue notch factor, K_f, of 2.4 was obtained from K_t by a highly stressed volume approach discussed in Ref. 12.

Life predictions were made for three sets of constant amplitude test results. These test results were referenced to a 1 g load that was selected to approximate the load applied to an airplane wing with the airplane in steady level flight. Tables 1 through 3 and Figs. 32 through 34 present the data for loads, P, of: 1 g to P, -g to P, and g ± P. All data are presented in terms of nominal outer fiber stresses that were reported in Refs. 48 through 50.

Variable load spectra as designated by military code MIL-A-8866 were also applied to the beams. Figure 35 shows a portion of one of the load spectra for different block sizes. Loads are in percent of a load limit, which is the load used as a reference for establishing the strength level for design. For these variable load spectra, the nominal outer fiber stresses were also reported (48-49).

Table 4 and Fig. 36 present the data for the beams subjected to test spectra A, B and C of MIL-A-8866. Two margins of safety, which denotes the excess in strength of a structure over the design load, were reported. Although the predicted results were acceptable, they did not show the block size effect demonstrated by the test results. If cyclic relaxation of mean stress was the cause of the block size effect, this same effect should have been reflected in the simulation results.

Shut-down periods existed during some of the tests. Upon releasing the load and reloading, the mean stress would be altered from its previous value. Impellizzeri (17) occasionally entered a zero load in the fatigue damage analyses and improved the life estimations.

Figure 37 compares actual and estimated data for all the box-beam test results. Estimations of variable load histories were more accurate than for the constant amplitude loads. At very long lives the fatigue life estimations were severely off for several points.

Application to Automotive Fan Blades

Constant amplitude and variable amplitude fatigue tests* were conducted on automotive fan blades, Fig. 38. Some of the constant amplitude data of the blades were generated on an electrodynamic shaker. All variable and the remainder of the constant amplitude tests were performed on a closed loop system. Figure 39 shows the blade in

*All tests were performed at the General Motors Proving Grounds.

the load fixture of the closed loop system load frame. All fan blades were subjected to load levels that produced the desired output from a strain gage mounted in the region where the crack initiates, Fig. 40.

Monotonic and stable cyclic stress-strain properties were determined. For the simulation, the monotonic curve was used until the initial yield stress was exceeded. After exceeding this yield stress, the model parameters were changed to fit the stable cyclic curve. A relaxing constant of 5×10^4 was determined. The fatigue notch factor, K_f, was determined from the constant amplitude data from both the fan blades and the sheet steel specimens, Fig. 41. At 2×10^6 reversals, K_f is approximately 1.9. Initial overstrain strain-life data were used in the analysis of the constant amplitude loading and periodic overstrain data for the variable load histories.

Table 5 lists the constant amplitude fan blade data that were not overstrained. Overstrain data and life estimations are given in Table 6. Figure 42 shows all the constant amplitude data and the fatigue life estimations for the overstrained data. A large amount of scatter exists for the fan blade data. Fatigue life estimations for other load histories could not be expected to be more accurate than the scatter of the constant amplitude data.

The fan blades were also subjected to two load histories that are cataloged by the Society of Automotive Engineers and are representative of service histories. Table 7 and Fig. 43 present the data of the "axle" history and the "suspension" are given in Table 8 and Fig. 44. Reference 54 lists the loading patterns for the different load histories. The suspension load history contains more large loads with mean load shifts. All life predictions were within the scatter band of the constant amplitude data.

Estimated and actual fatigue lives of all the fan blade data are shown in Fig. 45. All estimations are within the scatter of the constant amplitude data.

CONCLUDING REMARKS

Fatigue life estimations can be made by modeling the stress-strain response of the metal at the highly strained region and by applying a cumulative damage analysis to that region. Determination of the local stresses and strains is accomplished by combining Eq. 3 and the model of uniaxial stress-strain behavior. Damage is calculated from either elastic or plastic strain for each segment of the local stress-strain curve. Mean stress is corrected for at the end of each reversal and upon closure of a complete hysteresis loop.

Successful verification of the model of uniaxial stress-strain behavior was accomplished for 2024-T4 aluminum and A 36 steel (38). The models that simulated each of these metals were similar, indicating that the basic concepts for this type of model could be used for other metals. Simulation of cyclic hardening or softening is not always necessary for fatigue analyses. In many cases the structure is deformed during the manufacturing process to such a degree that will eliminate the initial transient period. Only stable cyclic stress strain properties were employed for the fatigue analysis of the box-beam structures. Cyclic hardening for the sheet steel from the fan blades was obtained by replacing the monotonic tension properties with the stable cyclic after the first reversal containing plastic strain. For both the analysis of the box-beams and the fan blades, cyclic relaxation of mean stress was modeled, although this might not have been necessary for the completely reversed and variable load histories.

Since many structures experience occasional large loads during service, appropriate fatigue data were included. Since periodic overstraining did not further reduce fatigue life, initial overstrain data were employed for all the analyses of the box-beams. For the fan blades, initial overstrain data were used to analyze the constant amplitude loadings and periodic overstrain data were employed for the variable load histories.

The type of data that is appropriate for a particular load history is not clear. For the fan blades, frequent overloads were apparent during the variable load histories. If initial overstrain data were employed for the analysis of the variable load histories, large errors would have occurred.

In general, good agreement was obtained between the actual and estimated fatigue lives of the box-beams and fan blades. Figure 37 summarizes the estimated and actual fatigue data for the box-beams. Several fatigue life estimations for the constant amplitude load data were in considerable error. However, the majority of the life estimations resulted in damage summations (estimated/actual) between 0.3 and 3. Figure 45 presents the estimated and actual fatigue data for the fan blades. Damage summations ranged from 0.2 to 5, which is within the scatter of the constant amplitude test results.

REFERENCES

1. J. A. Ewing and J. C. W. Humfrey, "The Fracture of Metals under Repeated Alternations of Stress," Philosophical Transactions, Royal Society, London, Series A, Vol. 200, 1903, pp. 241-250.

2. J. C. Grosskreutz, "The Mechanisms of Metal Fatigue (II)," (Review Article), physica status solidi (b), Vol. 47, No. 2, 1971, pp. 359-396.

3. C. R. Smith, "Small Specimen Data for Predicting Life of Full-Scale Structures," Fatigue Tests of Aircraft Structures: Low-Cycle, Full-Scale, and Helicopters, ASTM STP 338, American Society for Testing and Materials, 1962, pp. 241-250.

4. R. E. Peterson, "Fatigue of Metals-Engineering and Design Aspect," Materials Research and Standards, Vol. 3, No. 2, February 1963, pp. 122-139.

5. H. F. Hardrath, "Fatigue of Metals-Crack Propagation and Final Failure," Materials Research and Standards, Vol. 3, No. 2, February 1963, pp. 116-121.

6. T. J. Dolan, "Nonlinear Response under Cyclic Loading Conditions," Proceedings of the Ninth Midwestern Mechanics Conference, Madison, Wisconsin, August 1965, pp. 3-21.

7. JoDean Morrow, "Fatigue Properties of Metals," Section 3.2 of Fatigue Design Handbook, Society of Automotive Engineers, Vol. 4, 1968.

8. S. S. Manson and M. H. Hirschberg, "Crack Initiation and Propagation in Notched Fatigue Specimens," Proceedings of the First International Conference on Fracture, The Japanese Society for Strength and Fracture of Materials, Vol. 1, Sendai, Japan, September 1965, pp. 479-498.

9. J. H. Crews, Jr. and H. F. Hardrath, "A Study of Cyclic Plastic Stresses at a Notch Root," Experimental Mechanics, Vol. 6, No. 6, June 1966, pp. 313-320.

10. JoDean Morrow, R. M. Wetzel, and T. H. Topper, "Laboratory Simulation of Structural Fatigue Behavior," Effect of Environment and Complex Load History on Fatigue Life, ASTM STP 462, American Society for Testing and Materials, 1970, pp. 74-91. See also: R. M. Wetzel, JoDean Morrow, and T. H. Topper, "Fatigue of Notched Parts with Emphasis on Local Stresses and Strains," Naval Air Development Center Report No. NADC-ST-6818, September 1968.

11. T. H. Topper, R. M. Wetzel, and JoDean Morrow, "Neuber's Rule Applied to Fatigue of Notched Specimens," Journal of Materials, Vol. 4, No. 1, March 1969, pp. 200-209. See also: T. H. Topper, R. M. Wetzel, J. Morrow, "Neuber's Rule Applied to Fatigue of Notched Specimens," Aeronautical Structures Laboratory Report No. NAEC-ASL-1114, June 1967.

12. T. H. Topper and JoDean Morrow, Editors, "Simulation of the Fatigue Behavior at the Notch Root in Spectrum Loaded Notched Members (U)," T. & A. M. Report No. 333, Department of Theoretical and Applied Mechanics, University of Illinois, Urbana, January 1970, (Final Report for Aero Structures Department, Naval Air Development Center).

13. J. H. Crews, "Crack Initiation at Stress Concentrations as Influenced by Prior Local Plasticity," Achievement of High Fatigue Resistance in Metals and Alloys, ASTM STP 467, American Society for Testing and Materials, 1970, pp. 37-52.

14. R. M. Wetzel, "Smooth Specimen Simulation of Fatigue Behavior of Notches," Journal of Materials, Vol. 3, No. 3, September 1968, pp. 646-657. See also: R. M. Wetzel, "Smooth Specimen Simulation of Fatigue Behavior of Notches," T. & A. M. Report No. 295, Department of Theoretical and Applied Mechanics, University of Illinois, Urbana, May 1967.

15. S. J. Stadnick and JoDean Morrow, "Techniques for Smooth Specimen Simulation of the Fatigue Behavior of Notched Members," Testing for Prediction of Material Performance in Structures and Components, ASTM STP 515, American Society for Testing and Materials, 1972, pp. 229-252. See also: S. J. Stadnick, "Simulation of Overload Effects in Fatigue Based on Neuber's Analysis," T. & A. M. Report No. 325, Department of Theoretical and Applied Mechanics, University of Illinois, Urbana.

16. L. E. Tucker, "A Procedure for Designing Against Fatigue Failure of Notched Parts," Preprint of Society of Automotive Engineers, from Automotive Engineering Congress, Detroit, Michigan, January 10-14, 1972. See also: L. E. Tucker, "A Procedure for Designing Against Fatigue Failure of Notched Parts," M.S. Thesis, Department of Theoretical and Applied Mechanics, University of Illinois, Urbana, 1970.

17. L. F. Impellizzeri, "Cumulative Damage Analysis in Structural Fatigue," Effects of Environment and Complex Load History on Fatigue Life, ASTM STP 462, American Society for Testing and Materials, 1970, pp. 40-68.

18. J. Schijve, "The Accumulation of Fatigue Damage in Aircraft Materials and Structures," AGARD-AG-157, Advisory Group for Aerospace Research and Development, North Atlantic Treaty Organization, January 1972.

19. H. Neuber, "Theory of Stress Concentration for Shear-Strained Prismatical Bodies with Arbitrary Nonlinear Stress-Strain Law," Transactions, American Society of Mechanical Engineers, Journal of Applied Mechanics, Vol. 8, December 1961, pp. 544-550.

20. E. Z. Stowell, "Stress and Strain Concentration at a Circular Hole in an Infinite Plate," NACA Technical Note No. 2073, National Advisory Committee for Aeronautics, 1950.

21. A. Palmgren, "Die Lebensdauer von Kugellagern," Zeitschrift des Vereines Deutscher Ingenieure, Vol. 68, No. 14, April 1924, pp. 339-341. See also: NASA Technical Translation 1-13460.

22. M. A. Miner, "Cumulative Damage in Fatigue," Transactions, American Society of Mechanical Engineers, Vol. 67, 1945, p. A 159.

23. J. F. Martin, T. H. Topper, and G. M. Sinclair, "Computer Based Simulation of Cyclic Stress-Strain Behavior with Applications to Fatigue," Materials Research and Standards, Vol. 11, No. 2, February 1971, p. 23. See also: J. F. Martin, T. H. Topper, and G. M. Sinclair, "Computer Based Simulation of Cyclic Stress Strain Behavior," T. & A. M. Report No. 326, Department of Theoretical and Applied Mechanics, University of Illinois, Urbana, July 1969. See also Chapter V of: T. H. Topper and JoDean Morrow, Editors, "Simulation of the Fatigue Behavior in Spectrum Loaded Notched Members," T. & A. M. Report No. 333, Department of Theoretical and Applied Mechanics, University of Illinois, Urbana, January 1970. (Final Report for Aero Structures Department, Naval Air Development Center).

24. R. M. Wetzel, "A Method of Fatigue Damage Analysis," Technical Report No. SR 71-107, Scientific Research Staff, Ford Motor Company, August 1971. See also: R. M. Wetzel, "A Method of Fatigue Damage Analysis," Ph. D. Thesis, Department of Civil Engineering, University of Waterloo, Waterloo, Ontario, September 1971.

25. H. R. Jhansale and T. H. Topper, "Cyclic Deformation and Fatigue Behaviour of Axial and Flexural Members - A Method of Simulation and Correlation," Proceedings of the First International Conference on Structural Mechanics in Reactor Technology, Berlin, Germany, September 1972, Vol. 6, Part L, pp. 433-455. See also: H. R. Jhansale, "Inelastic Deformation and Fatigue Response of Spectrum Loaded Strain Controlled Axial and Flexural Members," Ph. D. Thesis, Department of Civil Engineering, University of Waterloo, Waterloo, Ontario, Canada, March 1971.

26. H. R. Jhansale and T. H. Topper, "A Conceptual Model for Cyclic Inelastic Response of a Structural Component Based on Material Deformation Studies," Mechanical Behavior of Materials, Proceedings of the 1971 International Conference on Mechanical Behavior of Materials, Kyoto, Japan, August 1971, Vol. II, pp. 489-500, The Society of Materials Science, Japan, 1972. See also: H. R. Jhansale, "Inelastic Deformation and Fatigue Response of Spectrum Loaded Strain Controlled Axial and Flexural Members," Ph. D. Thesis, Department of Civil Engineering, University of Waterloo, Waterloo, Ontario, Canada, March 1971.

27. C. V. B. Gowda and T. H. Topper, "On the Relations between Stress and Strain Concentration Factors in Notched Members with a Non-linear Stress-Strain Law," Transactions, American Society of Mechanical Engineers, Journal of Applied Mechanics, Vol. 37, Series E, No. 1, March 1970.

28. C. V. B. Gowda and T. H. Topper, "Cyclic Deformation Behavior of Notched Mild Steel Plates in Plane Stress," SESA Paper No. 1705, Society of Experimental Stress Analysis, presented at the 1970 SESA Fall meeting, Boston, Massachusetts, October 1970.

29. A. A. Blatherwick and B. K. Olson, "Stress Redistribution in Notched Specimens during Fatigue Cycling," Experimental Mechanics, Vol. 8, No. 8, August 1968, pp. 356-361.

30. G. E. Griffith, "Experimental Investigation of the Effects of Plastic Flow in a Tension Panel with a Circular Hole," NACA Technical Note No. 1705, National Advisory Committee for Aeronautics, 1949.

31. C. F. Jenkin, "Fatigue in Metals," The Engineer, Vol. 134, December 1922, pp. 612-614.

32. K. Koibuchi and M. Yamane, "Stress-Strain Curves under Variable Stresses," Bulletin of Japanese Society of Mechanical Engineers, Vol. 10, No. 40, August 1967, pp. 601-610.

33. W. D. Iwan, "The Steady-State Response of a Two-Degree-of-Freedom Bilinear Hysteretic System," Transactions, American Society of Mechanical Engineers, Journal of Applied Mechanics, Vol. 32, Series E, No. 1, March 1965, pp. 151-156.

34. W. D. Iwan, "A Distributed-Element Model for Hysteresis and Its Steady-State Dynamic Response," Transactions, American Society of Mechanical Engineers, Journal of Applied Mechanics, Vol. 33, Series E, No. 4, December 1966, pp. 893-900.

35. W. D. Iwan, "On a Class of Models for the Yielding Behavior of Continuous and Composite Systems," Transactions, American Society of Mechanical Engineers, Journal of Applied Mechanics, Vol. 34, Series E, No. 3, September 1967, pp. 612-617.

36. JoDean Morrow, "Cyclic Plastic Strain Energy and Fatigue of Metals," Internal Friction, Damping, and Cyclic Plasticity, ASTM STP 378, American Society for Testing and Materials, 1965, pp. 45-87.

37. R. W. Landgraf, JoDean Morrow, and T. Endo, "Determination of the Cyclic Stress-Strain Curve," Journal of Materials, Vol. 4, No. 1, March 1969, pp. 176-188.

38. F. B. Plummer, "Cyclic Plasticity and Structural Energy Dissipation," Ph.D. Thesis, Department of Theoretical and Applied Mechanics, University of Illinois, Urbana, 1973.

39. T. H. Topper and B. I. Sandor, "Effects of Mean Stress and Prestrain on Fatigue Damage Summation," Effects of Environment and Complex Load History on Fatigue Life, ASTM STP 462, American Society for Testing and Materials, 1970, pp. 93-104. See also: T. H. Topper and B. I. Sandor, "Effects of Mean Stress on Fatigue Damage Summation," T. & A.M. Report No. 318, Department of Theoretical and Applied Mechanics, University of Illinois, Urbana, August 1968. See also Chapter III of: T. H. Topper and JoDean Morrow, Editors, "Simulation of the Fatigue Behavior in Spectrum Loaded Notched Members," T. & A.M. Report No. 333, Department of Theoretical and Applied Mechanics, University of Illinois, Urbana, January 1970, (Final Report for Aero Structures Department, Naval Air Development Center).

40. N. E. Dowling, "Fatigue Failure Predictions for Complicated Stress-Strain Histories," Journal of Materials, Vol. 7, No. 1, March 1972, pp. 71-87. See also: N. E. Dowling, "Fatigue Failure Predictions for Complicated Stress-Strain Histories," T. & A. M. Report No. 337, Department of Theoretical and Applied Mechanics, University of Illinois, Urbana, January 1971.

41. P. Watson and T. H. Topper, "Fatigue Damage Evaluation for Mild Steel Incorporating Mean Stress and Overload Effects," Experimental Mechanics, Vol. 12, No. 1, January 1972, pp. 11-17.

42. P. Watson and T. H. Topper, "The Effects of Overstrain on the Fatigue Behaviour of Five Steels," presented at Fall meeting of the Metallurgical Society, Cleveland, Ohio, October 1970.

43. N. E. Dowling, "Fatigue Life and Inelastic Strain Response under Complex Histories for an Alloy Steel," Journal of Testing Evaluation, Vol. 1, No. 4, July 1973, pp. 271-287. See also: N. E. Dowling, "Fatigue Life and Inelastic Strain Response under Complex Histories for an Alloy Steel," T. & A. M. Report No. 354, Department of Theoretical and Applied Mechanics, University of Illinois, Urbana, April 1972.

44. J. O. Smith, "The Effect of Range of Stress on the Fatigue Strength of Metals," Bulletin No. 334, University of Illinois, Engineering Experiment Station, Urbana, February 1942.

45. F. L. Stulen, "Fatigue Life Data Displayed by a Single Quantity Relating Alternating and Mean Stress," AFML TR 65-121, Air Force Materials Lab., Wright-Patterson AFB, Ohio, July 1965.

46. K. N. Smith, P. Watson, and T. H. Topper, "A Stress-Strain Function for the Fatigue of Metals," Journal of Materials, Vol. 5, No. 4, December 1970, pp. 767-776.

47. R. B. Wilson, "Influence of Variable Mean Stress on Fatigue Damage," T. & A. M. Report No. 672, Department of Theoretical and Applied Mechanics, University of Illinois, Urbana, June 1967. See also: R. B. Wilson, "Influence of Variable Mean Stress on Fatigue Damage," M. S. Thesis, Department of Theoretical and Applied Mechanics, University of Illinois, Urbana, 1967.

48. W. Breyan, "Effects of Block Size, Stress Level, and Loading Sequence on Fatigue Characteristics of Aluminum-Alloy Box Beams," Effects of Environment and Complex Load History on Fatigue Life, ASTM STP 462, American Society for Testing and Materials, 1970, pp. 127-166.

49. W. Breyan, "Effects of Spectrum Block Size and Stress Level on Fatigue Characteristics of Aluminum Alloy Box Beams under Fixed-Sequence Unidirectional Loading," Report No. NADC-ST-6811, Naval Air Development Center, Johnsville, Pennsylvania, September 1968.

50. W. Breyan, "Constant-Load-Amplitude Fatigue Characteristics of Aluminum Alloy Box Beam under Partially Reversed Loading," Report No. NADC-ST-7011, Naval Air Development Center, Warminster, Pennsylvania, October 1970.

51. W. Breyan and E. P. Roeser, "Effects of Spectrum Block Size and Stress Level on Fatigue Characteristics of Aluminum Alloy Box Beams under Random-Sequence Unidirectional Loading," Report No. NADC-ST-7013, Naval Air Development Center, Warminster, Pennsylvania, December 1971.

52. W. Breyan, "Summary of Test Results for Aluminum Alloy Box Beam Fatigue Program, Test Phases I-IV," Report No. NADC-72056-VT, Naval Air Development Center, Warminster, Pennsylvania, June 1972.

53. J. W. Dally and A. J. Durelli, "Stresses in Perforated Panels," Product Engineering, Vol. 27, No. 3, March 1956, pp. 188-191.

54. H. O. Fuchs, D. V. Nelson, M. A. Burke, and T. L. Toomay, "Shortcuts in Cumulative Damage Analysis," Preprint of Society of Automotive Engineers, Paper No. 730565, Automobile Engineering meeting, Detroit, Michigan, May 1973.

55. T. Endo and JoDean Morrow, "Cyclic Stress-Strain and Fatigue Behavior of Representative Aircraft Metals," Journal of Materials, Vol. 4, No. 1, March 1969, pp. 159-175. See also: T. Endo and JoDean Morrow, "Monotonic and Completely Reversed Cyclic Stress-Strain and Fatigue Behavior of Representative Aircraft Metals," Aeronautical Structures Laboratory Report No. NAEC-ASL-1105, June 1966.

56. J. F. Martin, "Cyclic Stress-Strain Behavior and Fatigue Resistance of Two Structural Steels," FCP Report No. 9, College of Engineering, University of Illinois, Urbana, Illinois, October 1973.

57. O. C. Zienkiewicz, The Finite Element Method in Engineering Science, McGraw-Hill Publishing Company, Limited, London, 1971.

58. P. V. Marcal, "Finite Element Analysis of Combined Problems of Nonlinear Material and Geometric Behavior," Proceedings ASME Joint Computer Conference on Computational Approach to Applied Mechanics, Chicago, 1969, pp. 133-149.

59. P. V. Marcal, "Finite Element Analysis with Material Nonlinearities--Theory and Practice," Japan-U.S. Seminar on Matrix Methods of Structural Analysis and Design, Tokyo, Japan, August 1969.

60. S. Valliappan, "Elasto-Plastic Analysis of Anisotropic Work-Hardening Materials," UNICIV Report No. R-70, University of South Wales, Kensington, New South Wales, Australia, August 1971.

61. G. C. Nayak and O. C. Zienkiewecz, "Elasto-Plastic Stress Analysis. A Generalization for Various Constitutive Relations Including Strain Softening," International Journal for Numerical Methods in Engineering, Vol. 5, 1972, pp. 113-135.

62. C. A. Griffis, "Finite Element Analysis of Notched Tensile Specimens in Plane Stress," NRL Report 7278, Naval Research Laboratory, Washington, D.C., September 1971.

63. J. A. Stricklin, W. E. Haisler, and W. A. Von Riesemann, "Evaluation of Solution Procedures for Material and/or Geometrically Nonlinear Structural Analysis by the Direct Stiffness Method," presented at AIAA/ASME 13th Structures, Structural Dynamics, and Materials Conference, San Antonio, Texas, April 1972.

64. G. Isakson, H. Armen, Jr. and A. Pifko, "Discrete-Element Methods for the Plastic Analysis of Structures," NASA CR-803, National Aeronautics and Space Administration, October 1967.

65. H. Armen, Jr. and A. Pifko, "Computer Programs for the Plastic Analysis of Structures Using Discrete Element Methods," NASA CR-66364, National Aeronautics and Space Administration, July 1965.

66. G. E. Dieter, Jr., Mechanical Metallurgy, McGraw-Hill Book Company, Inc., New York, 1961, pp. 251-252.

67. P. W. Bridgman, "The Stress Distribution at the Neck of a Tension Specimen," Transactions, American Society of Metals, Vol. 32, 1944, pp. 553-574.

TABLE 1

CONSTANT AMPLITUDE LOADING (1 g TO P)[1] OF THE BOX-BEAMS

Nominal Stress Amplitude $\Delta S/2$, ksi	Fatigue Test Results, Reversals to Failure $2N_f$	Estimated Reversals to Failure $2N_f$
38	748 766	287
37	1,100 1,300	295
36	1,130 1,780	531
34	2,470 3,650 3,840 5,430	691
25	9,830 11,500 11,840 12,100	3,260
20	16,200 18,800 19,900 21,100 22,500 25,900	10,900
14	48,600 59,100	71,700
7	261,000 276,000 282,000 443,000	6,020,000
6	230,000 241,000	15,000,000
4	569,000 No failure	114,000,000

[1] The minimum load, 1 g, for all tests was 588 pounds corresponding to a stress of 7.8 ksi, except for test results below 14 ksi for which the minimum load was 529 pounds and the stress 7 ksi.

TABLE 2

CONSTANT AMPLITUDE LOADING (-g TO P)[1] OF THE BOX-BEAMS

Nominal Stress Amplitude $\Delta S/2$, ksi	Fatigue Test Results, Reversals to Failure $2N_f$	Estimated Reversals to Failure $2N_f$
42	926	424
	1,220	
36	2,190	798
	3,080	
25	11,500	3,810
	13,400	
18	30,700	26,100
	33,600	
	35,900	
	39,900	
13	132,000	226,000
	144,000	
	160,000	
	173,000	
10	706,000	1,360,000
	1,360,000	
7	1,370,000	8,060,000
	2,220,000	

[1]The value of 1 g for all tests was 588 pounds corresponding to a stress of 7.5 ksi.

TABLE 3

CONSTANT AMPLITUDE LOADING (1 g TO ±P)[1] OF THE BOX-BEAMS

Nominal Stress Amplitude S/2, ksi	Fatigue Test Results, Reversals to Failure $2N_f$	Estimated Reversals to Failure $2N_f$
69	190 274	81
50	1,290 2,100	328
36	3,120 4,730	1,060
25	17,400 26,500	4,120
15	40,200 55,500 69,500	87,600
11	163,000 162,000	722,000
8	276,000 290,000	3,550,000

[1] The value of 1 g for all tests was 588 pounds corresponding to a stress of 7.5 ksi.

TABLE 4

VARIABLE LOAD FLIGHT SPECTRA FOR THE BOX-BEAMS

Spectrum	Margin of Safety	Block Size	Fatigue Test Results, Flight Hours to Failure	Estimated Flight Hours to Failure
A	0%	20	1,360 1,400	1,610
A	0%	60	1,500 1,620	1,580
A	0%	100	3,500 3,900	1,440
A	11%	20	3,300 3,360	2,900
A	11%	60	4,260 4,440	2,860
A	11%	100	7,100 7,100	2,610
B	0%	20	9,500 10,300	7,310
B	0%	60	6,660 7,020	7,040
B	0%	100	7,900 8,300	6,750
B	11%	20	12,300 13,300	12,600
B	11%	60	16,000 18,800	12,200
B	11%	100	21,300 22,600	11,900
C	0%	20	11,900 12,300	11,400
C	0%	60	16,600 17,600	11,000

TABLE 4 (Continued)

VARIABLE LOAD FLIGHT SPECTRA FOR THE BOX-BEAMS

Spectrum	Margin of Safety	Block Size	Fatigue Test Results, Flight Hours to Failure	Estimated Flight Hours to Failure
C	0%	100	18,900 25,900	10,300
C	11%	20	22,900 22,900	19,800
C	11%	60	33,900 35,100	19,400
C	11%	100	31,300 50,900	18,300

TABLE 5

CONSTANT AMPLITUDE FATIGUE DATA FOR THE FAN BLADES

Nominal Strain Amplitude $\Delta e/2$	Fatigue Test Results, Reversals to Failure $2N_f$
0.00388	1,360
0.00330	4,600
0.00285	5,530
0.00230	5,560
0.00189	12,500
0.00148	34,100
0.00092	160,000
0.00079	206,000
0.00069	355,000
0.00059	719,000
0.00059	407,000
0.00058	2,730,000
0.00056	566,000
0.00055	898,000
0.00053	1,170,000

TABLE 6

INITIALLY OVERSTRAINED CONSTANT AMPLITUDE
FATIGUE DATA FOR FAN BLADES

Nominal Strain Amplitude $\Delta e/2$	Fatigue Test Results, Reversals to Failure $2N_f$	Estimated[1] Reversals to Failure $2N_f$	Estimated[2] Reversals to Failure $2N_f$
0.00394	1,460	2,510	365
0.00393	1,280	3,340	368
0.00337	2,960	3,870	674
0.00334	2,700	3,960	707
0.00296	2,000	5,470	1,060
0.00293	1,880	5,630	1,110
0.00293	2,930	5,630	1,110
0.00230	6,870	11,600	2,720
0.00224	4,940	11,900	3,020
0.00218	8,160	12,800	3,340
0.00184	24,700	21,000	6,600
0.00181	6,870	22,100	6,870
0.00178	7,540	23,400	7,120
0.00154	29,700	39,000	13,100
0.00148	44,600	40,900	15,300
0.00145	69,100	42,700	16,200
0.00139	19,800	49,800	19,700
0.00118	36,900	84,700	38,500
0.00116	55,600	91,300	42,000
0.00096	205,000	165,000	91,000
0.00095	161,000	177,000	100,000
0.00094	267,000	185,000	106,000

[1] Plastic nominal stress-strain behavior, Eq. 3, is accounted for.

[2] Elastic nominal stress-strain behavior, Eq. 5, is assumed.

TABLE 6 (Continued)

INITIALLY OVERSTRAINED CONSTANT AMPLITUDE
FATIGUE DATA FOR FAN BLADES

Nominal Strain Amplitude $\Delta e/2$	Fatigue Test Results, Reversals to Failure $2N_f$	Estimated[1] Reversals to Failure $2N_f$	Estimated[2] Reversals to Failure $2N_f$
0.00089	128,000	229,000	127,000
0.00066	282,000	684,000	482,000
0.00064	1,040,000	785,000	600,000
0.00060	760,000	1,080,000	824,000
0.00059	2,120,000	1,140,000	877,000
0.00058	3,800,000	1,210,000	948,000
0.00056	808,000	1,530,000	1,190,000
0.00055	1,250,000	1,580,000	1,220,000

[1]Plastic nominal stress-strain behavior, Eq. 3, is accounted for.

[2]Elastic nominal stress-strain behavior, Eq. 5, is assumed.

TABLE 7

FATIGUE DATA FOR FAN BLADES SUBJECTED TO 'AXLE' LOAD HISTORIES

Maximum Nominal Strain	Test Results, Blocks to Failure	Estimated[1] Blocks to Failure	Estimated[2] Blocks to Failure	Estimated[3] Blocks to Failure
0.00370	90	68	38	164
0.00343	107	82	46	216
0.00300	103	113	65	353
0.00250	87	220	102	688
0.00200	244	406	242	1,560
0.00150	353	683	567	4,460

[1]Plastic nominal stress-strain behavior, Eq. 3, is accounted for.

[2]Elastic nominal stress-strain behavior, Eq. 5, is assumed.

[3]Damage is summed based on nominal strains.

TABLE 8

FATIGUE DATA FOR FAN BLADES SUBJECTED TO THE 'SUSPENSION' LOAD HISTORIES

Maximum Nominal Strain	Test Results, Blocks to Failure	Estimated[1] Blocks to Failure	Estimated[2] Blocks to Failure	Estimated[3] Blocks to Failure
0.00370	33	89	57	304
0.00258	159	284	191	1,140
0.00146	537	1,910	1,090	9,140
0.00128	No failure	4,020	2,910	15,000

[1]Plastic nominal stress-strain behavior, Eq. 3, is accounted for.

[2]Elastic nominal stress-strain behavior, Eq. 5, is assumed.

[3]Damage is summed based on nominal strains.

TABLE 9

COMPLETELY REVERSED STRAIN CONTROLLED TEST
RESULTS OF 7075-T6 ALUMINUM

Total Strain Amplitude $\Delta\epsilon/2$	Total Stress Amplitude $\Delta\sigma/2$, ksi	Plastic Strain $\Delta\epsilon_p/2$	Reversals to Failure $2N_f$
0.0185	88	0.0100	131
0.0121	78	0.0045	323
0.0084	75	0.0011	1,160
0.0079	73	0.0008	1,000
0.0072	72	0.0002	2,350
0.0063	66	--	3,360
0.0057	62	--	4,660
0.0050	54	--	14,400
0.0043	45	--	51,000
0.0038	38	--	123,000
0.0032	33	--	686,000

TABLE 10

INITIALLY OVERSTRAINED TEST RESULTS
OF 7075-T6 ALUMINUM

Total Strain Amplitude $\Delta\epsilon/2$	True Stress Amplitude $\Delta\sigma/2$, ksi	Reversals to Failure $2N_f$
0.0040	41	25,800
0.0037	38	35,300
0.0031	34	63,500
0.0021	22	554,000

TABLE 11

PERIODICALLY OVERSTRAINED TEST RESULTS
OF 7075-T6 ALUMINUM

Total Strain Amplitude $\Delta\epsilon/2$	True Stress Amplitude $\Delta\sigma/2$, ksi	Reversals to Failure $2N_f$
0.0032	32	119,000
0.0029	29	447,000

TABLE 12

MONOTONIC TENSION PROPERTIES OF BAR AND SHEET STEELS

	Sheet Steel	Bar Steel
Modulus of Elasticity, ksi	27,000	30,000
Upper Yield Strength, ksi	--	50
Lower Yield Strength, ksi	--	42
0.2% Offset Yield Strength, ksi	37	42
Ultimate Strength, ksi	57	66
True Fracture Strength, ksi[1]	113/96	128/111
Strength Coefficient, ksi[2]	58/97	49/120
Percent Reduction in Area, %	64	59
True Fracture Ductility	1.02	0.90
Strain Hardening Exponent[2]	0.072/0.198	0.024/0.228

[1]The first value is the final load at fracture divided by the final cross-sectional area at fracture. The second value is corrected for triaxial stress due to necking as proposed by Bridgman (66,67).

[2]The first value represents the initial portion of the stress-strain curve (approximately up to 0.02 strain). The second value represents the remainder to the curve.

TABLE 13

COMPLETELY REVERSED STRAIN CONTROLLED
TEST RESULTS OF THE SHEET STEEL

Total Strain Amplitude $\Delta\epsilon/2$	Total Stress Amplitude $\Delta\sigma/2$, ksi	Plastic Strain $\Delta\epsilon_p/2$	Reversals to Failure $2N_f$
0.0079	46	0.0063	3,480
0.0054	42	0.0039	6,690
0.0026	30	0.0016	49,400
0.0020	28	0.0011	126,000
0.0016	25	0.0008	194,000
0.0013	22	0.0006	484,000
0.0011	20	0.0004	3,840,000
0.0008	20	0.00014	4,480,000

TABLE 14

STABLE CYCLIC STRESS-STRAIN PROPERTIES

	Sheet Steel	Bar Steel
Cyclic Strength Coefficient, ksi[1]	202/109/70	209/134/88
Cyclic Strain Hardening Exponent[1]	0.288/0.167/0.105	0.283/0.204/0.135

[1]The values represent those obtained by companion specimen, incremental strain step, and precycled monotonic tension test results, respectively.

TABLE 15

INITIALLY OVERSTRAINED TEST RESULTS
OF THE SHEET STEEL

Total Strain Amplitude $\Delta\epsilon/2$	True Stress Amplitude $\Delta\sigma/2$, ksi	Plastic Strain $\Delta\epsilon_p/2$	Reversals to Failure $2N_f$
0.0011	20	0.0004	634,000
0.0008	19	0.00018	6,330,000

TABLE 16

PERIODICALLY OVERSTRAINED TEST RESULTS
OF THE SHEET STEEL

Total Strain Amplitude $\Delta\epsilon/2$	True Stress Amplitude $\Delta\sigma/2$, ksi	Plastic Strain $\Delta\epsilon_p/2$	Reversals to Failure $2N_f$
0.0011	19	0.0004	464,000
0.0008	20	0.00013	1,070,000
0.0008	21	0.00011	1,470,000

TABLE 17

FATIGUE PROPERTIES

	Sheet Steel	Bar Steel
Fatigue Strength Coefficient, ksi[1]	119/130/153	128/134/140
Fatigue Ductility Coefficient[1]	0.207/0.270/1.31	0.160/0.240/0.242
Fatigue Strength Exponent[1]	-0.121/-0.130/-0.147	-0.118/-0.125/-0.131
Fatigue Ductility Exponent[1]	-0.447/-0.478/-0.637	-0.412/-0.462/-0.465

[1]The values represent those obtained from non-overstrained, initial cyclic overstrain, and periodic cyclic overstrain data, respectively.

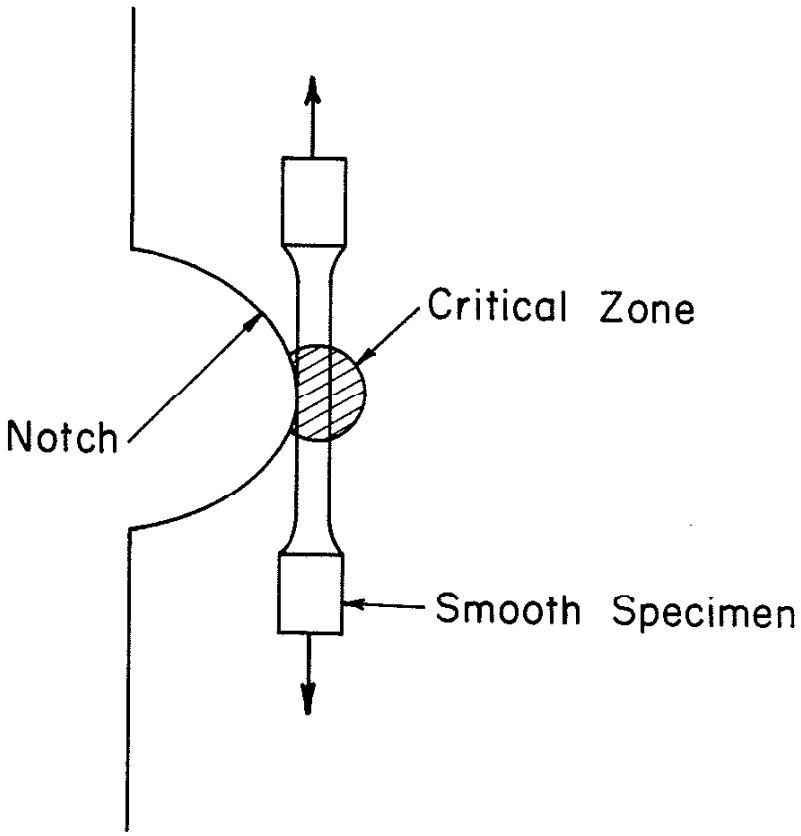

Fig. 1 Smooth Specimen Representation of Material at the Critical Zone

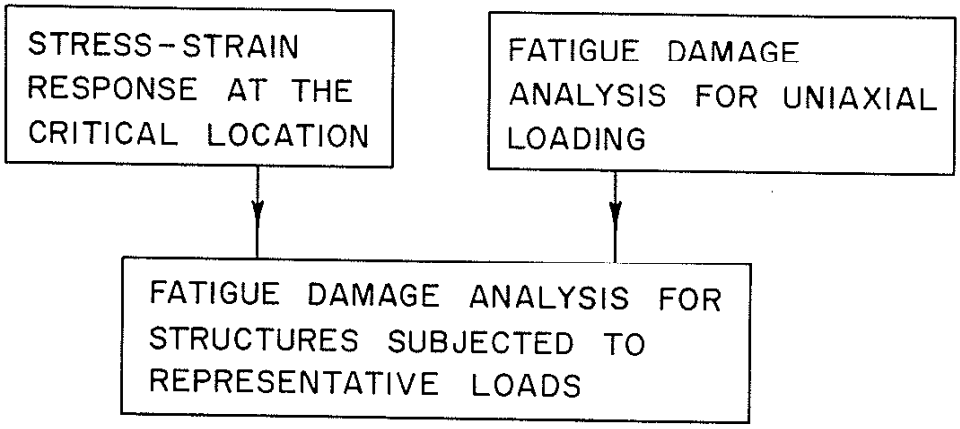

Fig. 2 Schematic of Fatigue Damage Analysis

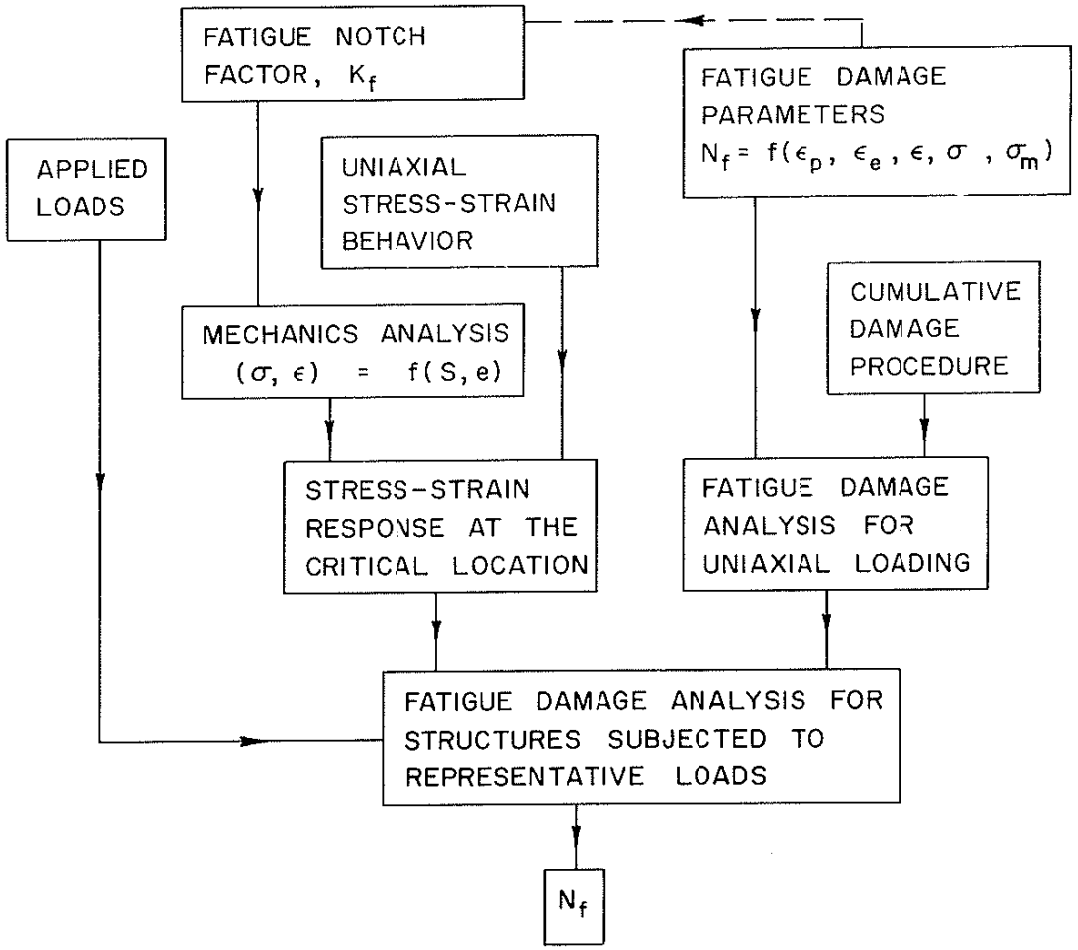

Fig. 3 Necessary Inputs for Fatigue Damage Analysis

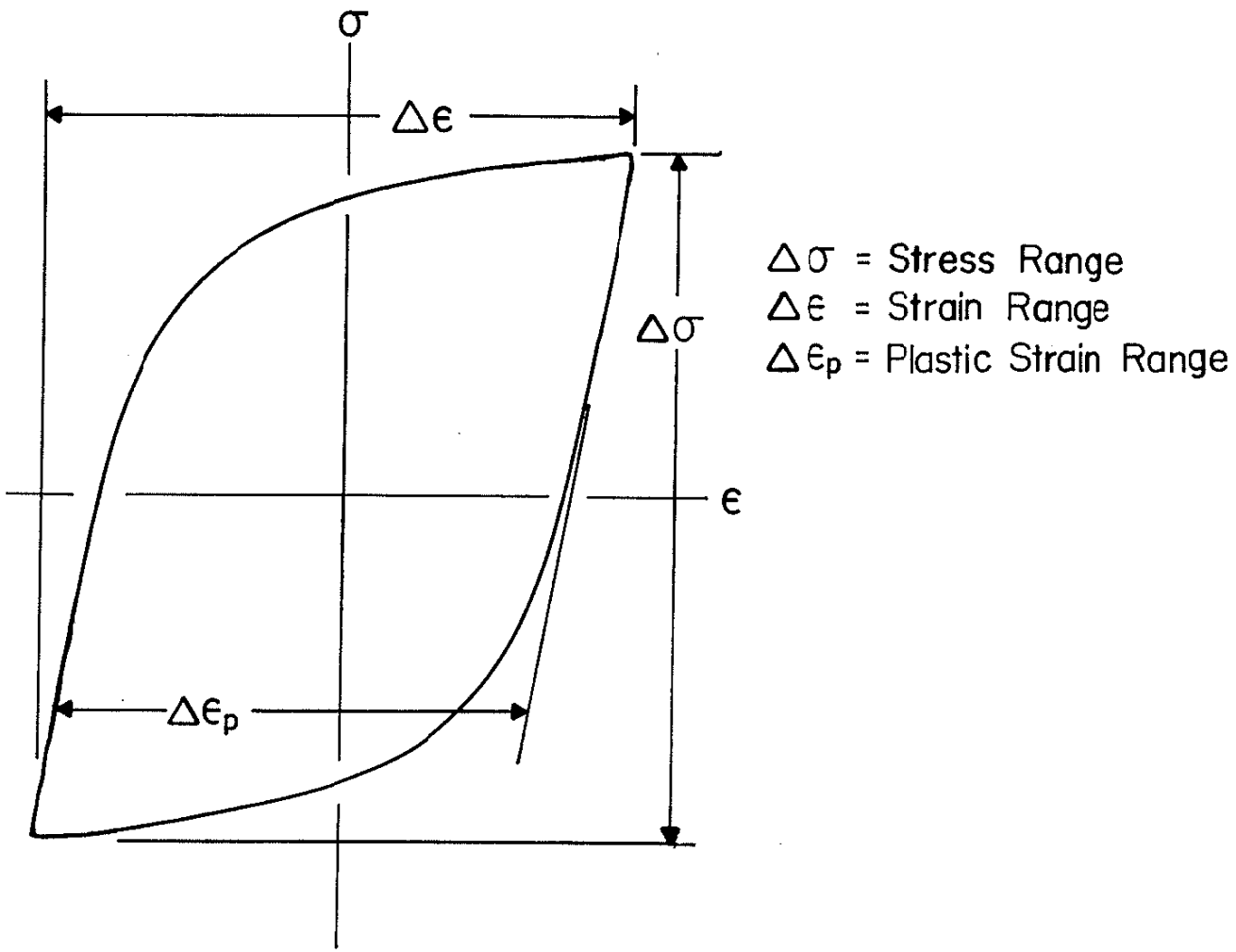

Fig. 4 Stress and Strain Ranges from a Hysteresis Loop

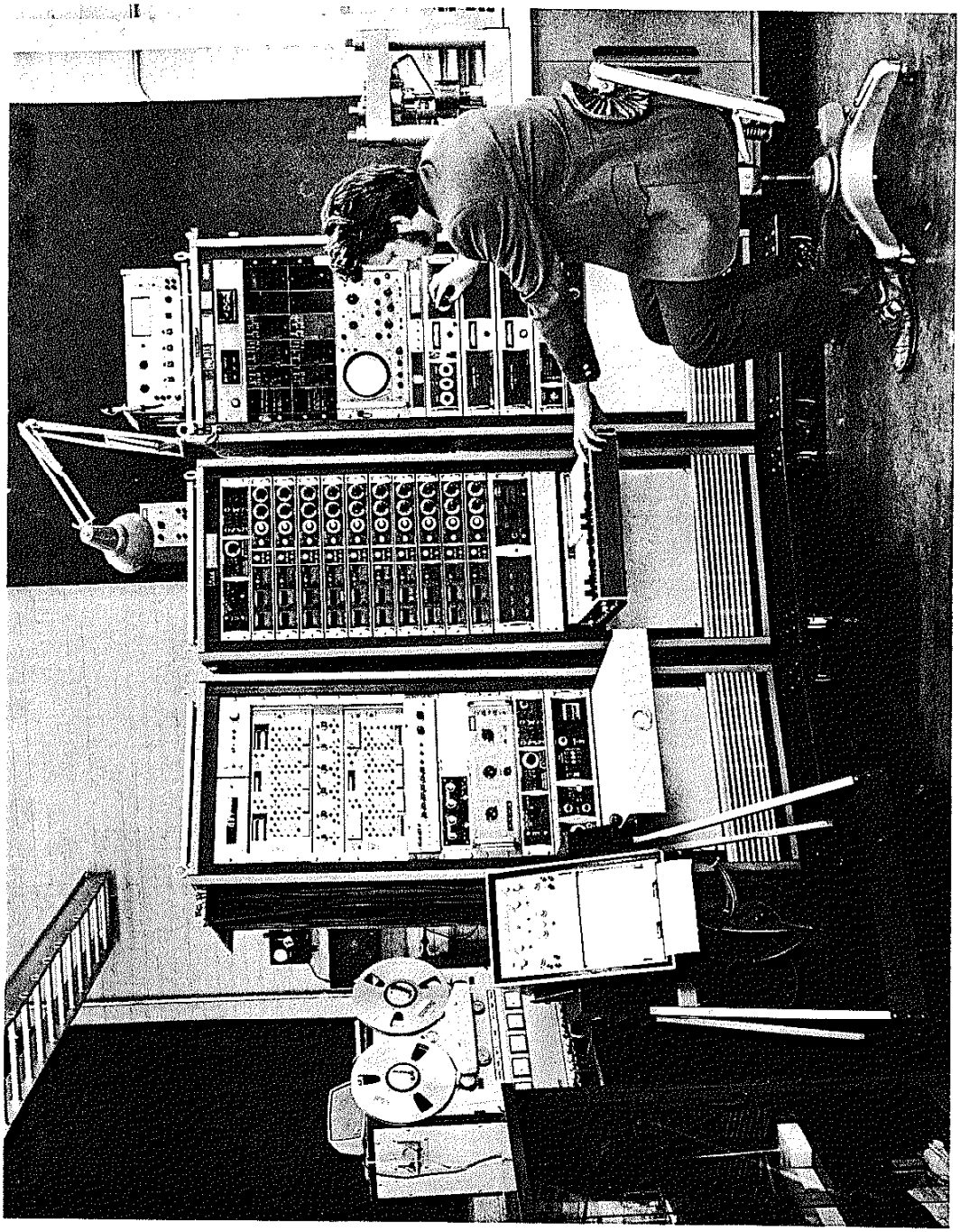

Fig. 5 Mechanical Test System

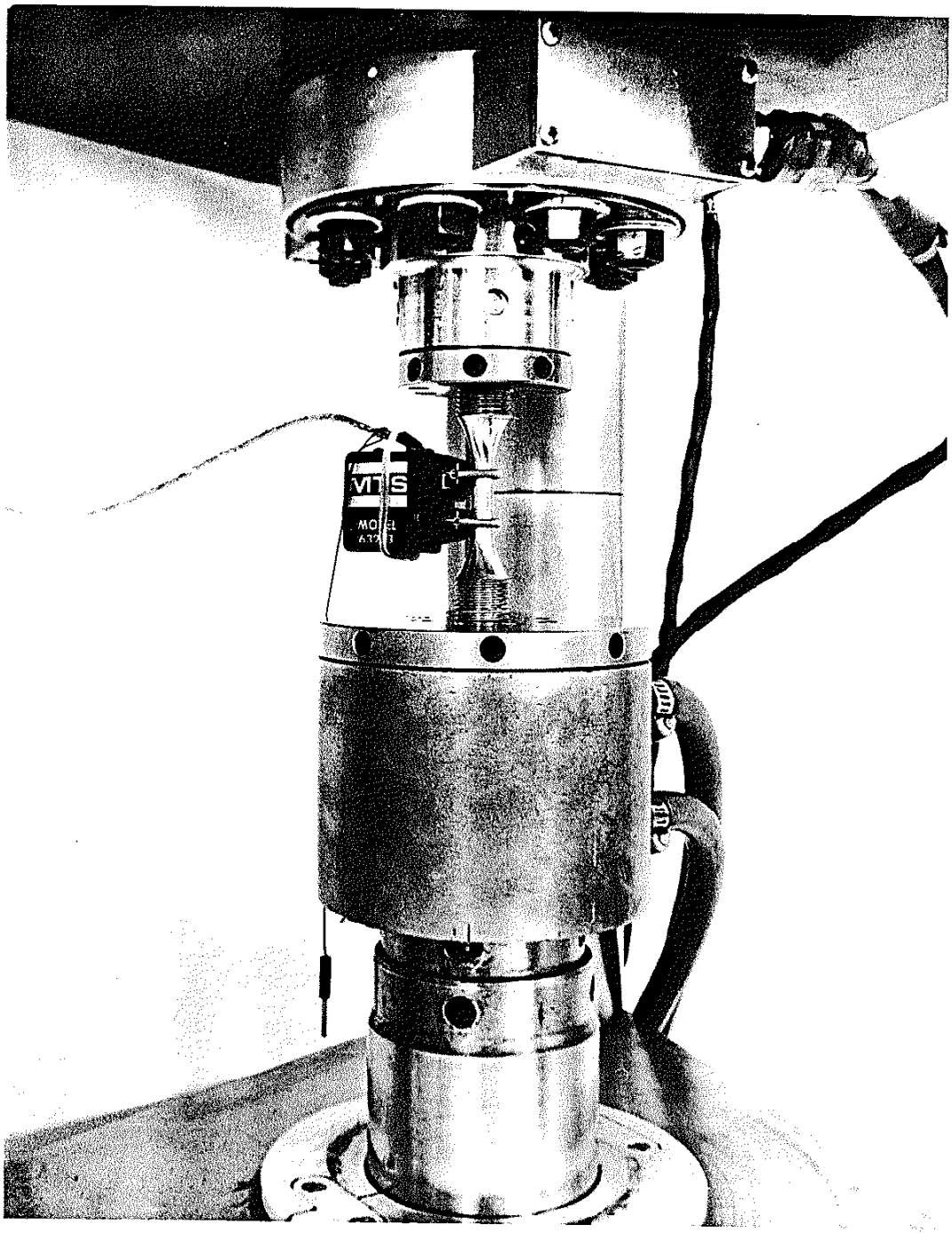

Fig. 6 Bar Steel Specimen Mounted in Load Frame

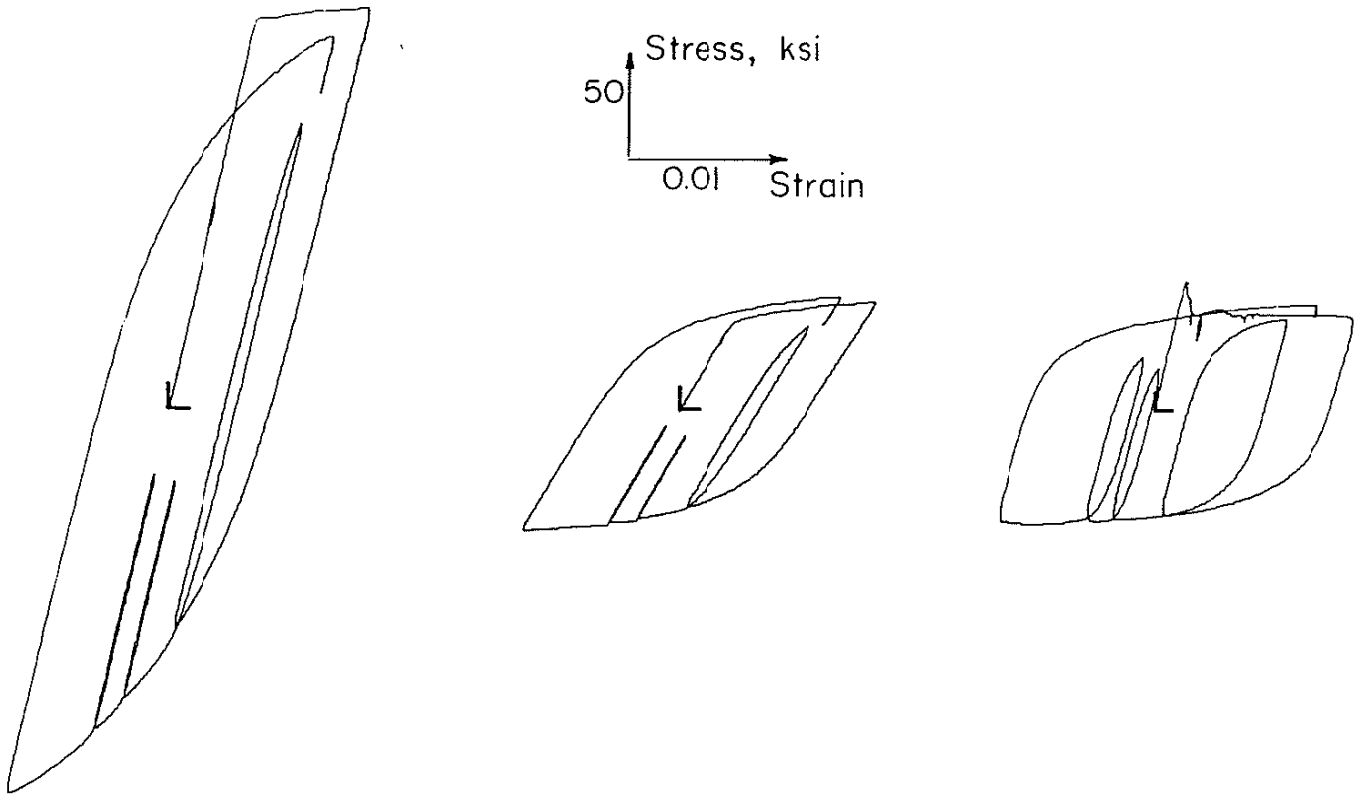

(a) 4340 Steel (b) 2024-T4 Aluminum (c) Structural Bar Steel

Fig. 7 Initial Stress-Strain Response of Three Metals Subjected to the Same Sequence of Strain Limits

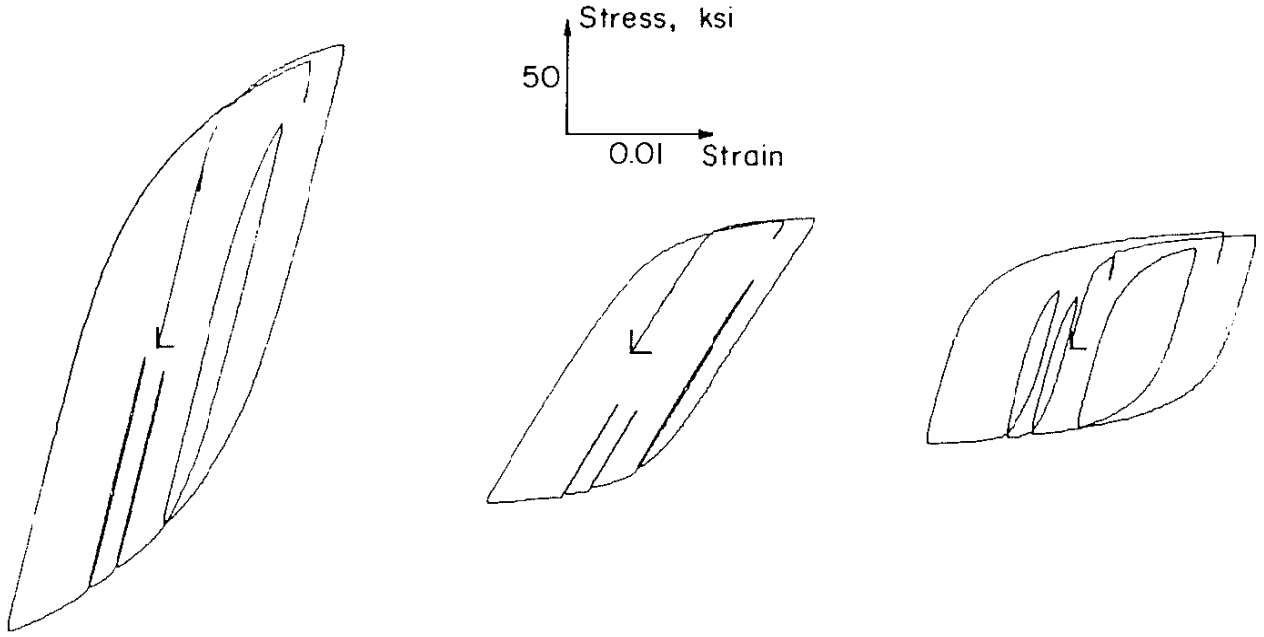

(a) 4340 Steel (b) 2024-T4 Aluminum (c) Structural Bar Steel

Fig. 8 Stress-Strain Response of Three Metals Subjected to the Same Sequence of Strain Limits after Initial Precycling

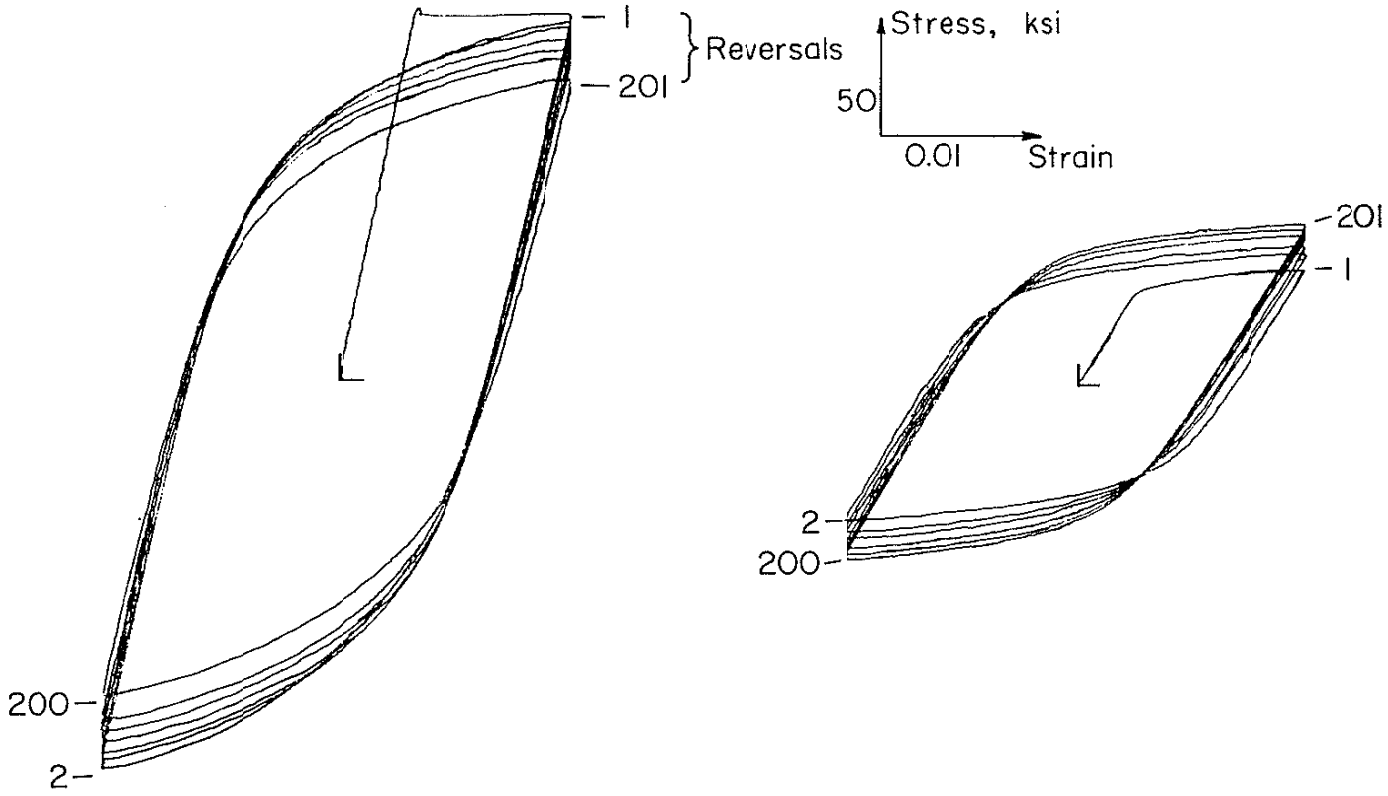

(a) 4340 Steel (Cyclic Softening) (b) 2024-T4 Aluminum (Cyclic Hardening)

Fig. 9 Transient Stress-Strain Behavior of Two Metals Subjected to Constant Strain Limits (Cycles 1, 2, 5, 10, 20, and 100 are Plotted)

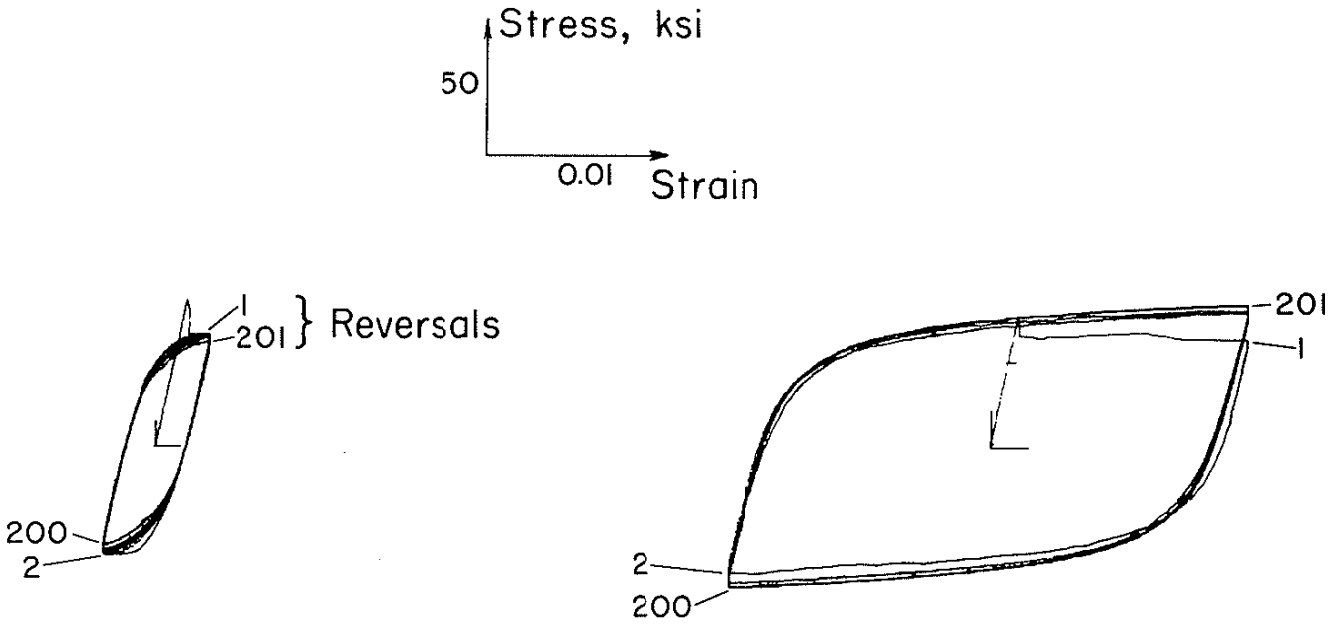

(a) Cyclic Softening (b) Cyclic Hardening

Fig. 10 Transient Stress-Strain Behavior of Bar Steel (Cycles 1, 2, 5, 10, 20, and 100 Are Plotted)

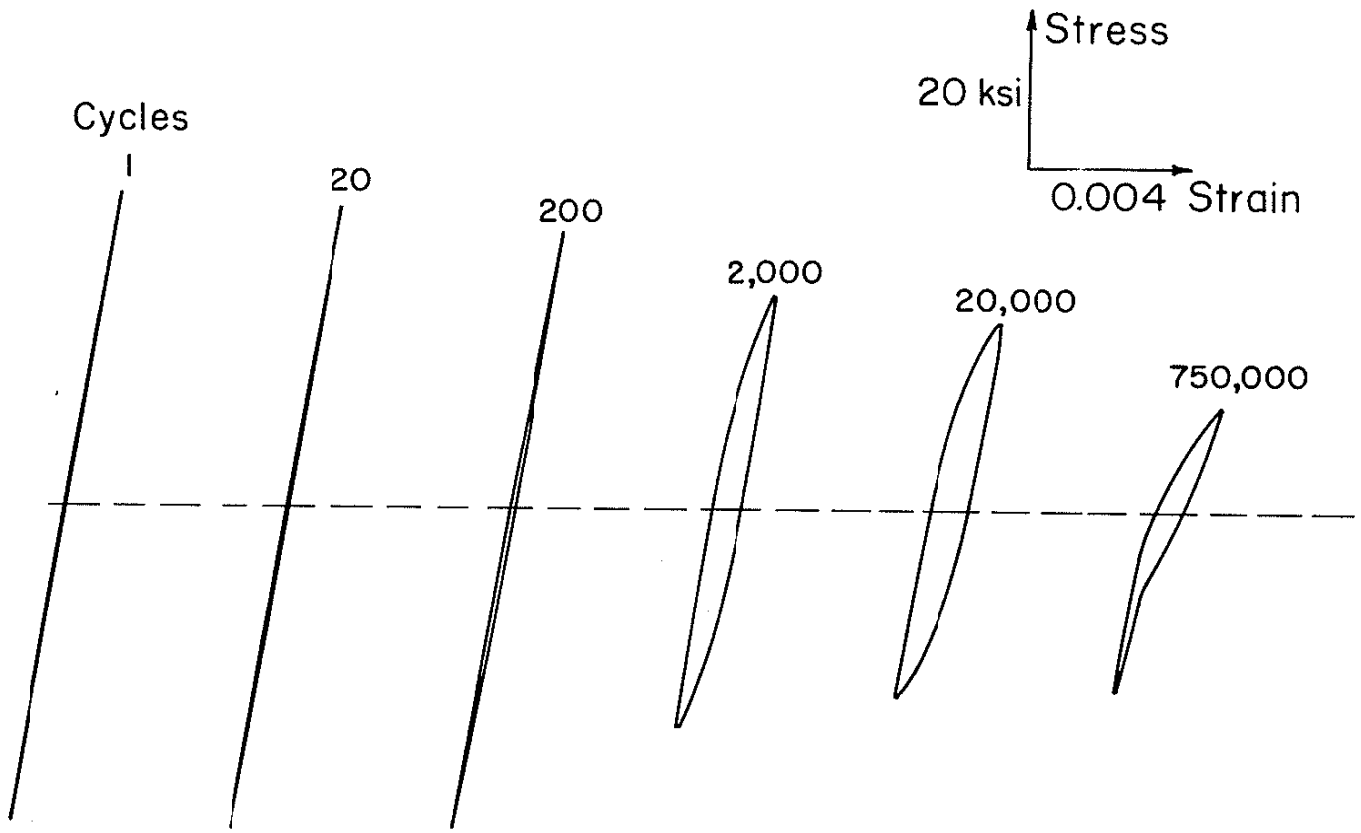

Fig. 11 Example of Cyclic Softening of the Bar Steel during a Constant Strain of $\Delta\epsilon/2 = \pm 0.0013$

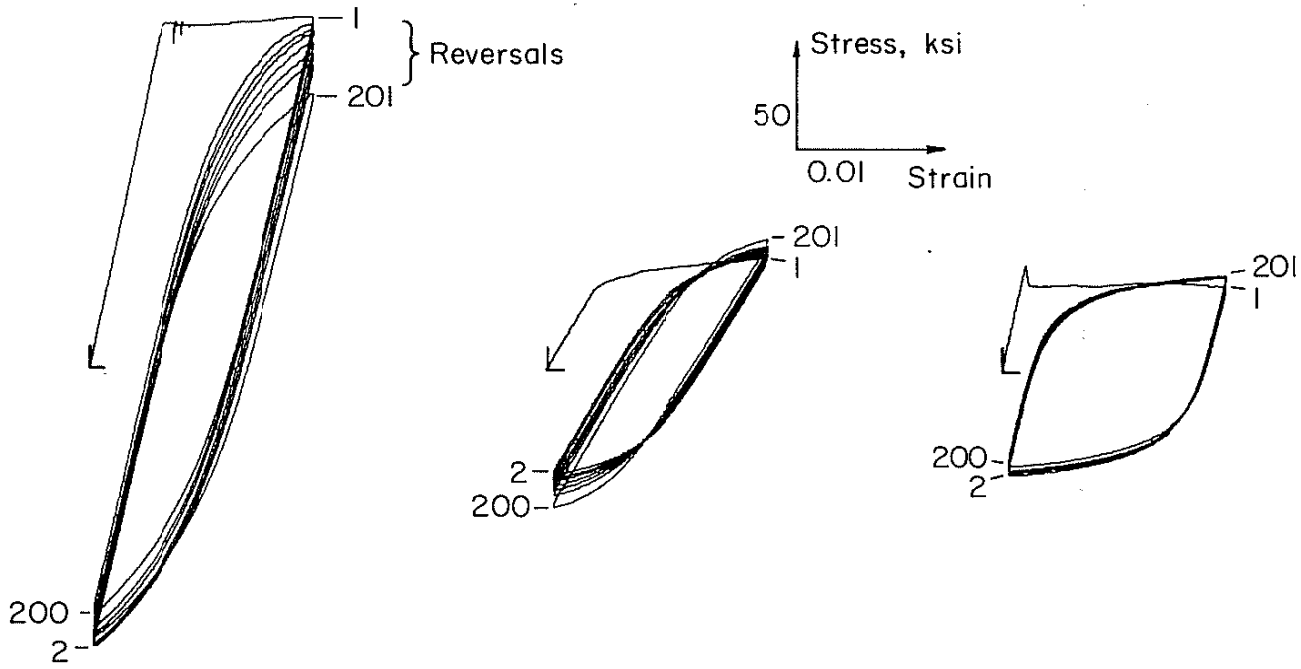

Fig. 12 Stress-Strain Response of Three Metals Subjected to the Same 0-Max. Strain Limits (Cycles 1, 2, 5, 10, 20, and 100 are Plotted)

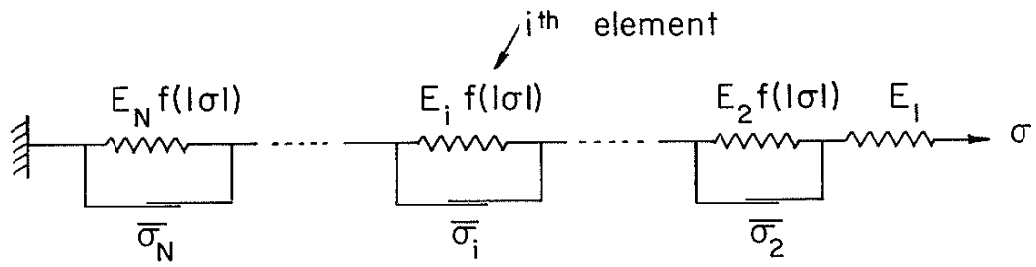

(a) Schematic of Mechanical Model

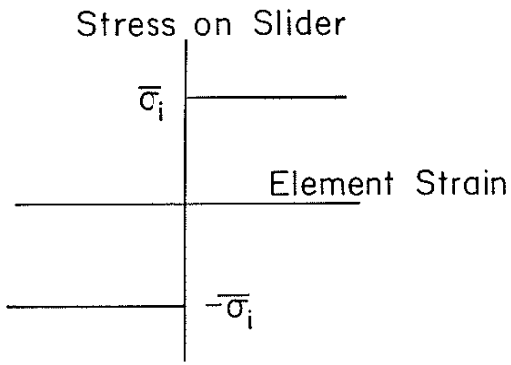

(b) Yield Stress Response of Frictional Slider

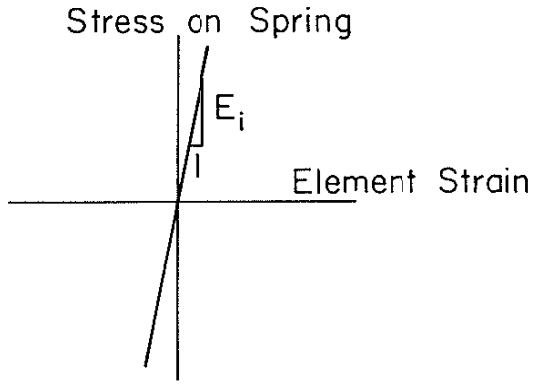

(c) Response of Spring without Relaxing Function

Fig. 13 Mechanical Model of Stress–Strain Behavior

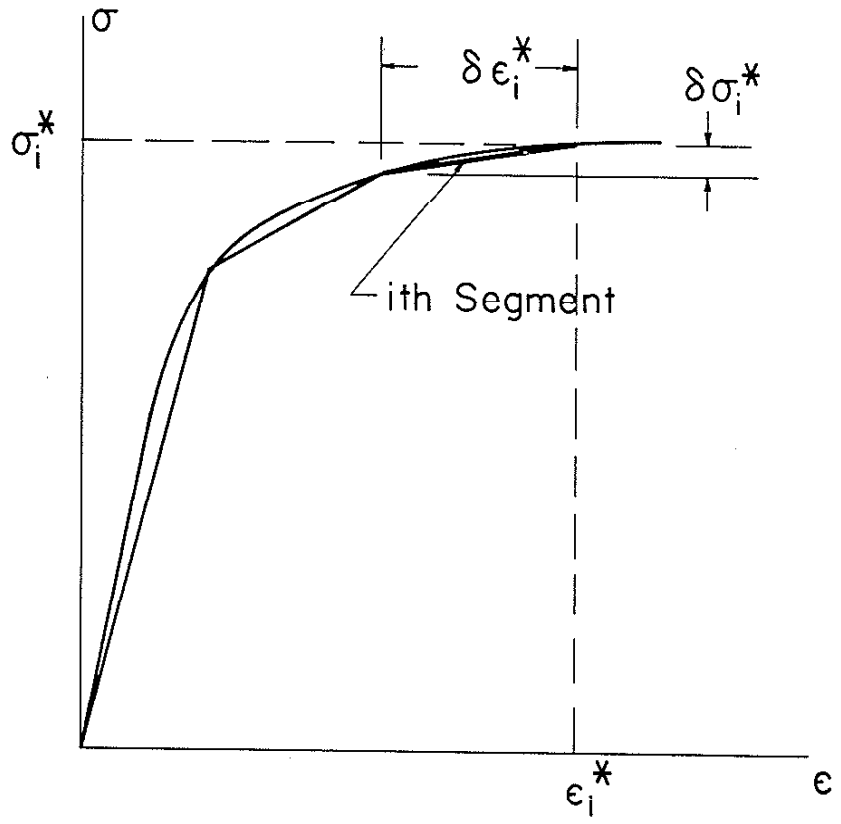

Fig. 14 Mechanical Model Approximation of Stress–Strain Curve

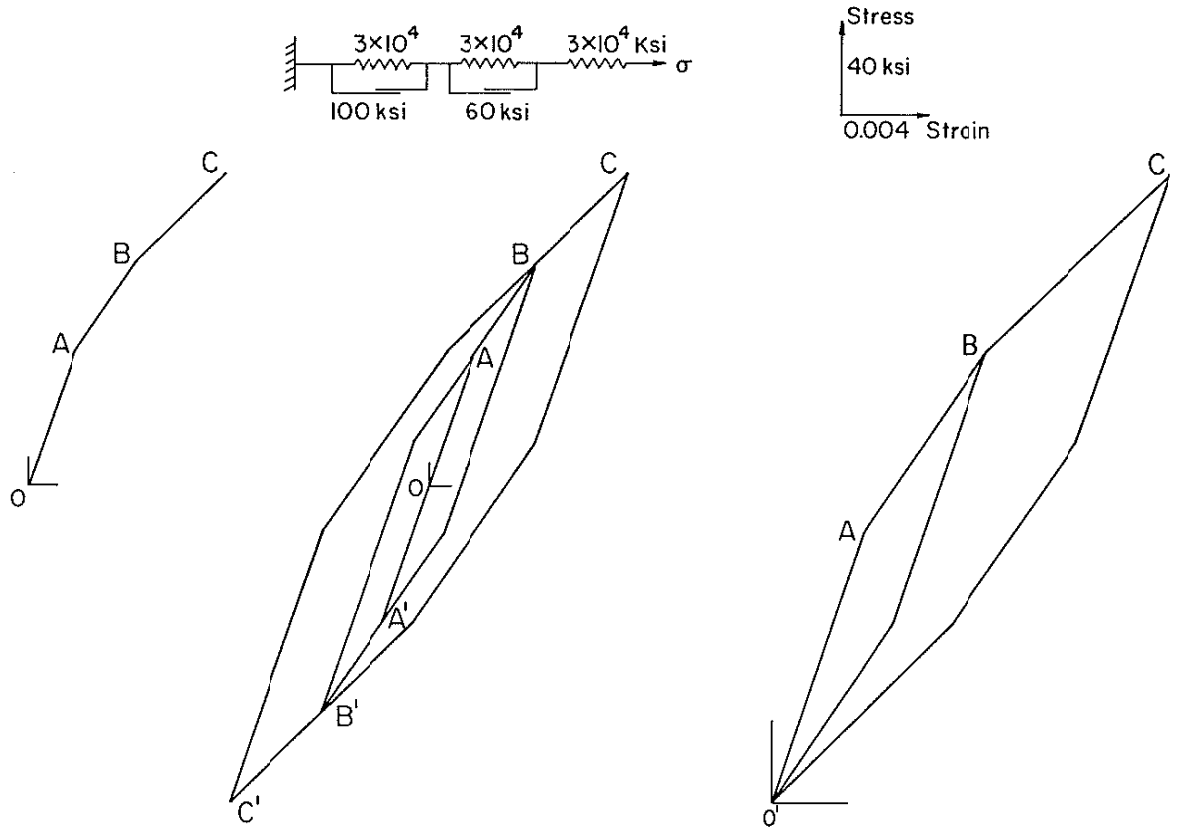

(a) Initial Curve (b) Completely Reversed Curves (c) Completely Reversed Curves with Origin Shifted

Fig. 15 Simulation of Stress–Strain Behavior by Three Element Model

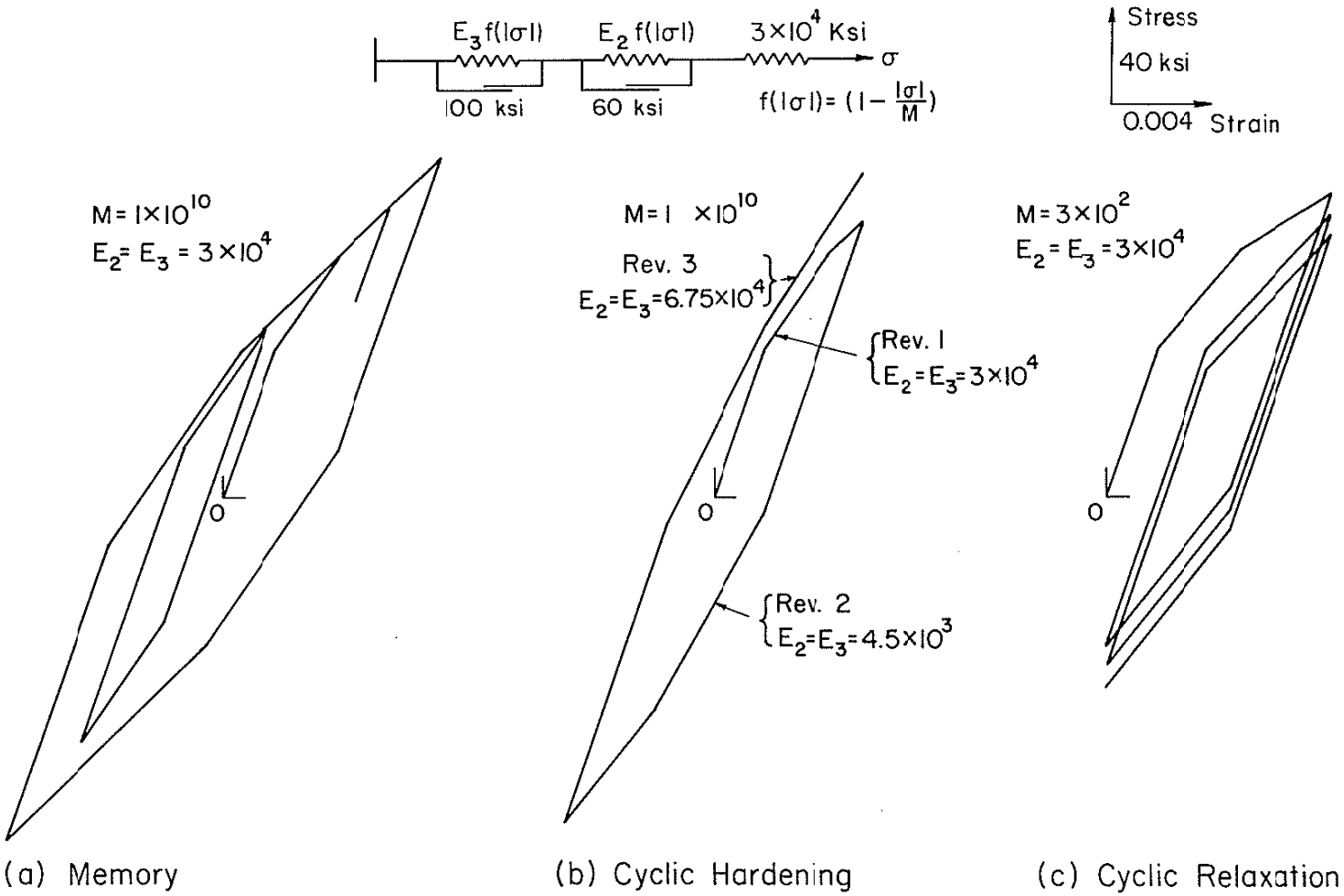

(a) Memory (b) Cyclic Hardening (c) Cyclic Relaxation

Fig. 16 Simulation of Memory, Cyclic Hardening, and Cyclic Relaxation of Mean Stress by Three Element Model

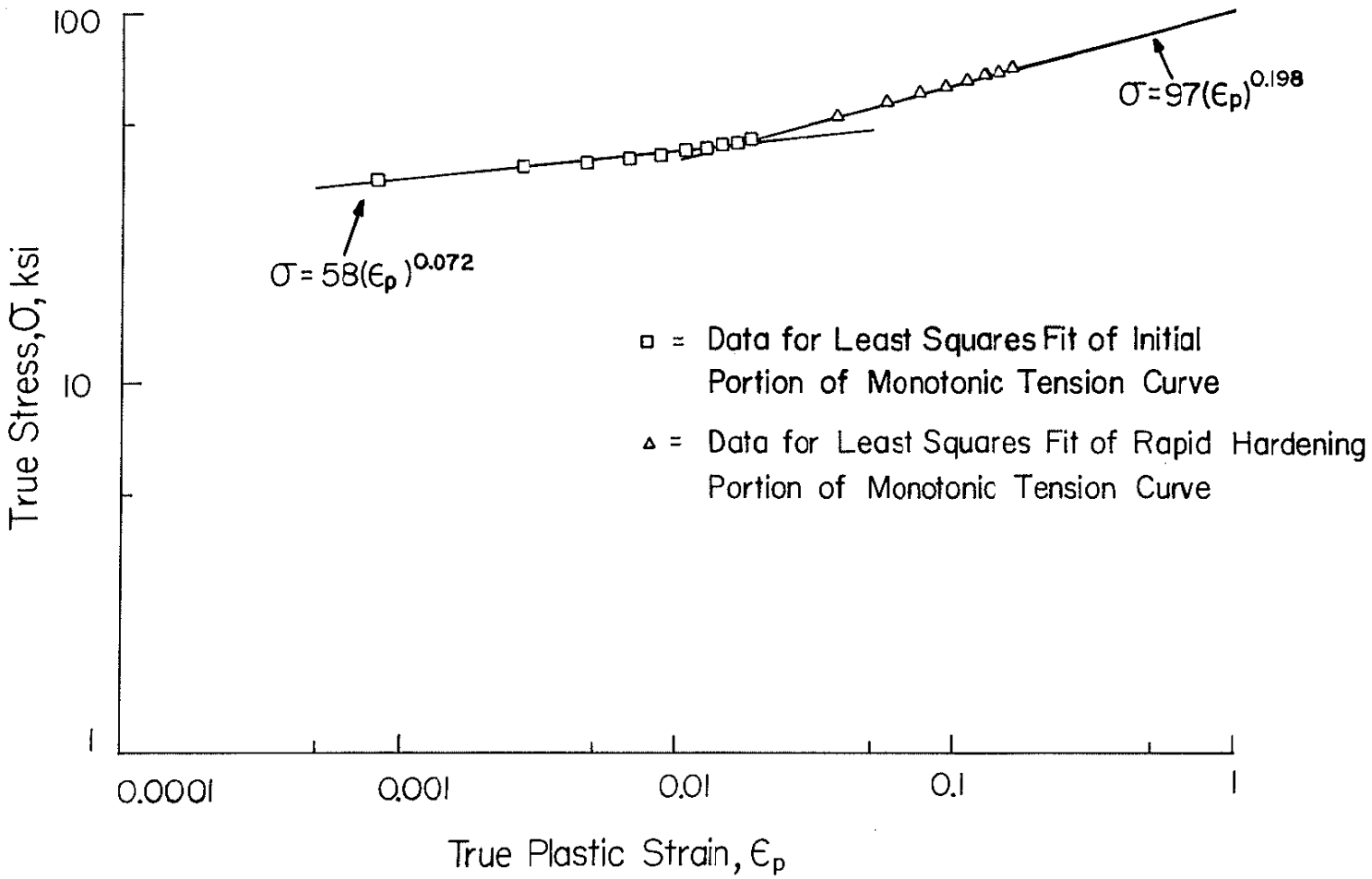

Fig. 17 Stress-Plastic Strain Data for Monotonic Tension of Sheet Steel Specimen

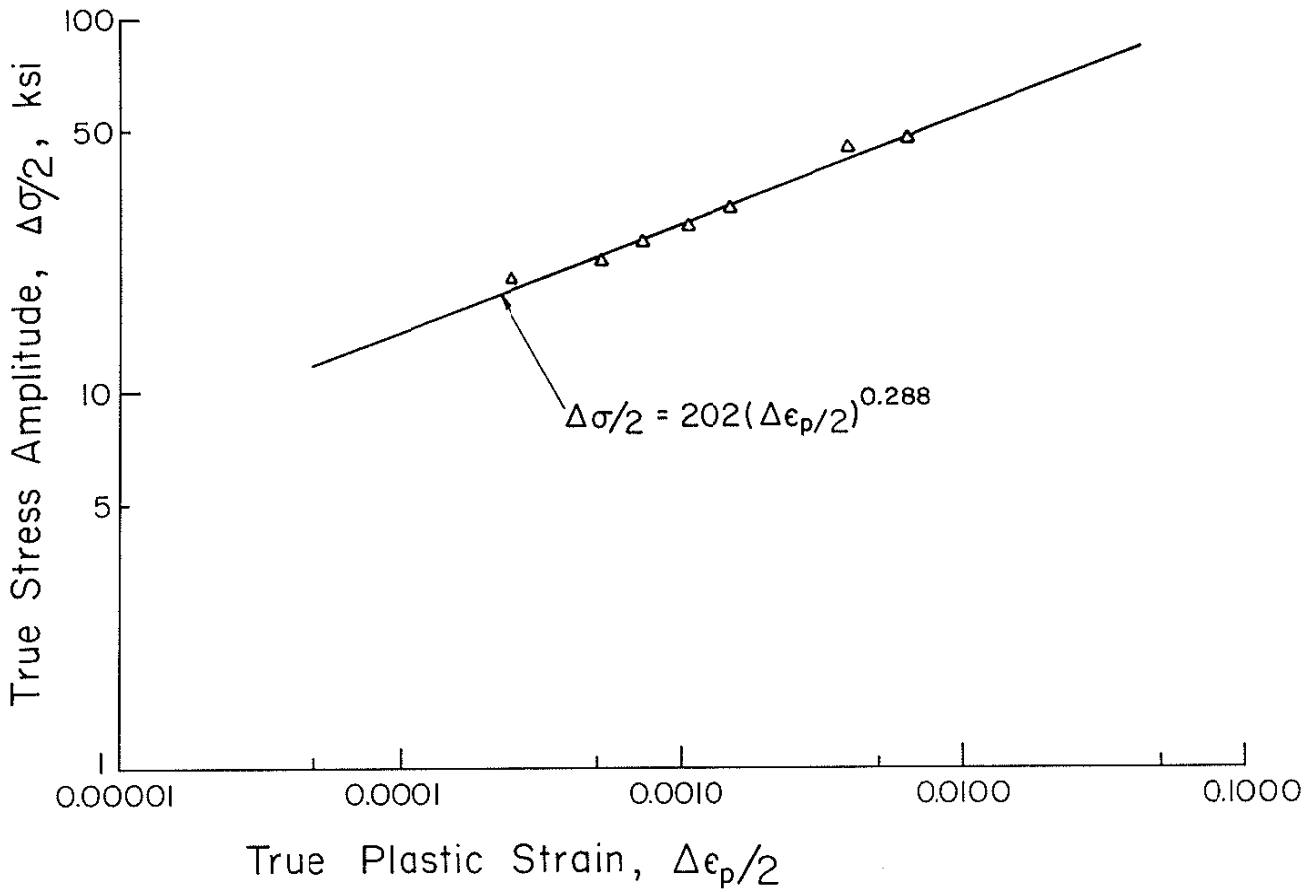

Fig. 18 Stress-Plastic Strain Data from Companion Specimens of the Sheet Steel

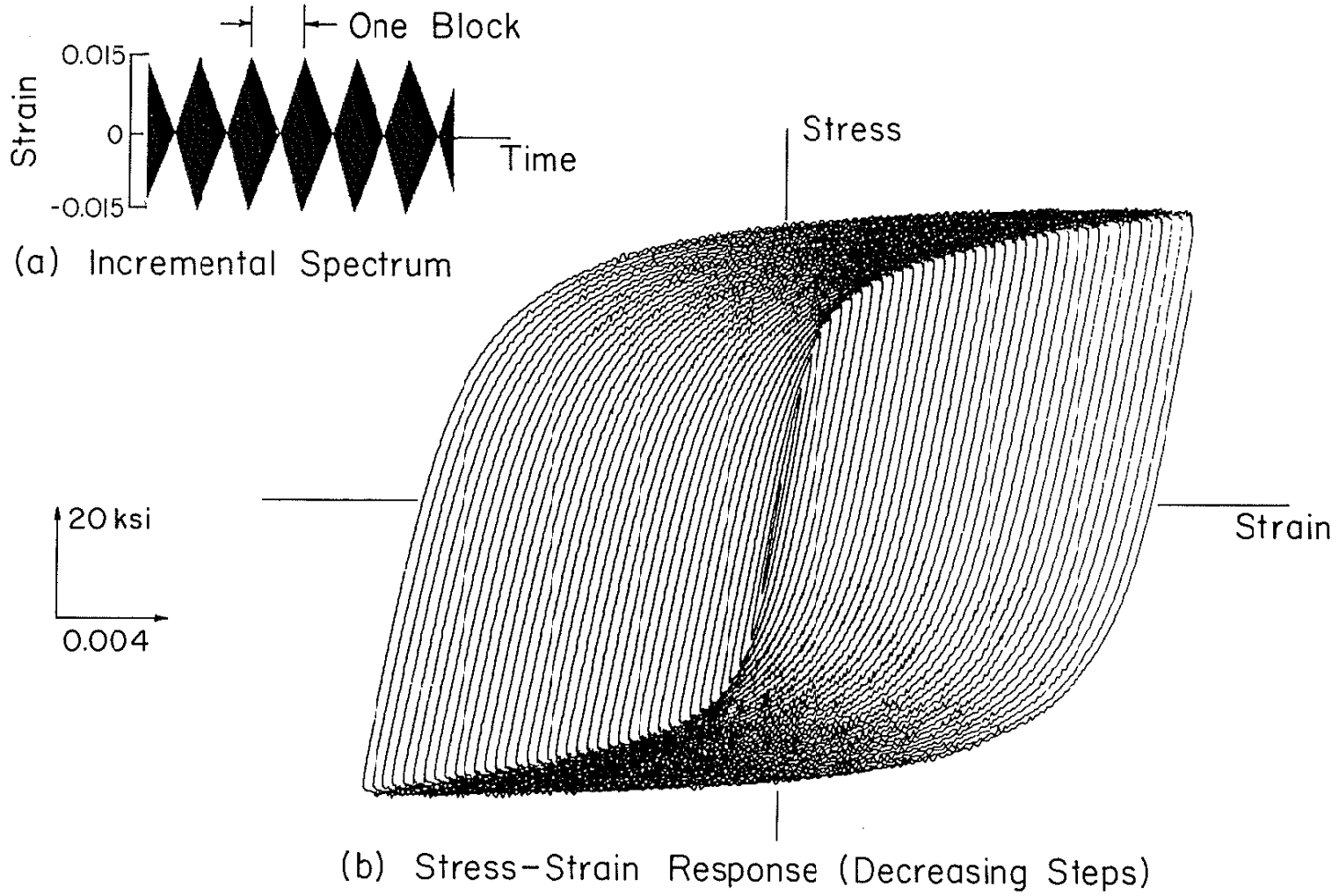

Fig. 19 Incremental Step Straining of Sheet Steel

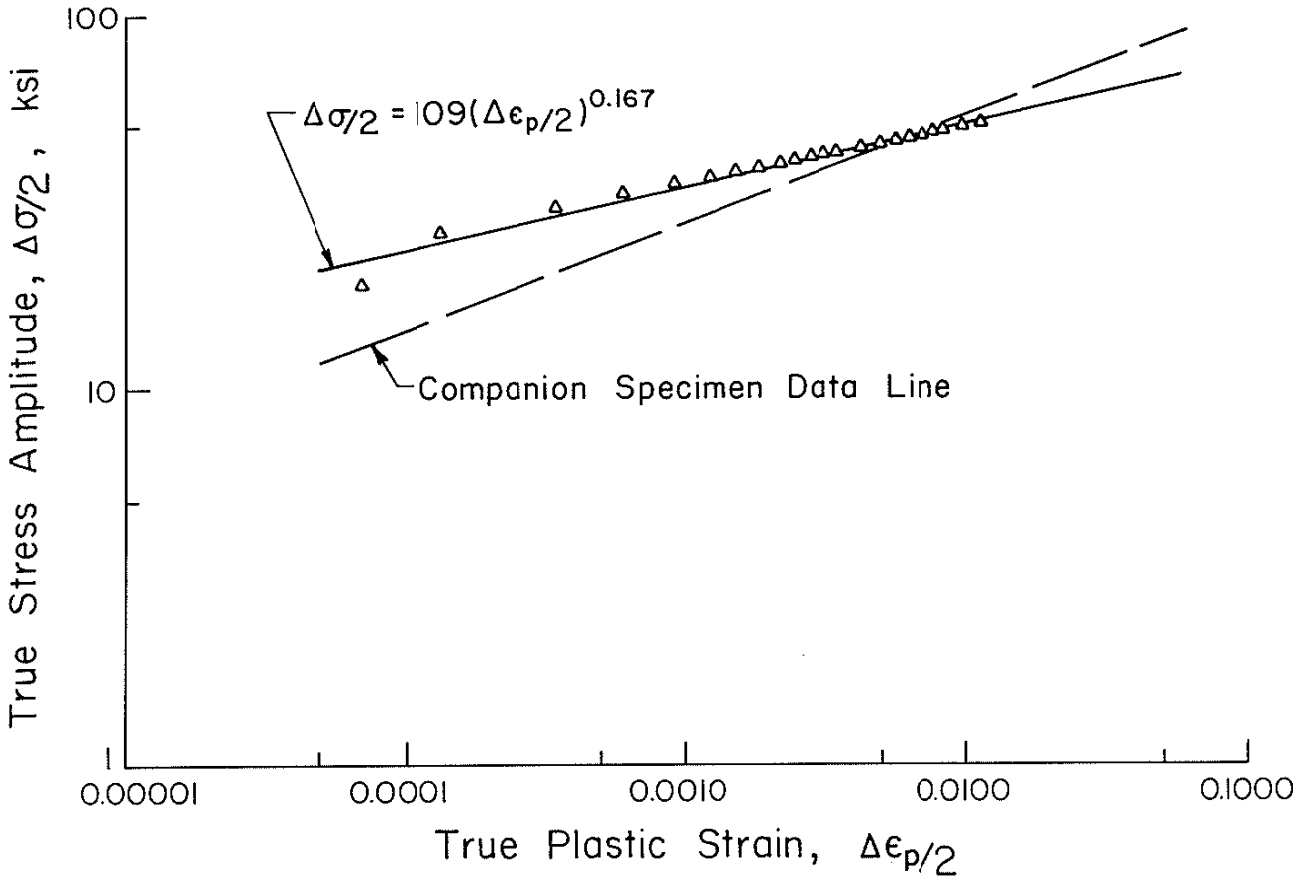

Fig. 20 Stress-Plastic Strain Data from Incremental Step Strain Test Results of the Sheet Steel

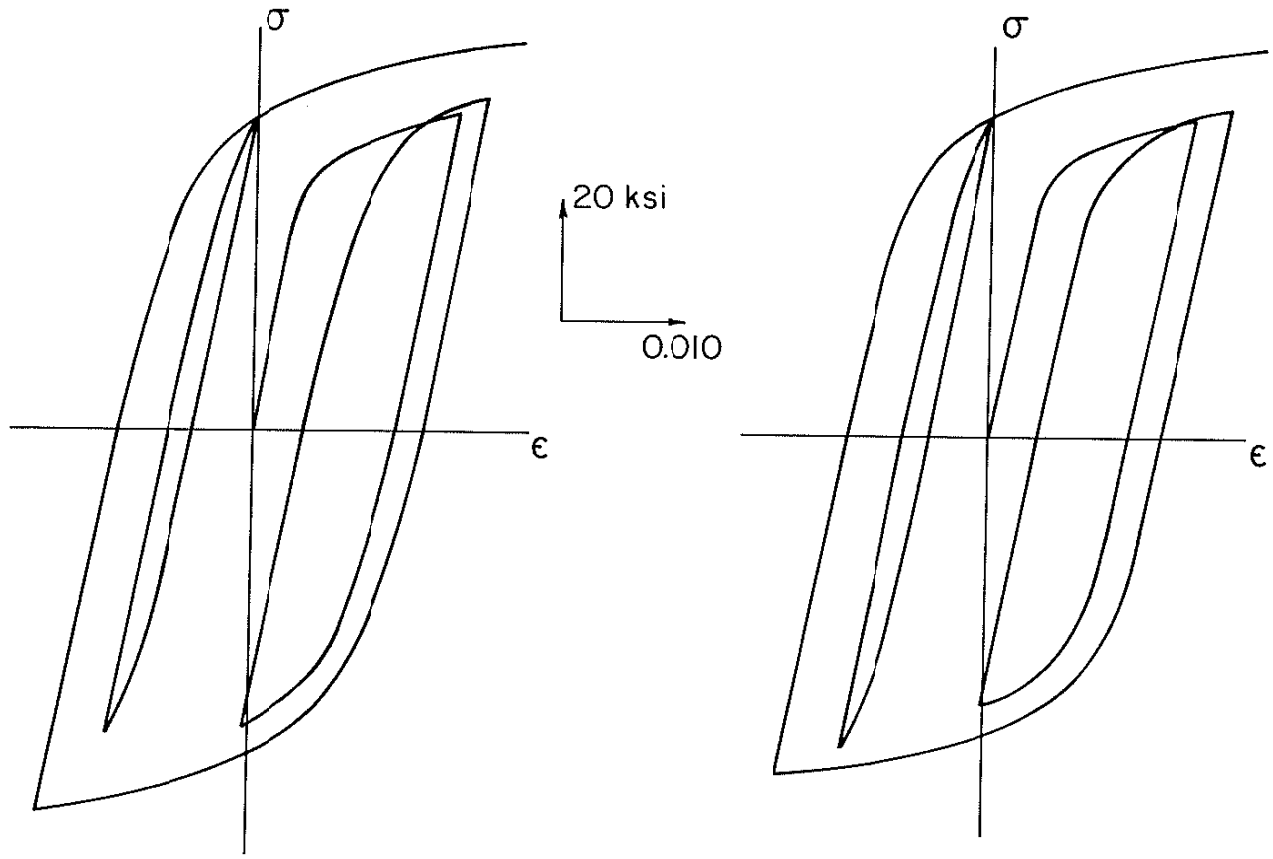

(a) Test Results

(b) Simulation

Fig. 21 Actual and Simulated Stress-Strain Response of 2024-T4 Aluminum

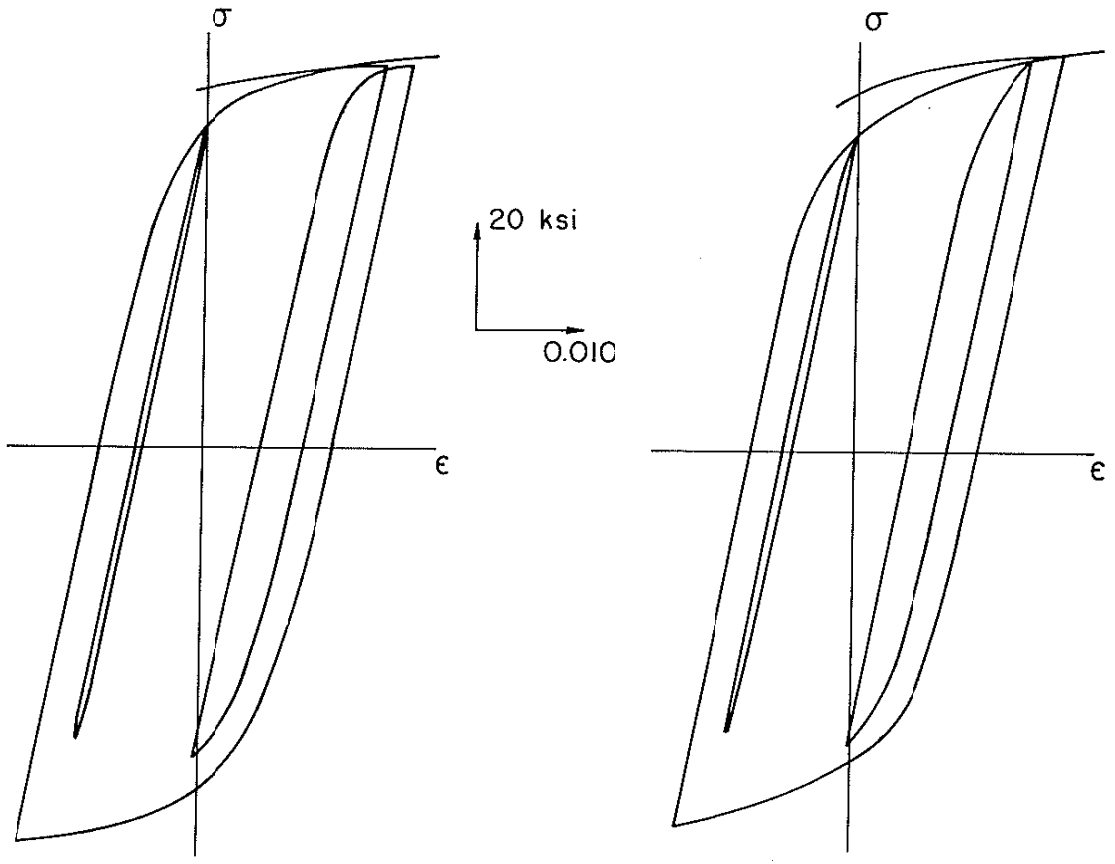

(a) Test Results

(b) Simulation

Fig. 22 Actual and Simulated Stable Stress-Strain Response of 2024-T4 Aluminum

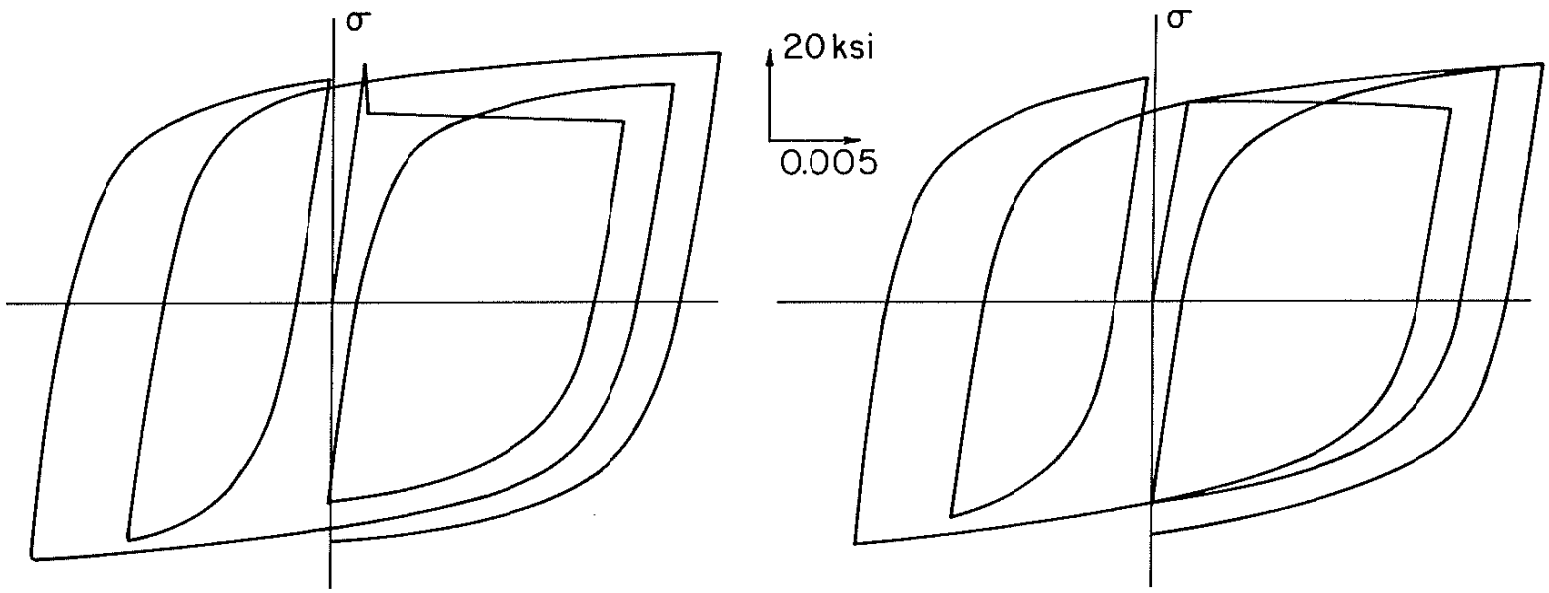

(a) Test Results (b) Simulation

Fig. 23 Actual and Simulated Stress–Strain Response of A36 Steel (Ref. 38)

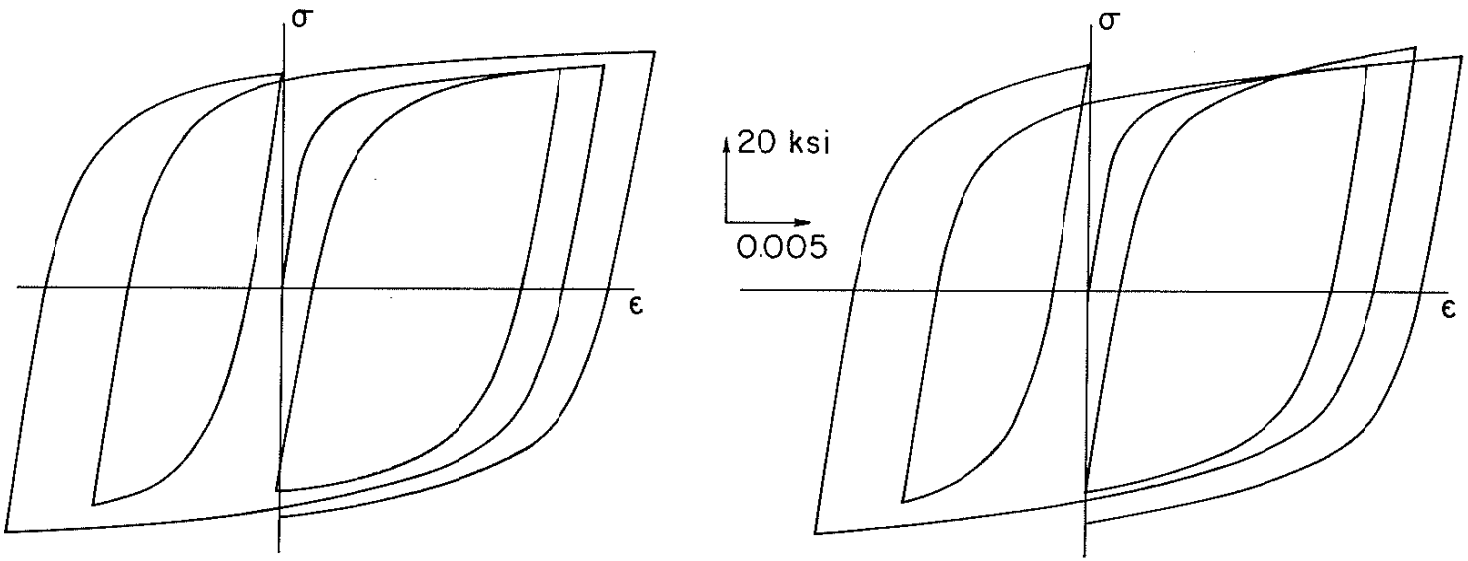

(a) Test Results (b) Simulation

Fig. 24 Actual and Simulated Stable Stress-Strain Response of A36 Steel (Ref. 38)

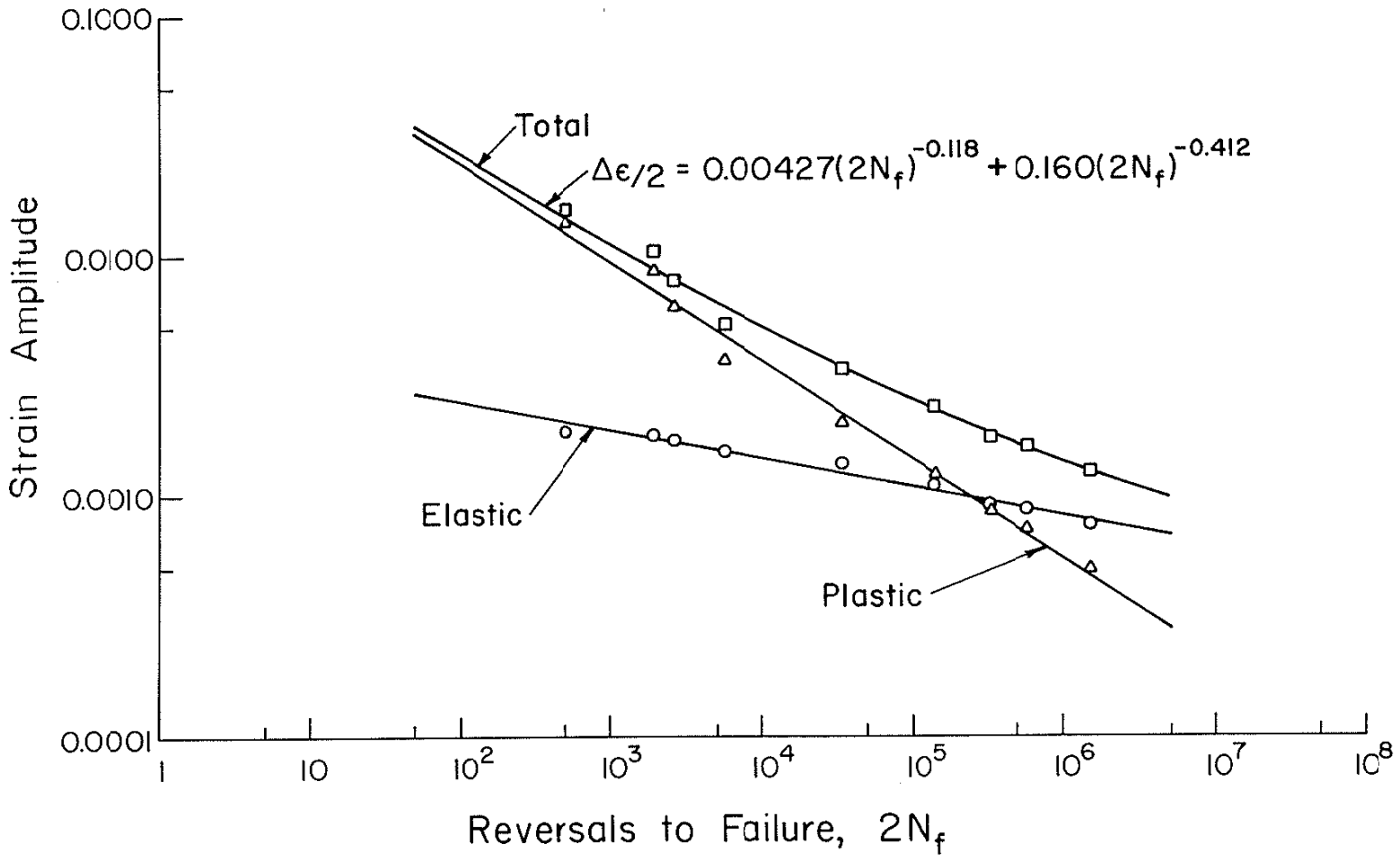

Fig. 25 Strain-Reversals to Failure Data for Bar Steel

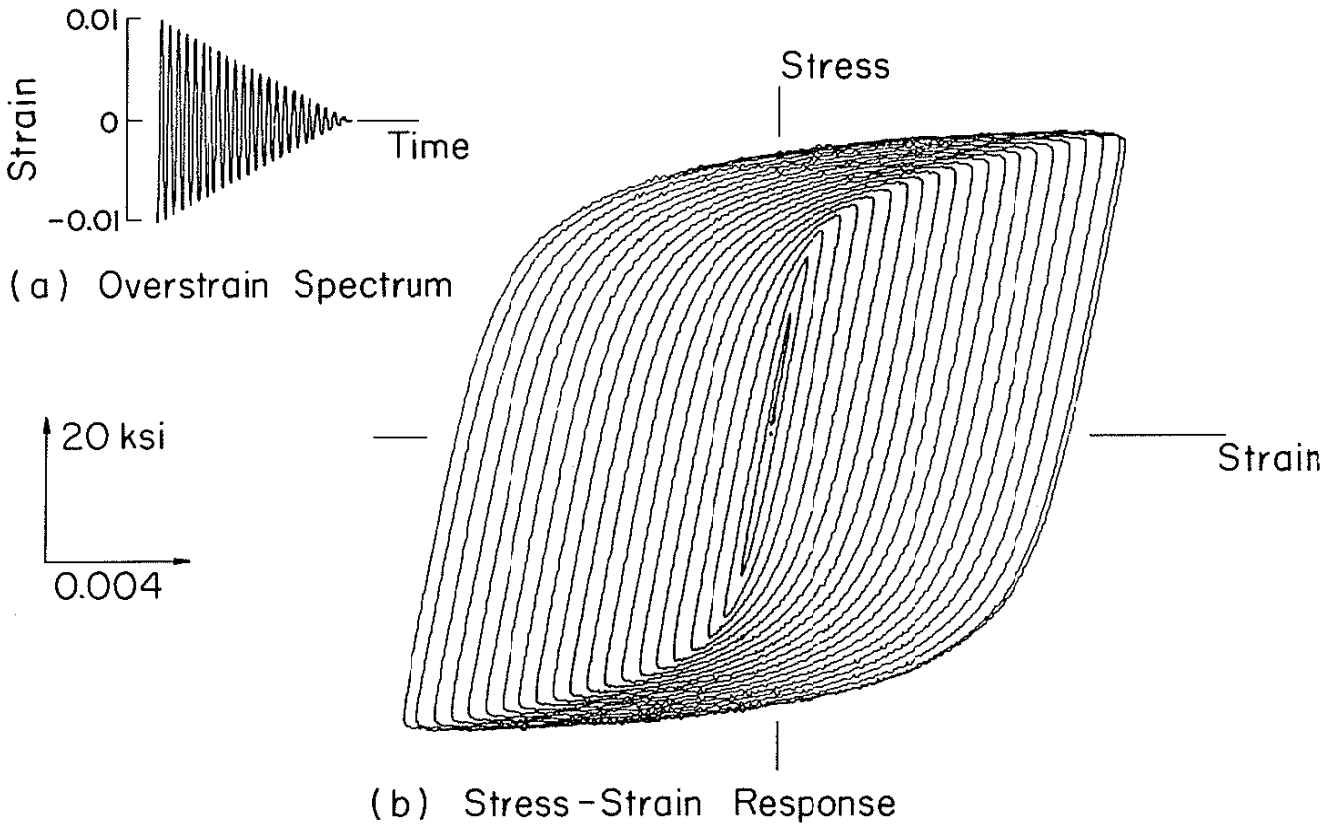

Fig. 26 Overstrain of Sheet Steel

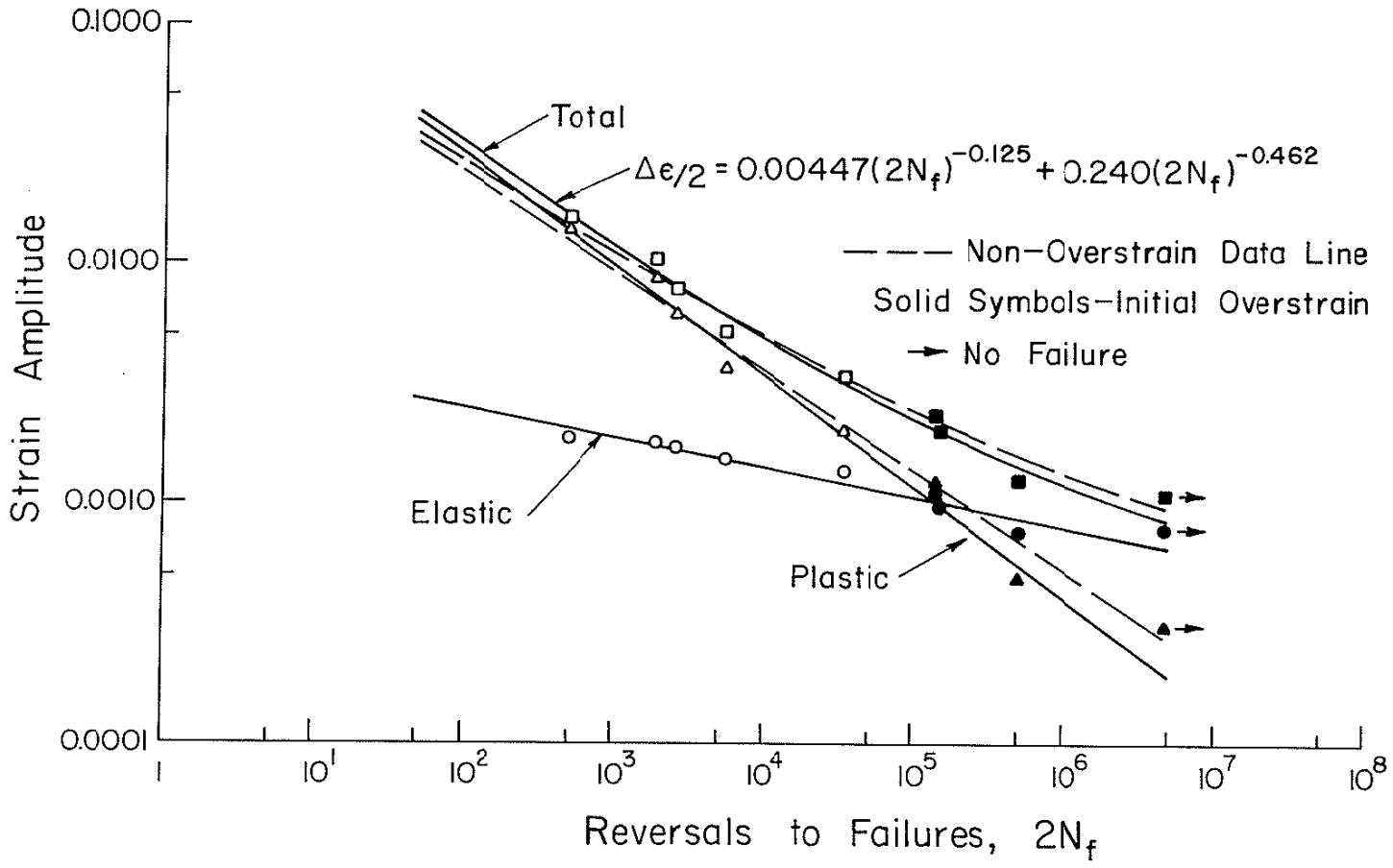

Fig. 27 Strain-Reversals to Failure Data for Bar Steel Subjected to Initial Cyclic Overstrains

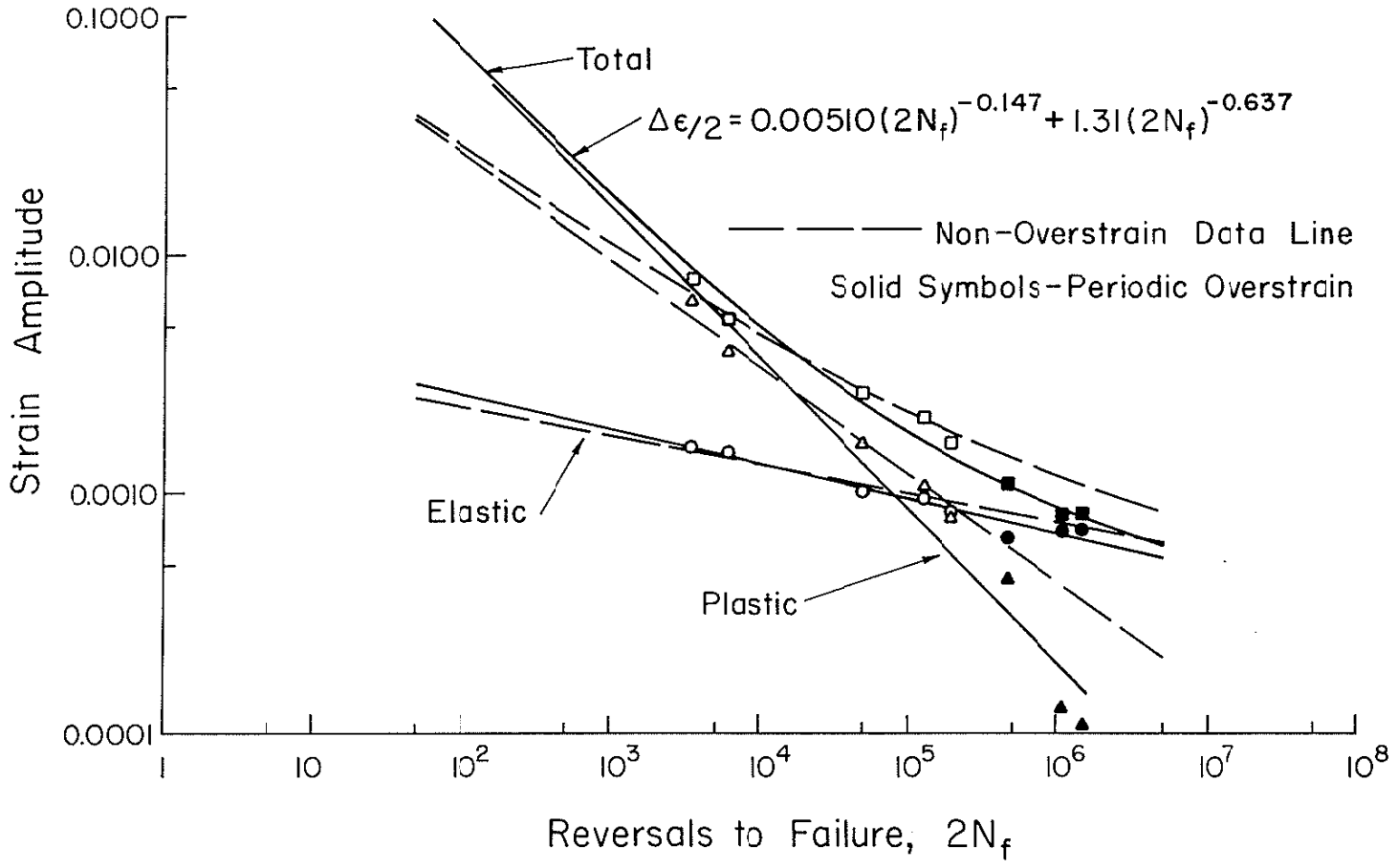

Fig. 28 Strain- Reversals to Failure Data for Sheet Steel Subjected to Periodic Cyclic Overstrains

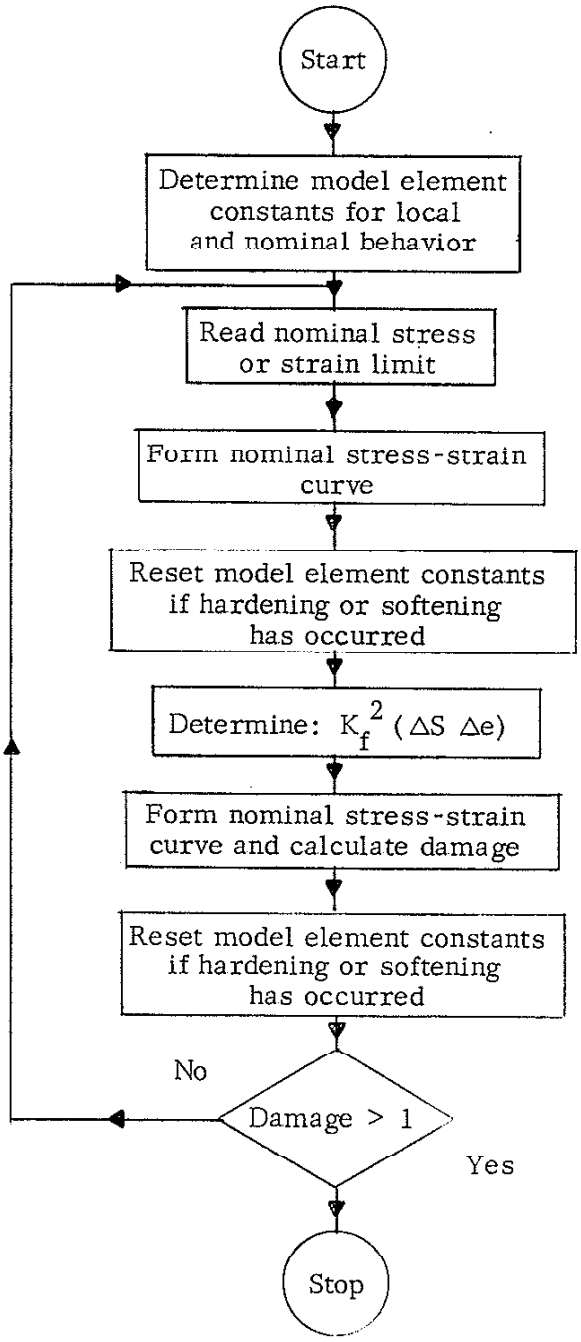

Fig. 29 Main Flow Chart of Fatigue Damage Procedure

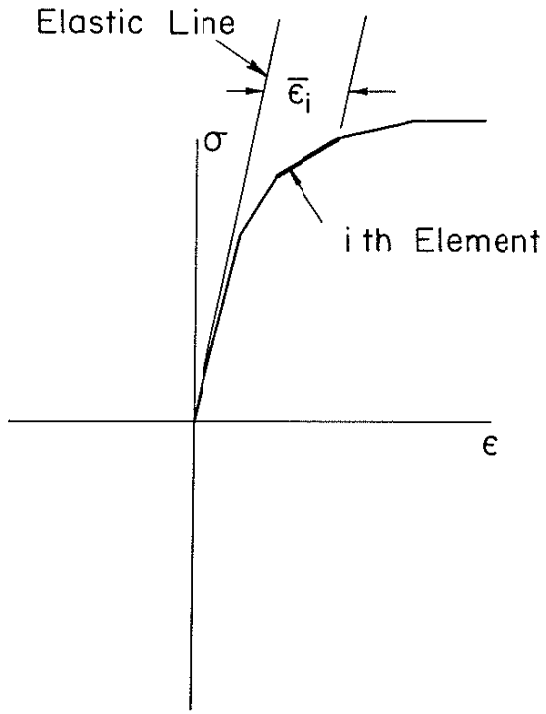

(a) Determination of $\bar{\epsilon}_i$

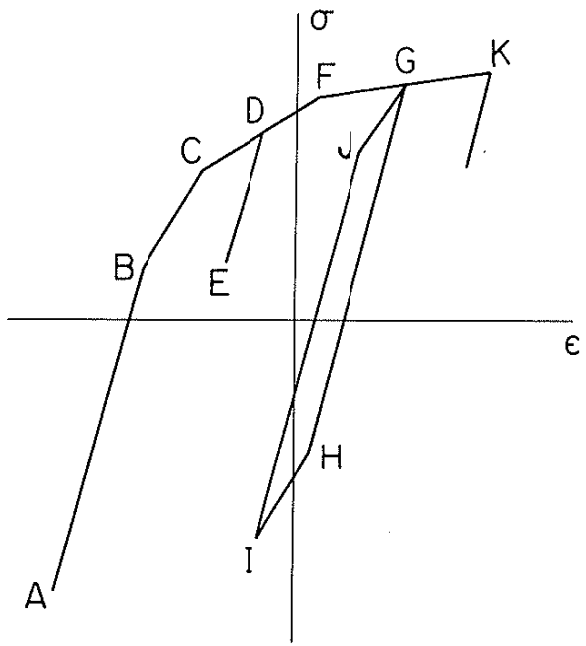

(b) Example for Damage Summation

Fig. 30 Examples for Incremental Damage Procedure

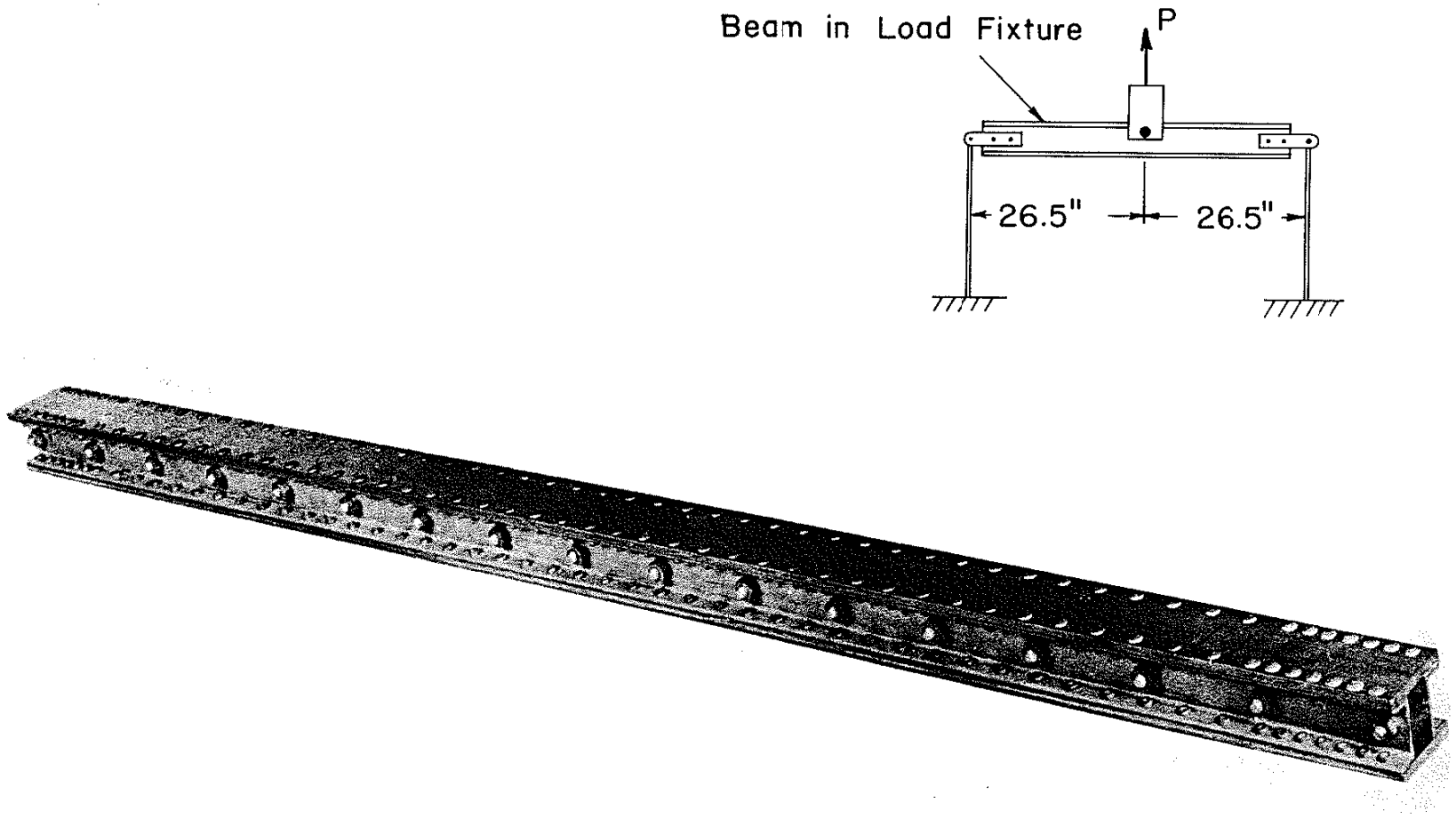

Fig. 31 Box-Beam Structure

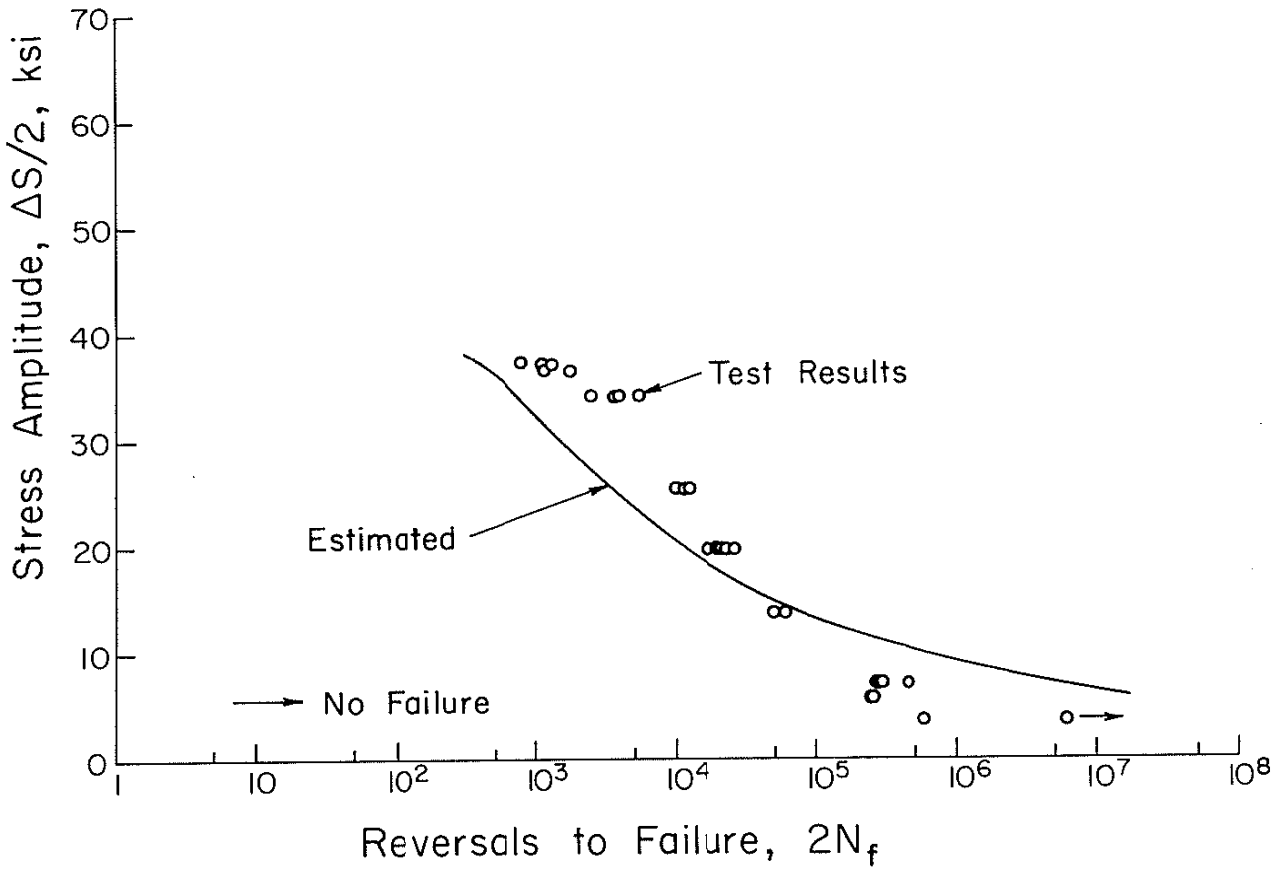

Fig. 32 Estimated and Actual Fatigue Results for Constant Amplitude (1g to P) Loading of Box-Beams

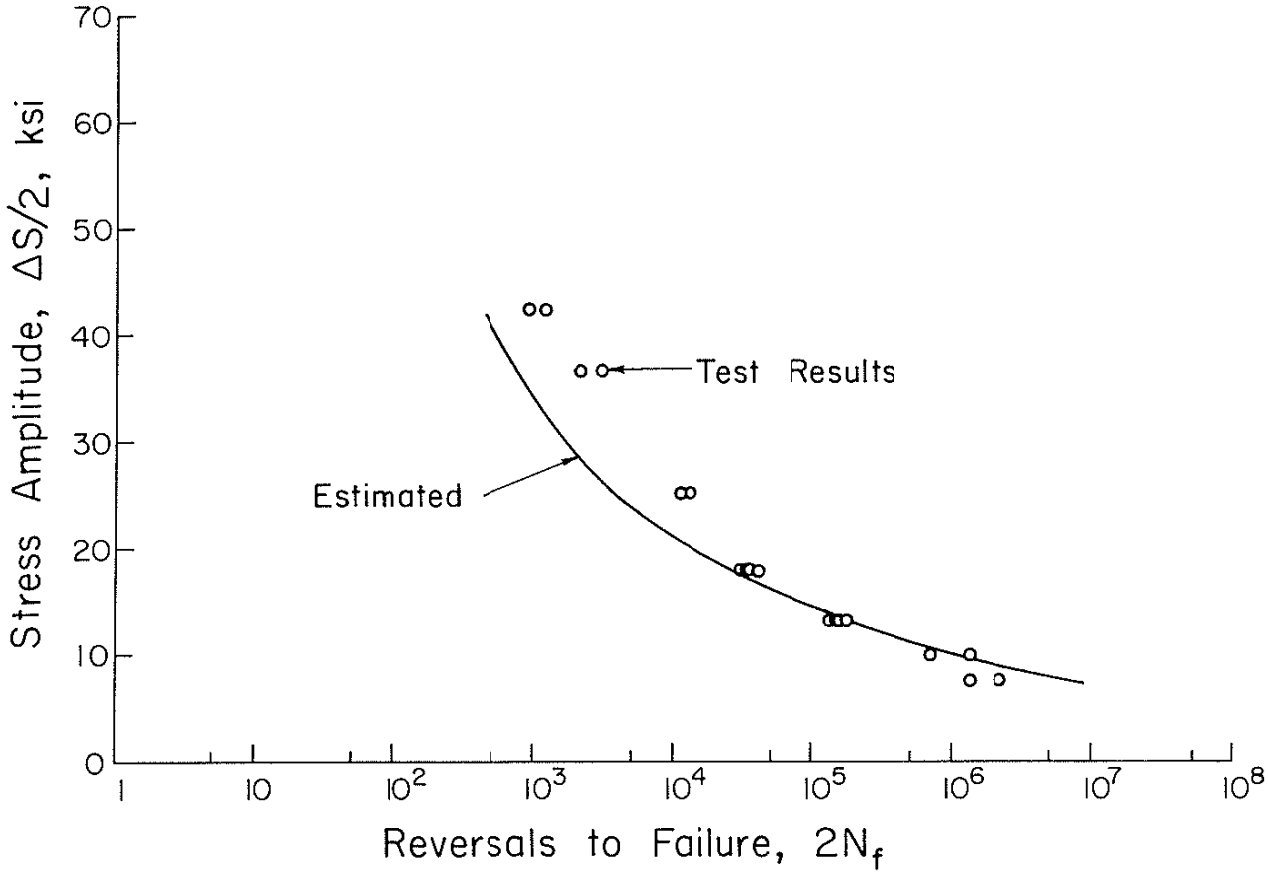

Fig. 33 Estimated and Actual Fatigue Results for Constant Amplitude (-g to P) Loading of Box-Beams

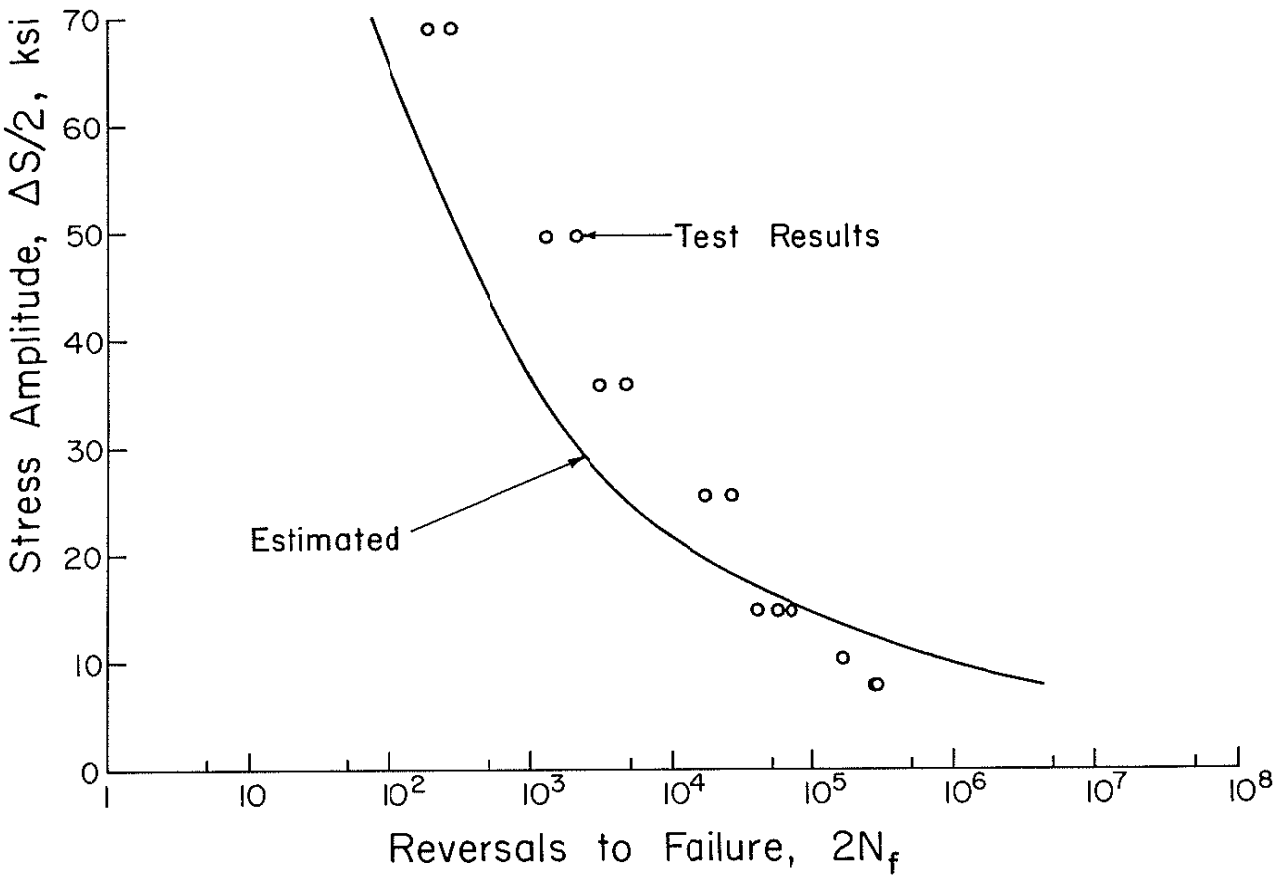

Fig. 34 Estimated and Actual Fatigue Results for Constant Amplitude (lg ± P) Loading of Box-Beams

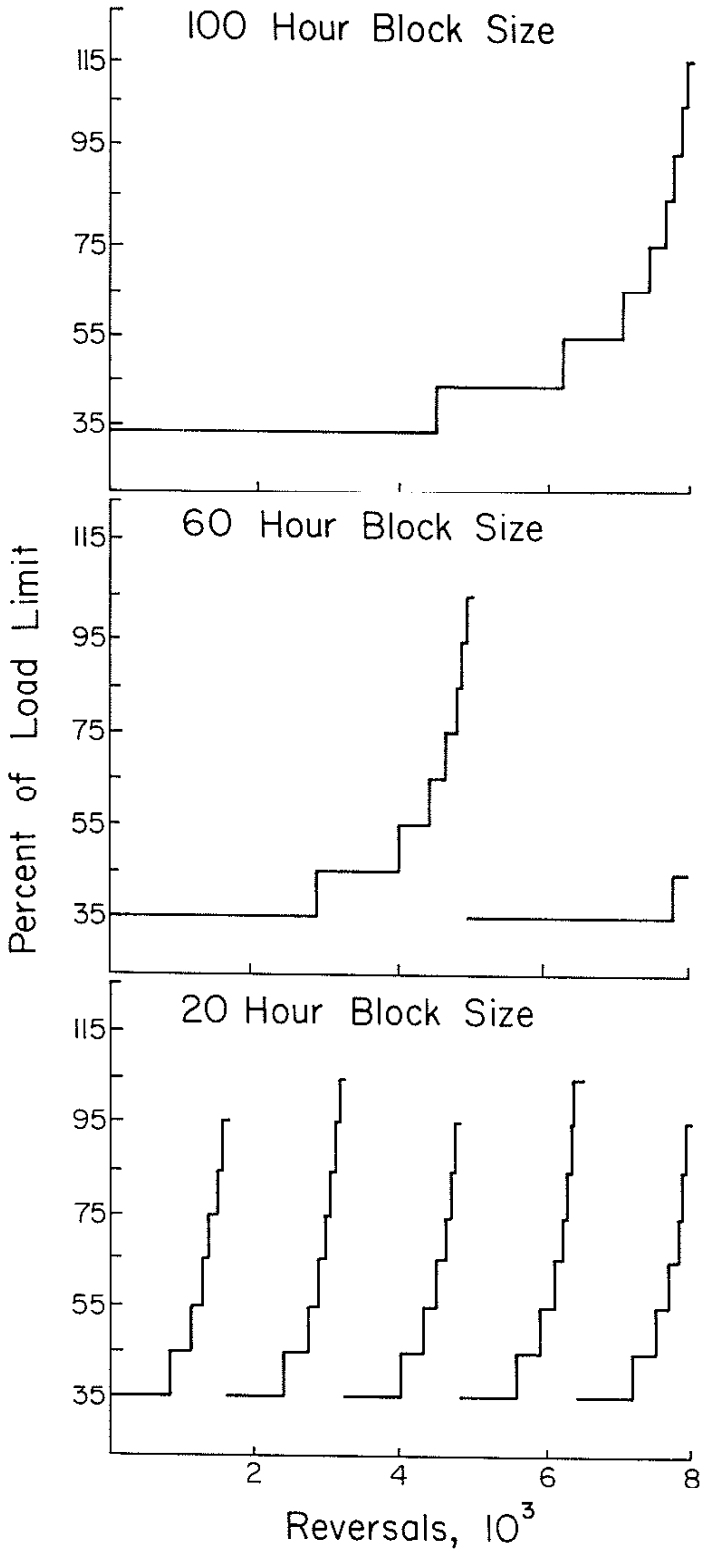

Fig. 35 Examples of Block Spectra Applied to Box-Beams

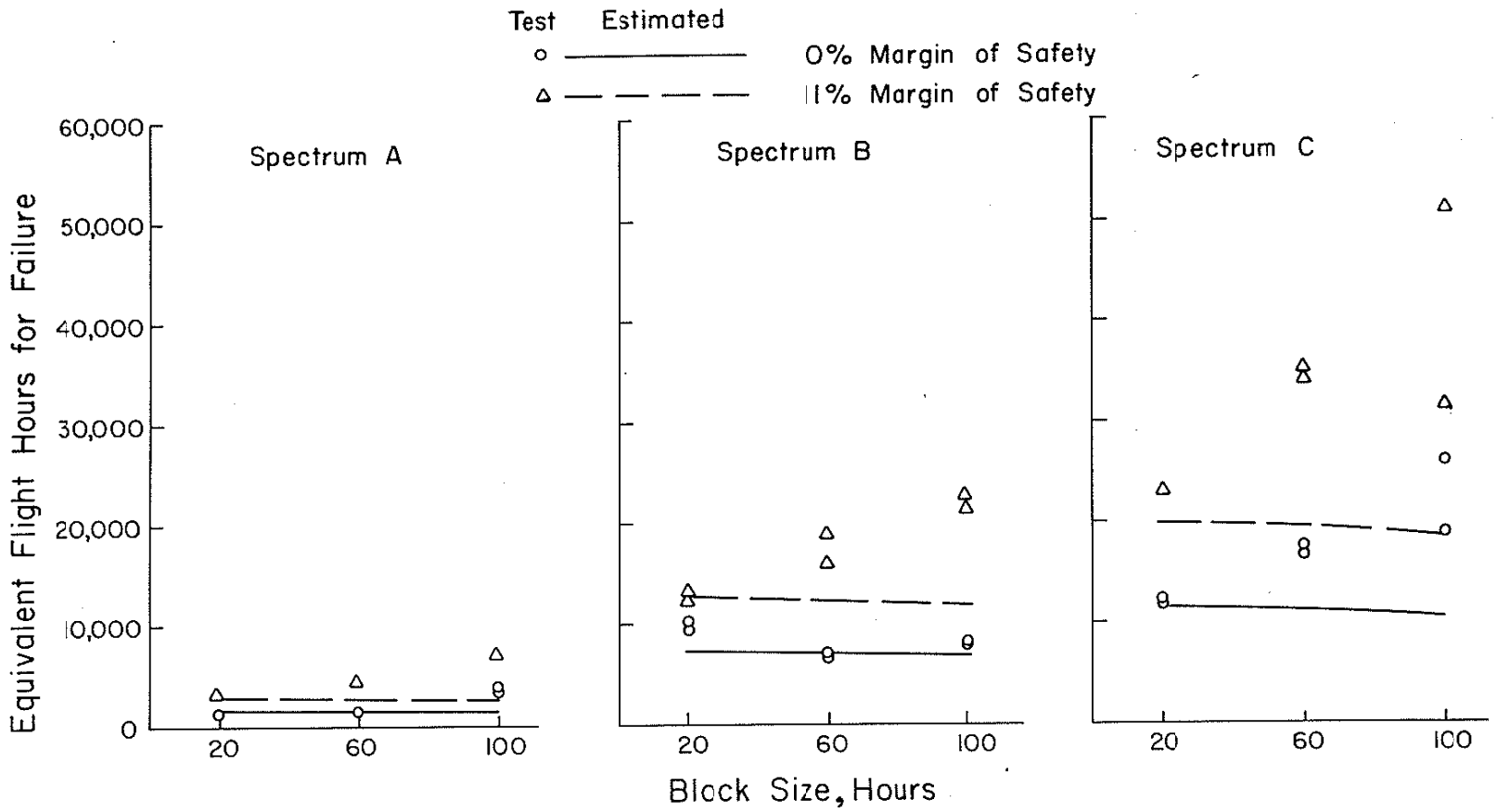

Fig. 36 Estimated and Actual Fatigue Results for Box—Beams Subjected to Variable Load Spectra

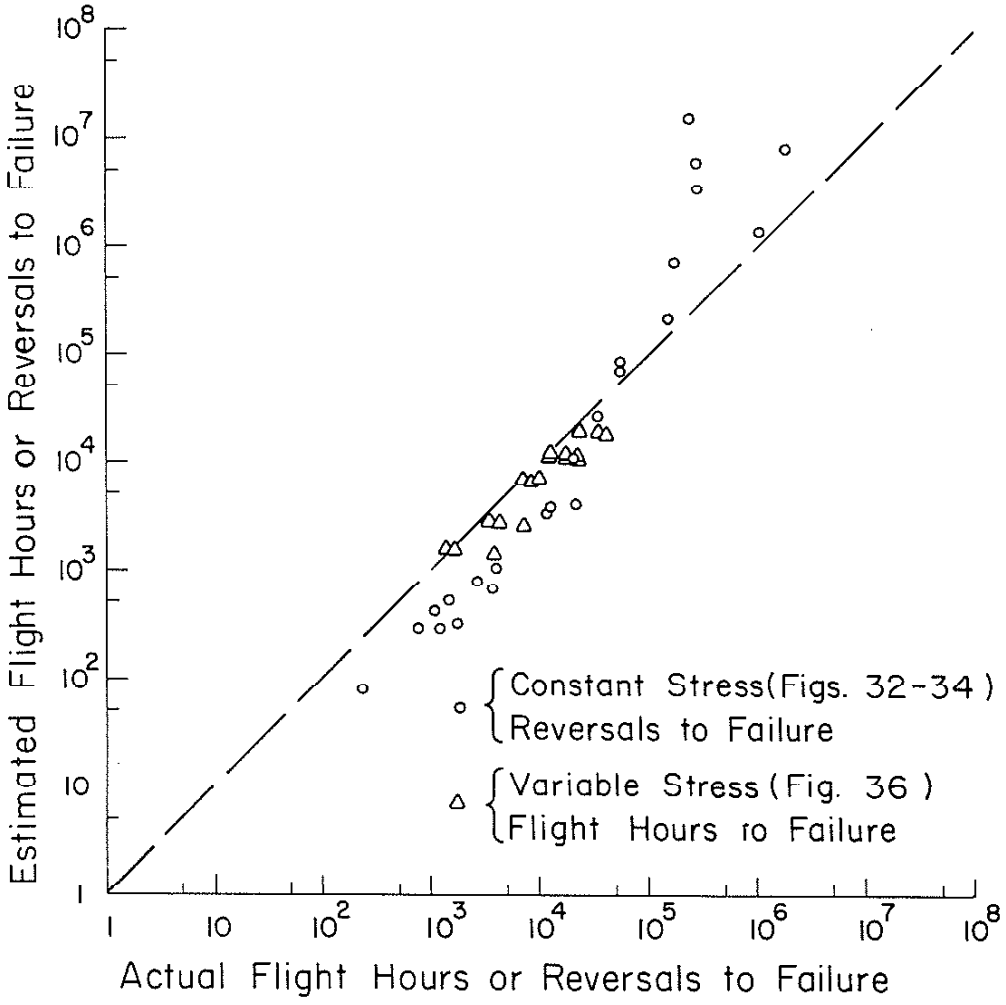

Fig. 37 Estimated vs. Actual Fatigue Results for Box-Beams

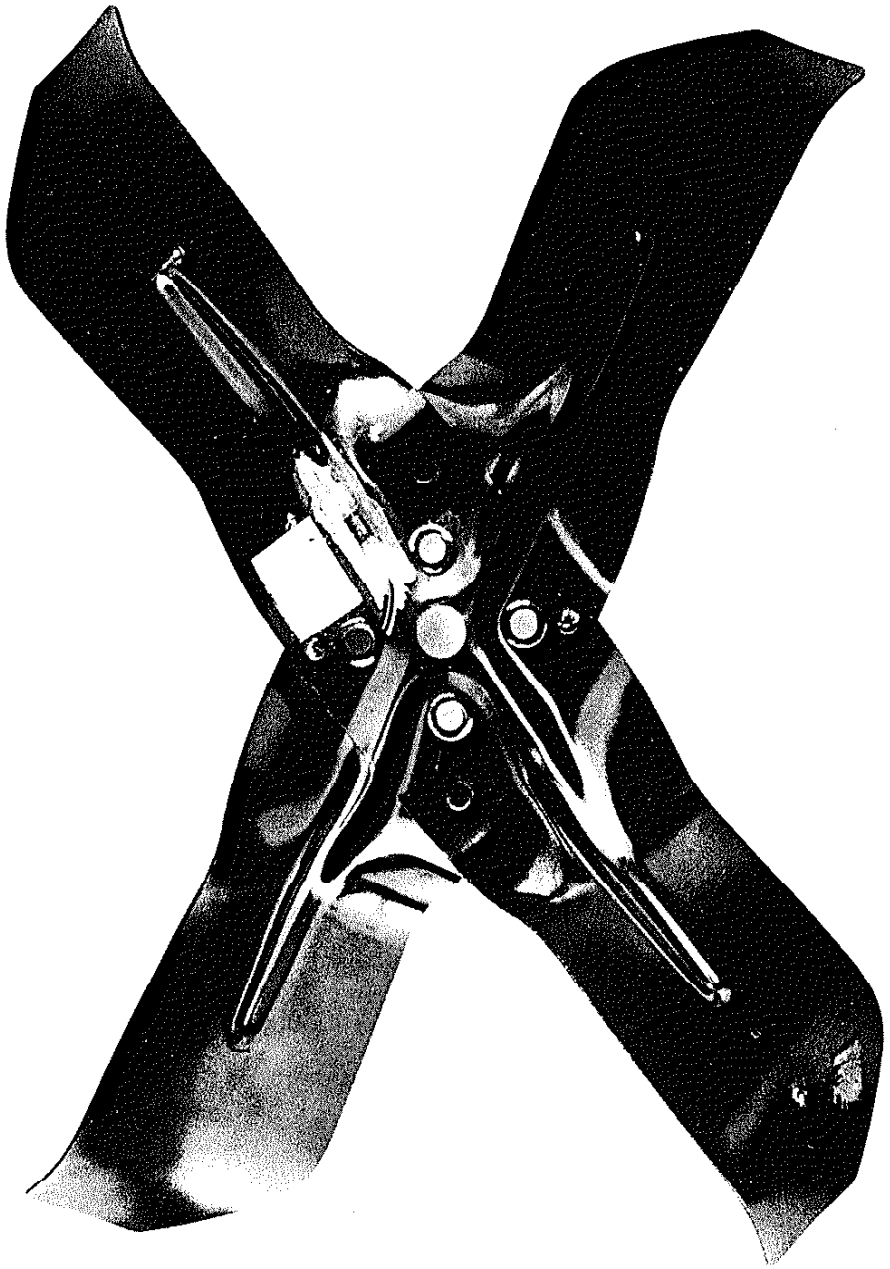

Fig. 38 Automotive Fan Blade

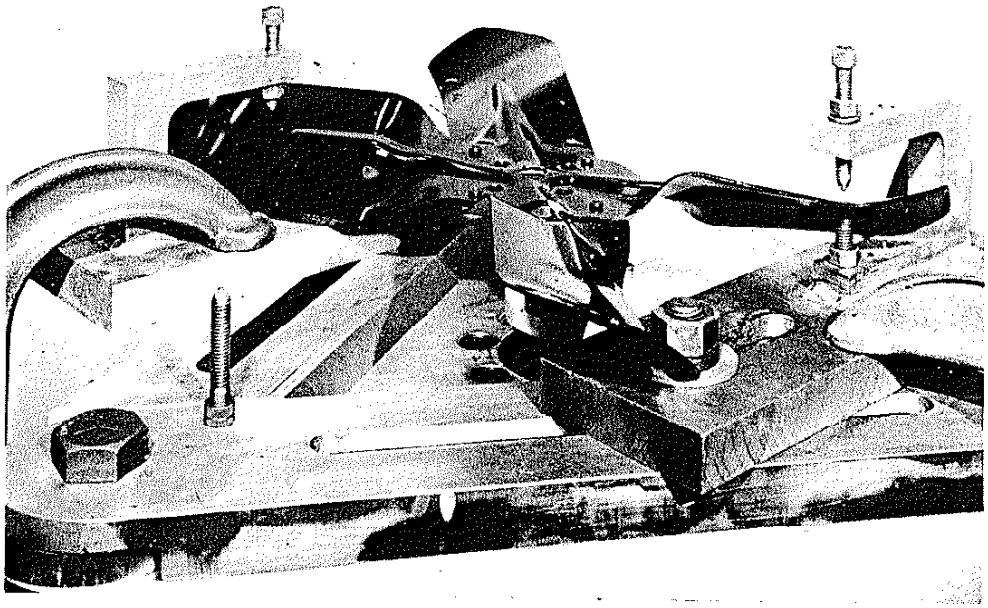

Fig. 39 Load Fixture for the Fan Blade

Fig. 40 Strain Gaged Region of the Fan Blade

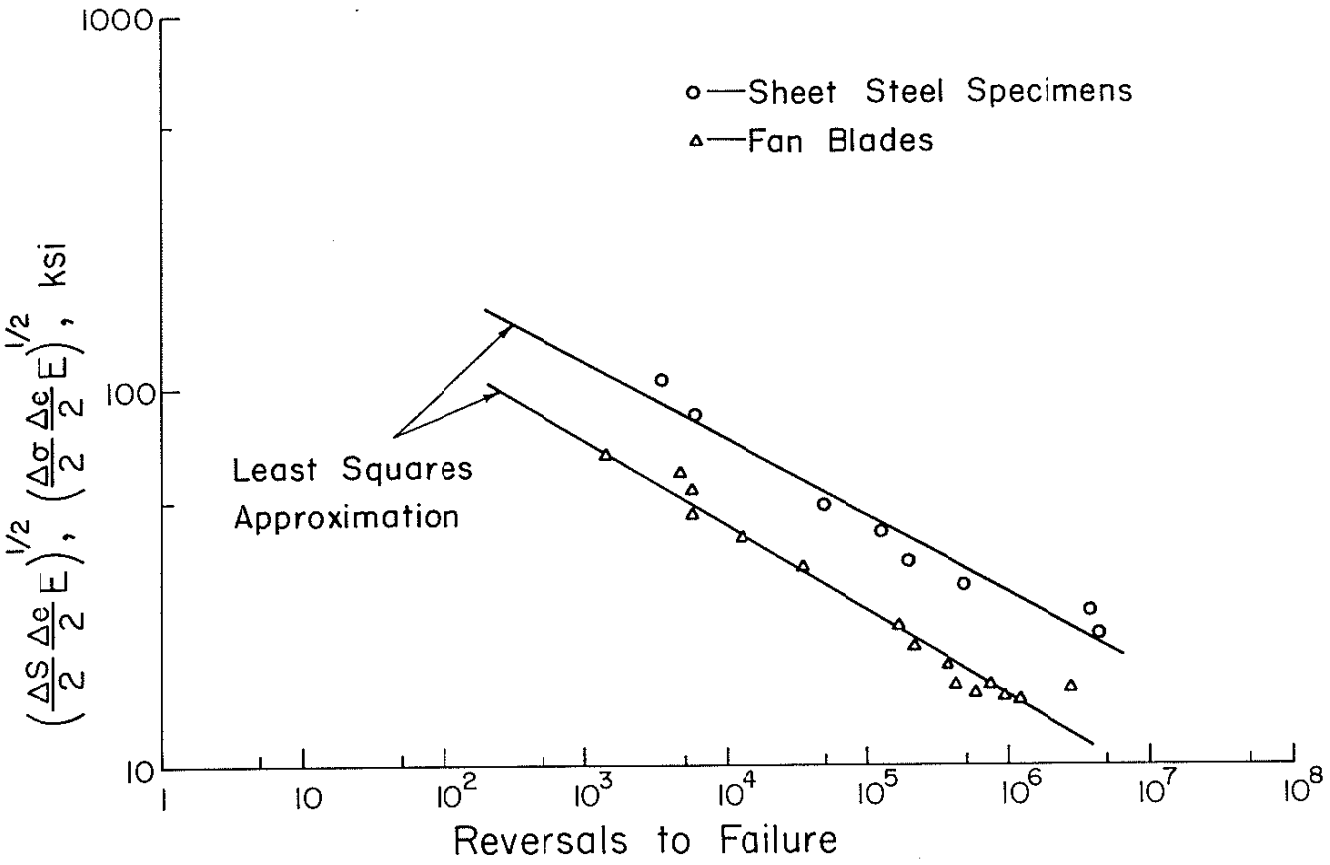

Fig. 41 Non-Overstrained Constant Amplitude Data for Sheet Steel and Fan Blades

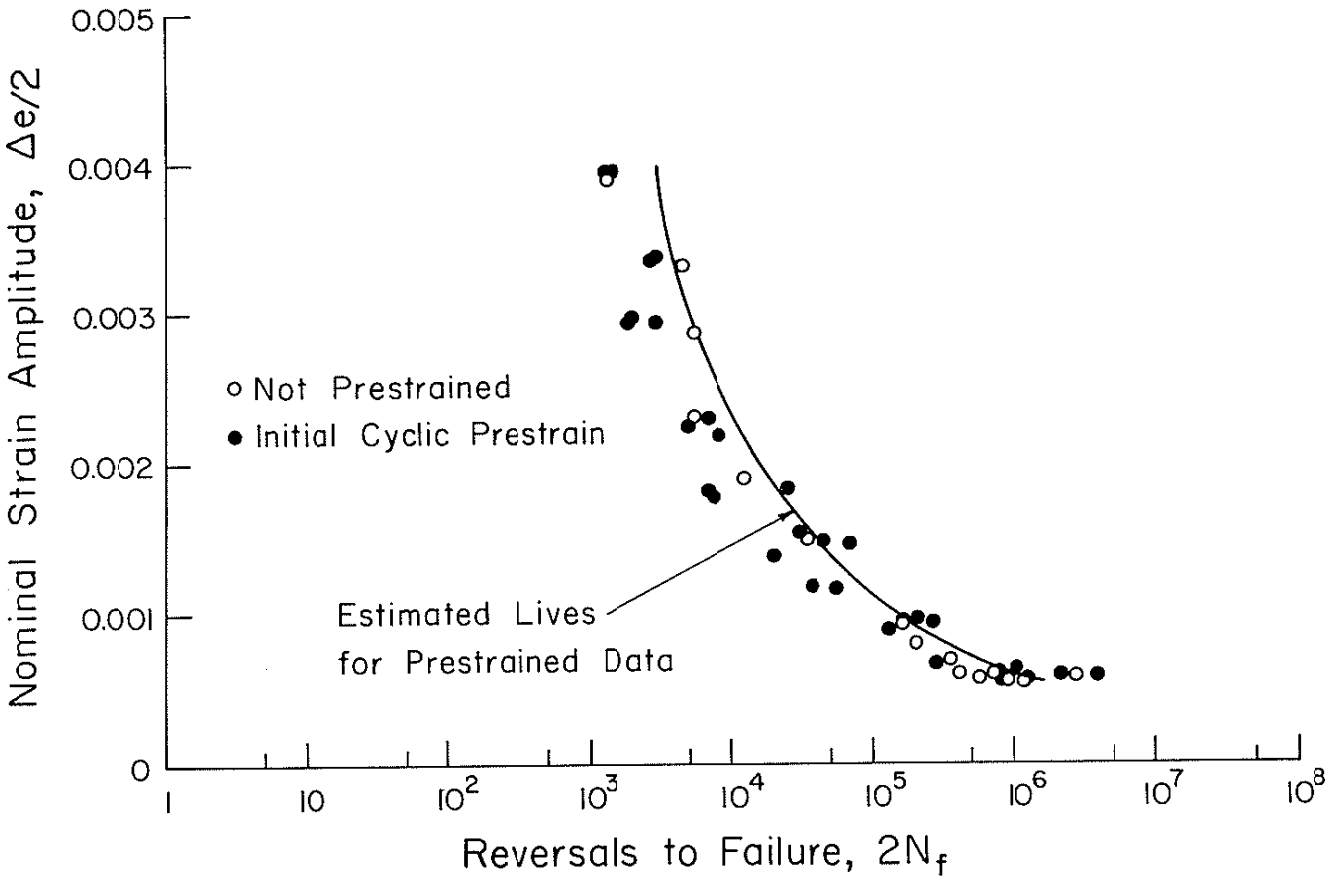

Fig. 42 Estimated and Actual Fatigue Results for Constant Amplitude Straining of Fan Blades

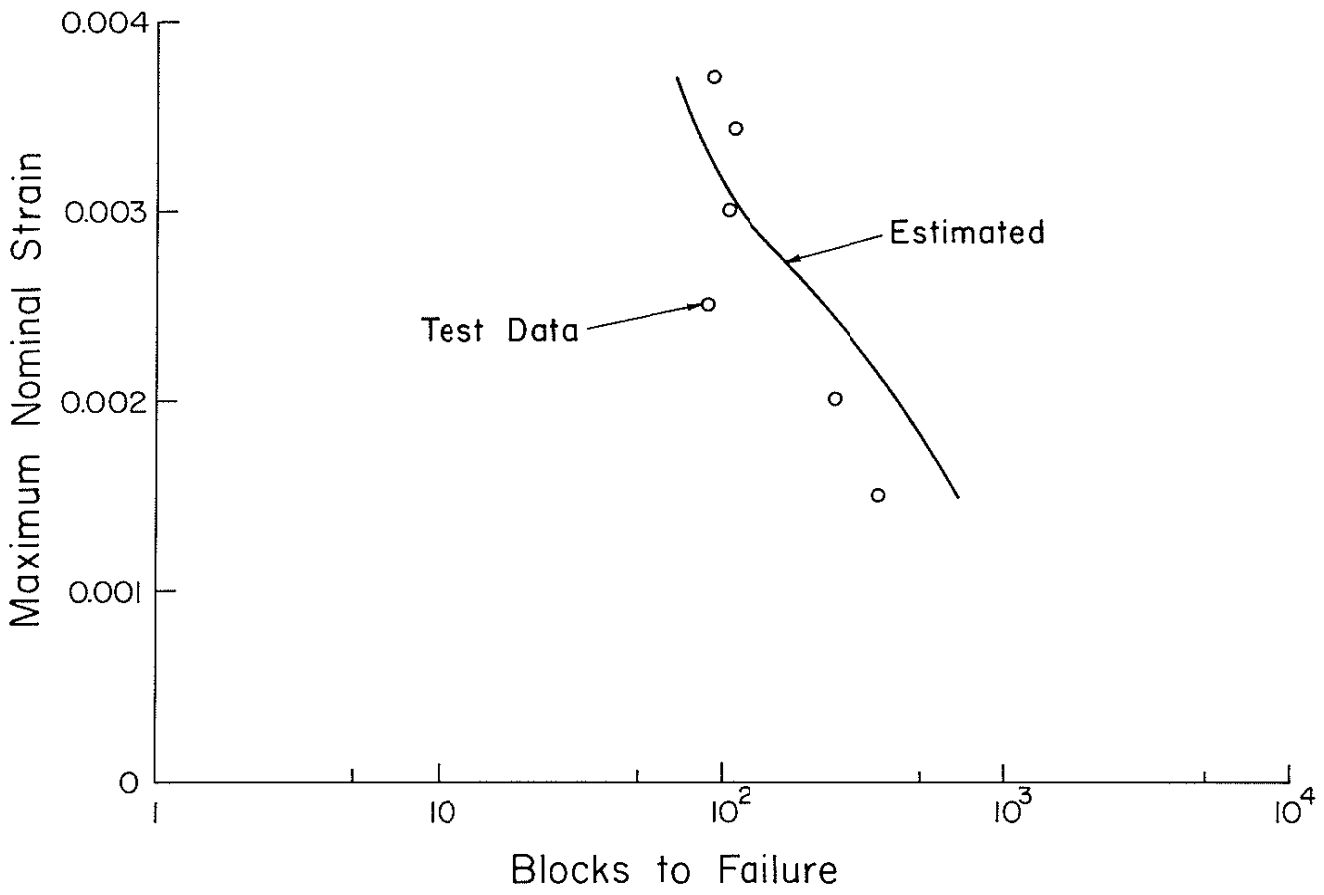

Fig. 43 Estimated and Actual Fatigue Results for Fan Blades Subjected to Axle Load History

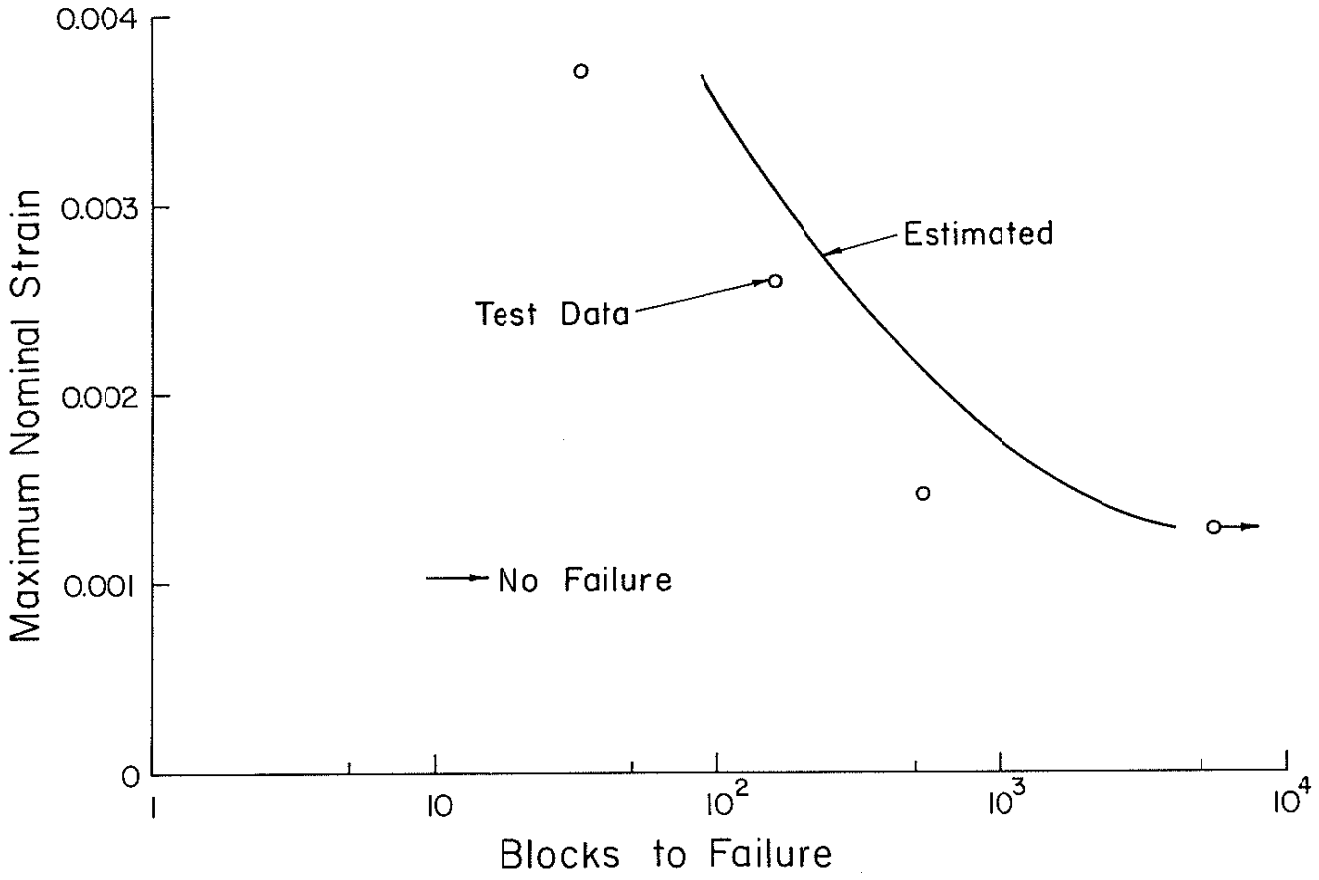

Fig. 44 Estimated and Actual Fatigue Results for Fan Blades Subjected to Suspension Load Histories

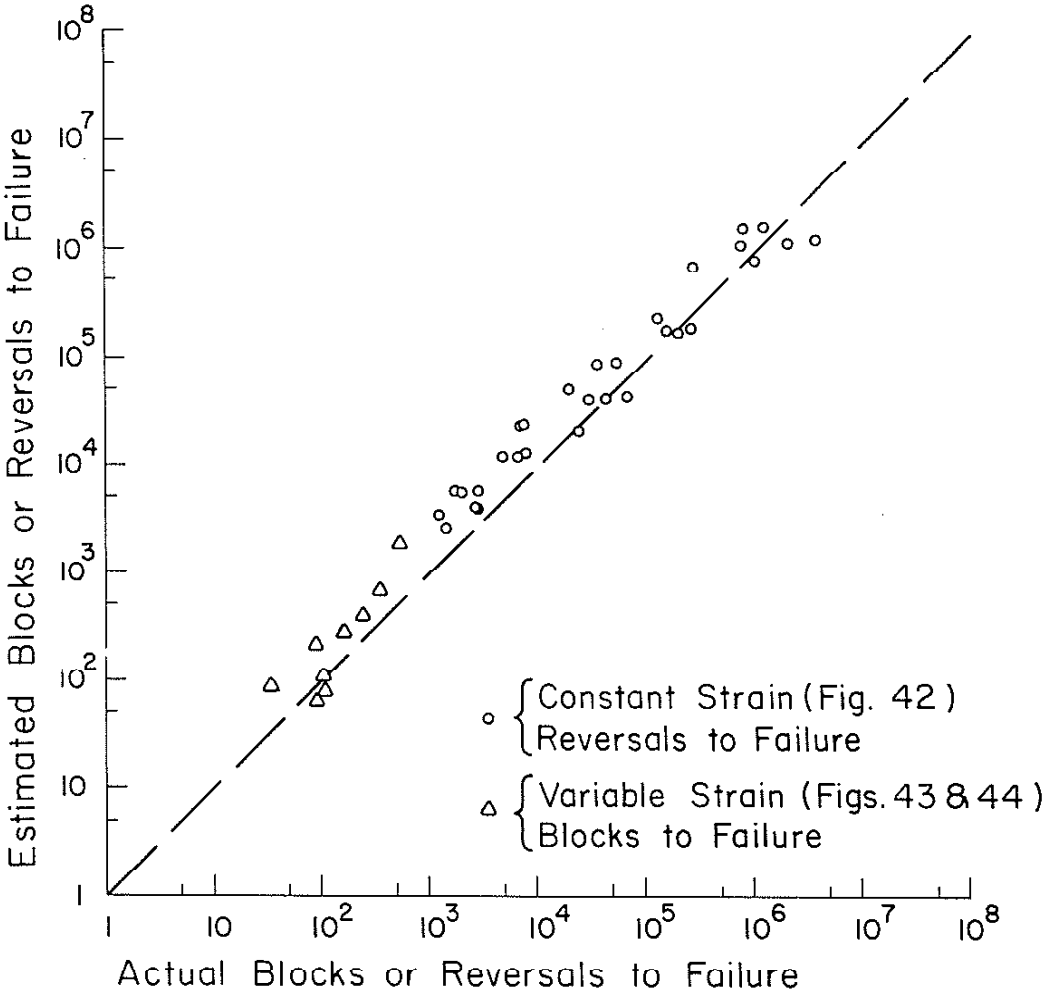

Fig. 45 Estimated vs. Actual Fatigue Results for Fan Blades

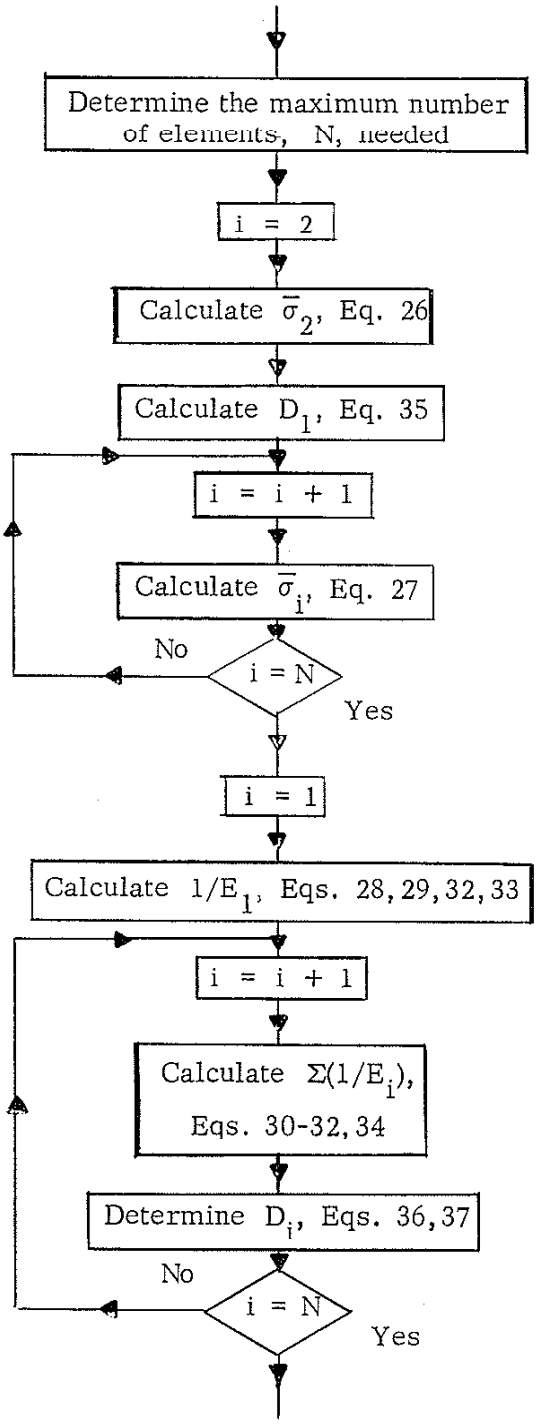

Fig. 46 Determination of the Stress-Strain and Damage Constants for the Model

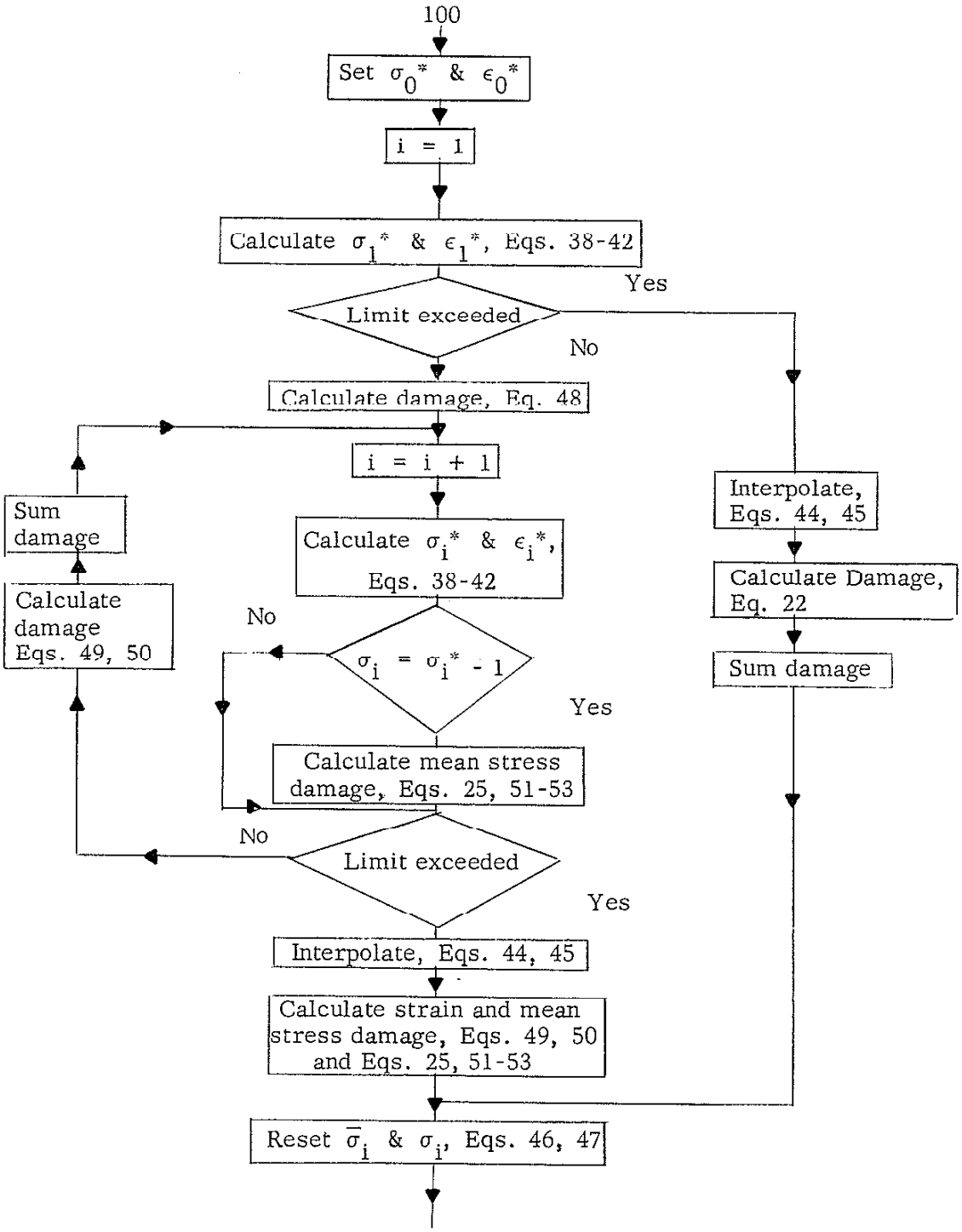

Fig. 47 Model Simulation of Stress-Strain Behavior

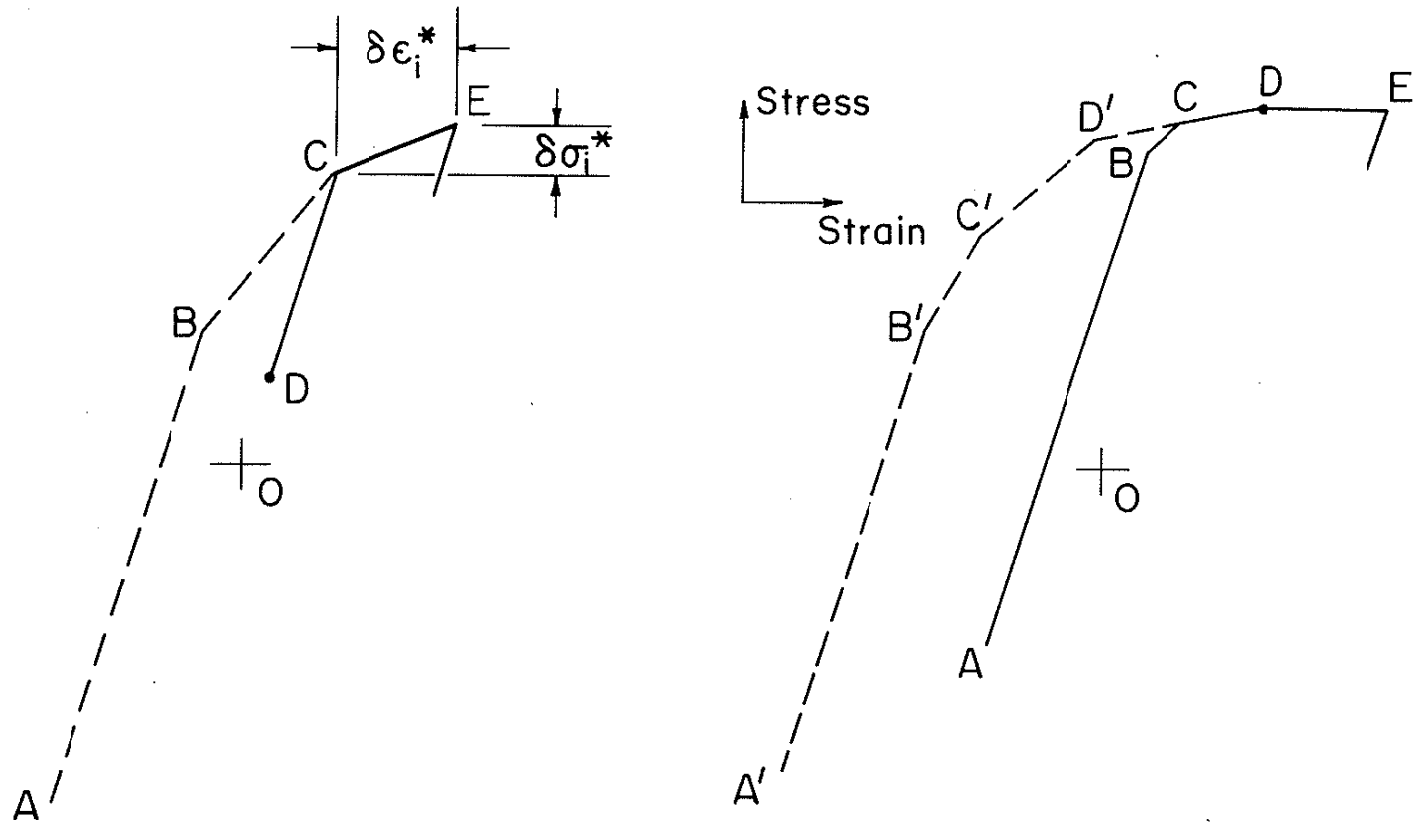

(a) Plastic Strain Damage (b) Mean Stress Damage

Fig. 48 Examples of Damage Calculations

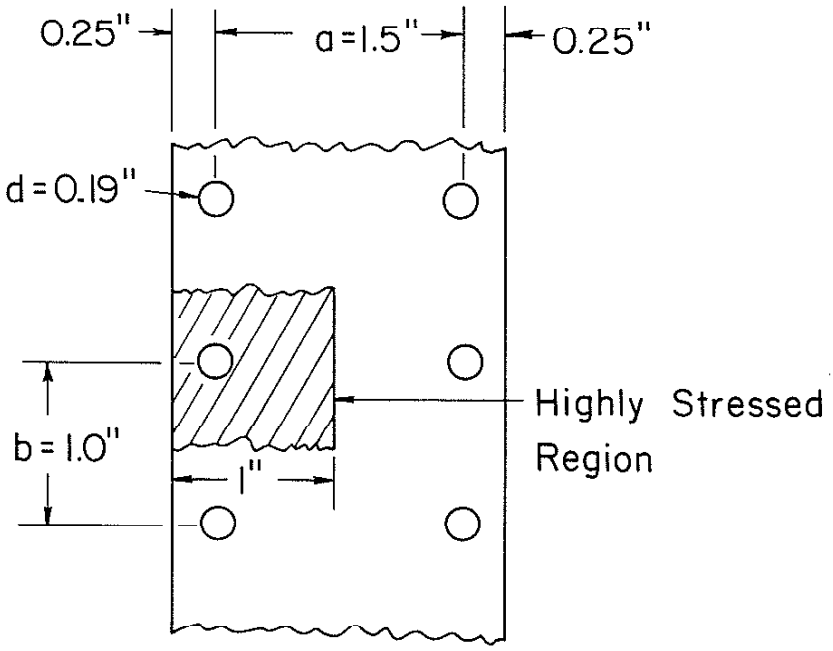

Fig. 49 Highly Stressed Area of Box-Beam Cover Plate

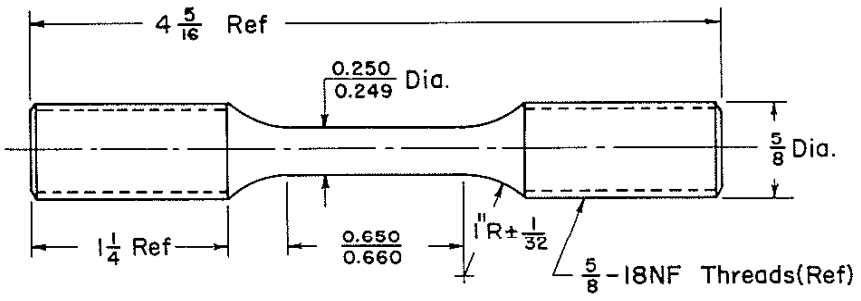

(a) Cylindrical Fatigue Specimen

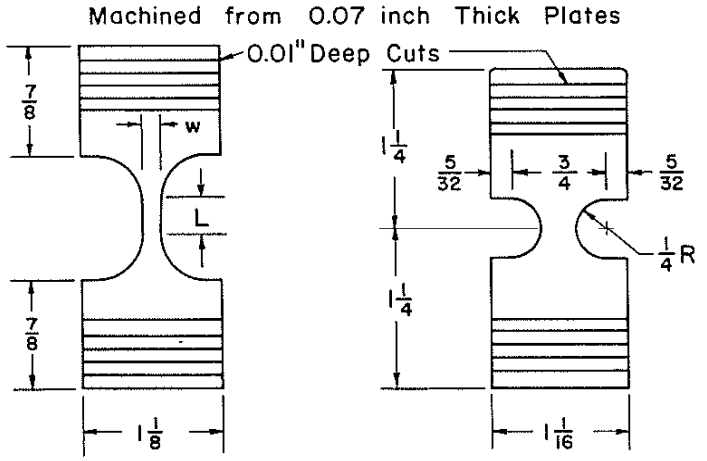

(b) Sheet Steel Axial Specimen

(c) Sheet Steel Transverse Specimen

Fig. 50 Specimen Configurations

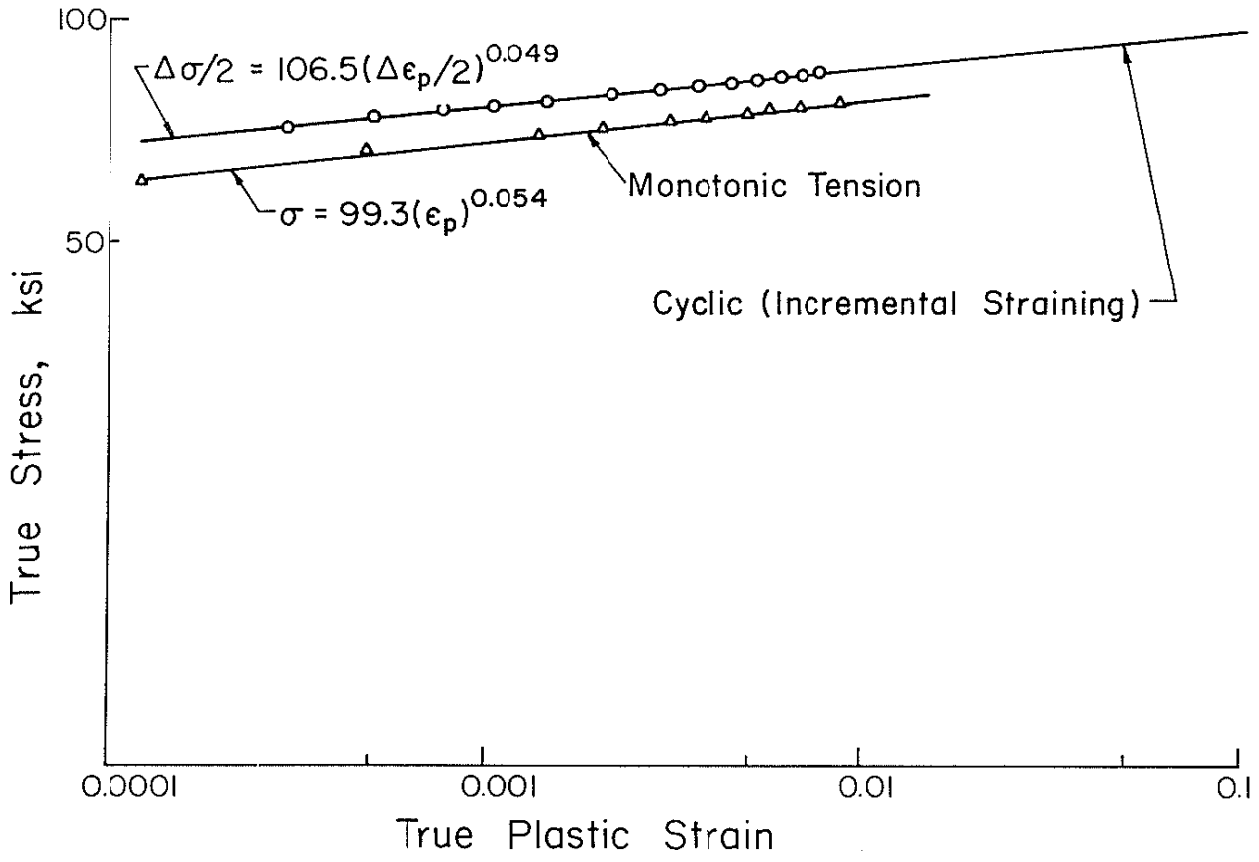

Fig. 51 Monotonic and Cyclic Stress-Strain Data for 7075-T6 Aluminum

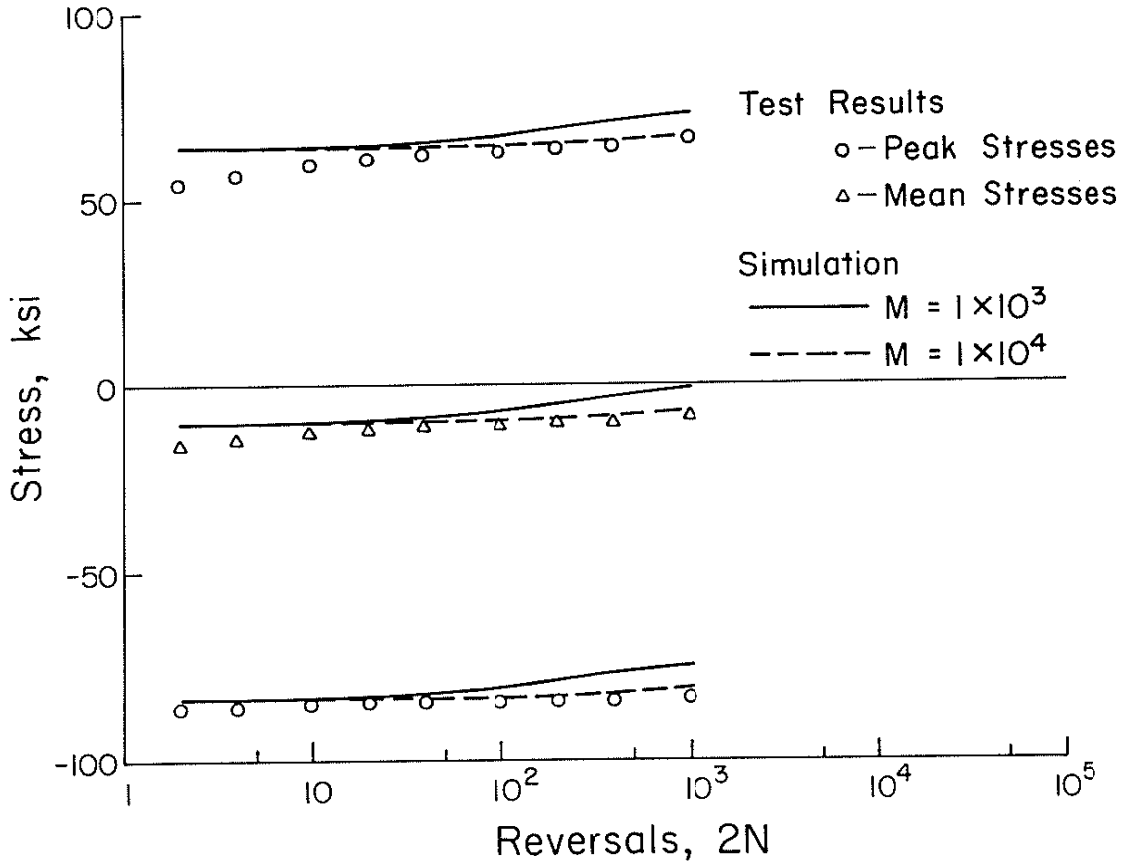

Fig. 52 Cyclic Relaxation Data for a Strain Range from 0.0 to -0.0155 for 7075-T6 Aluminum

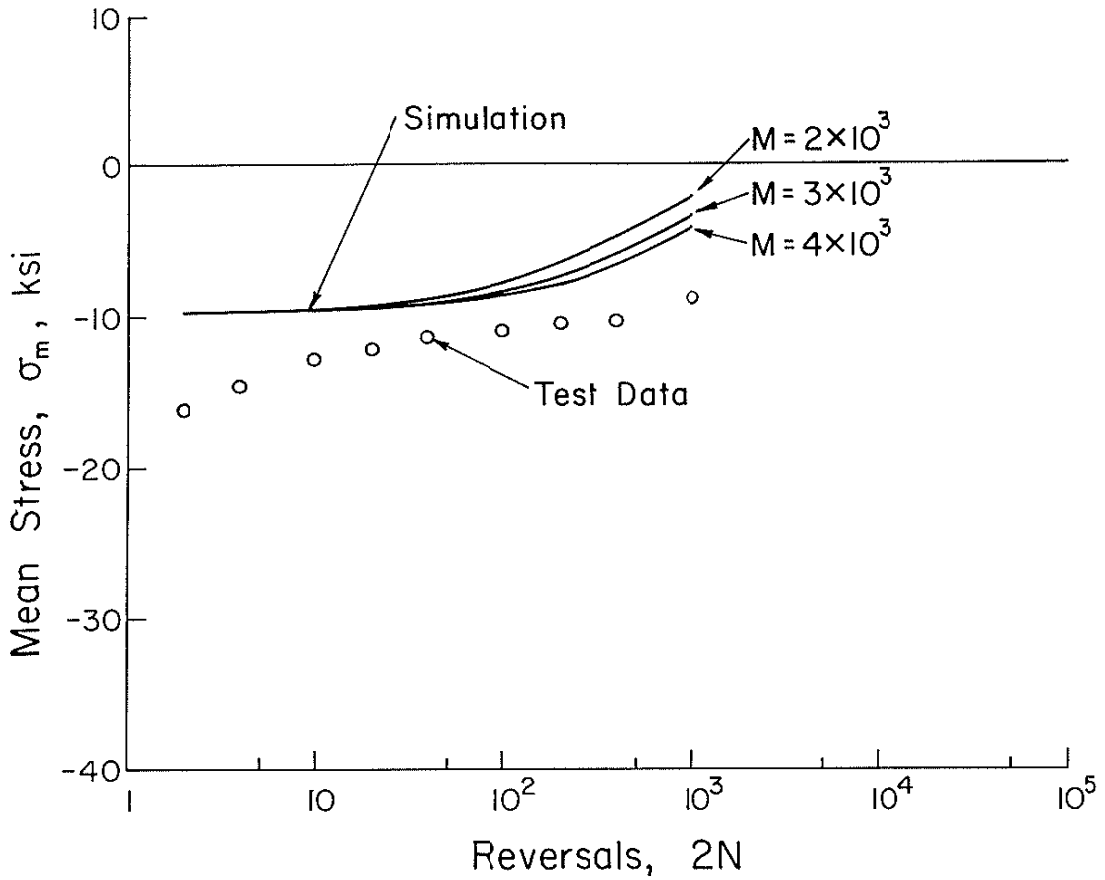

Fig. 53 Mean Stress Relaxation Data of 7075-T6 Aluminum for a Strain Range from 0.0 to -0.0155

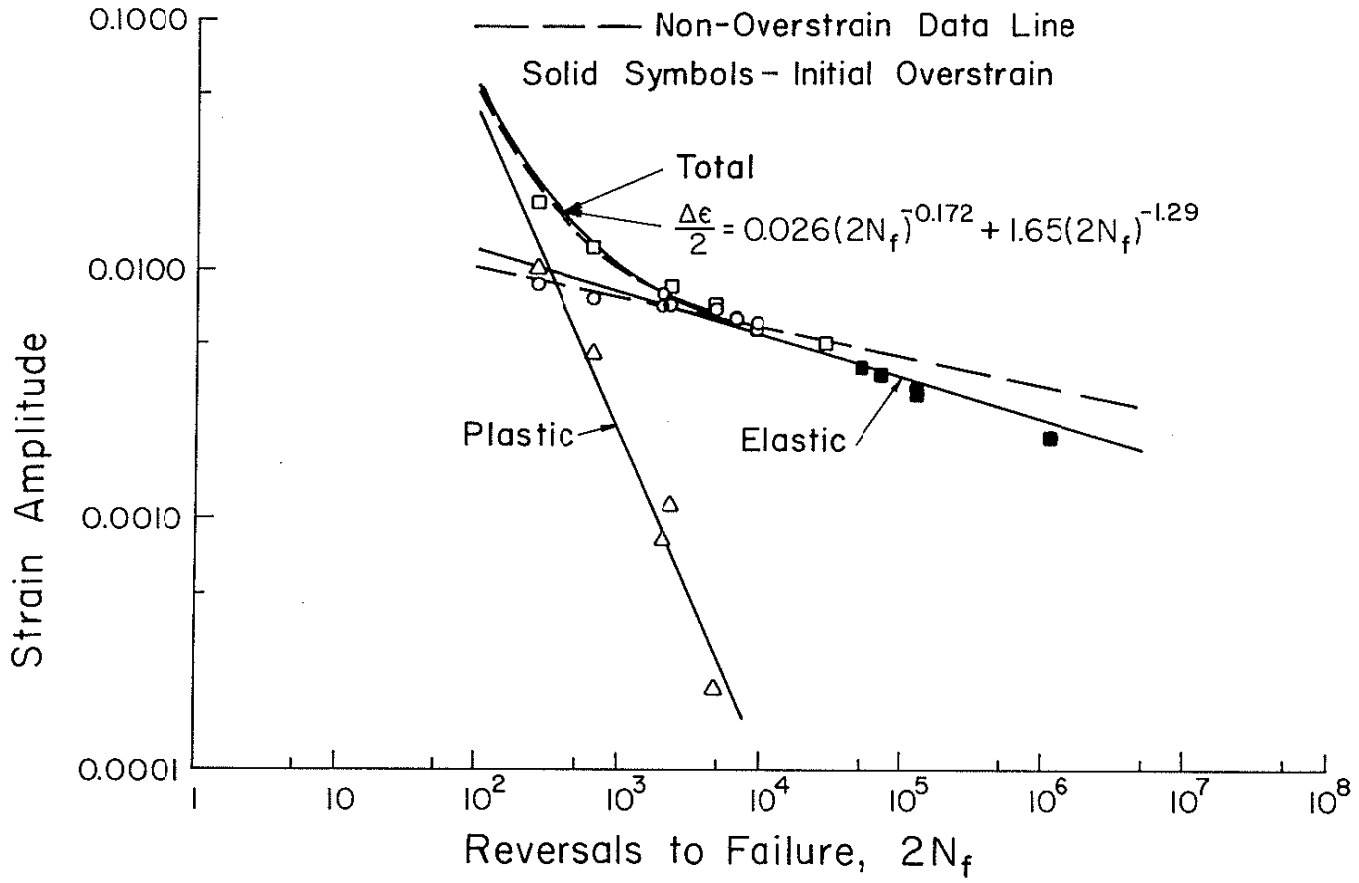

Fig. 54 Strain-Reversals to Failure Data for 7075-T6 Aluminum with Small Strain Amplitude Data Initially Overstrained

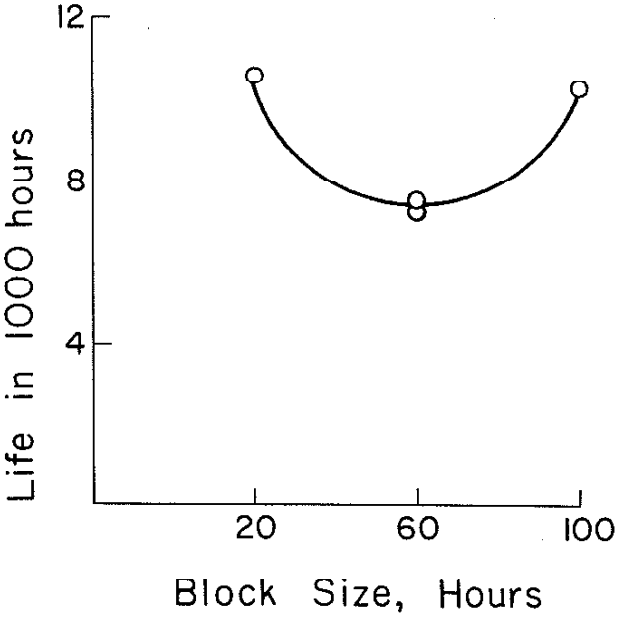

Fig. 55 Test Results of Notched Plates of 7075 Aluminum Subjected to Same Nominal Stresses as Box-Beams Loaded According to Spectrum B, 0% M.S.

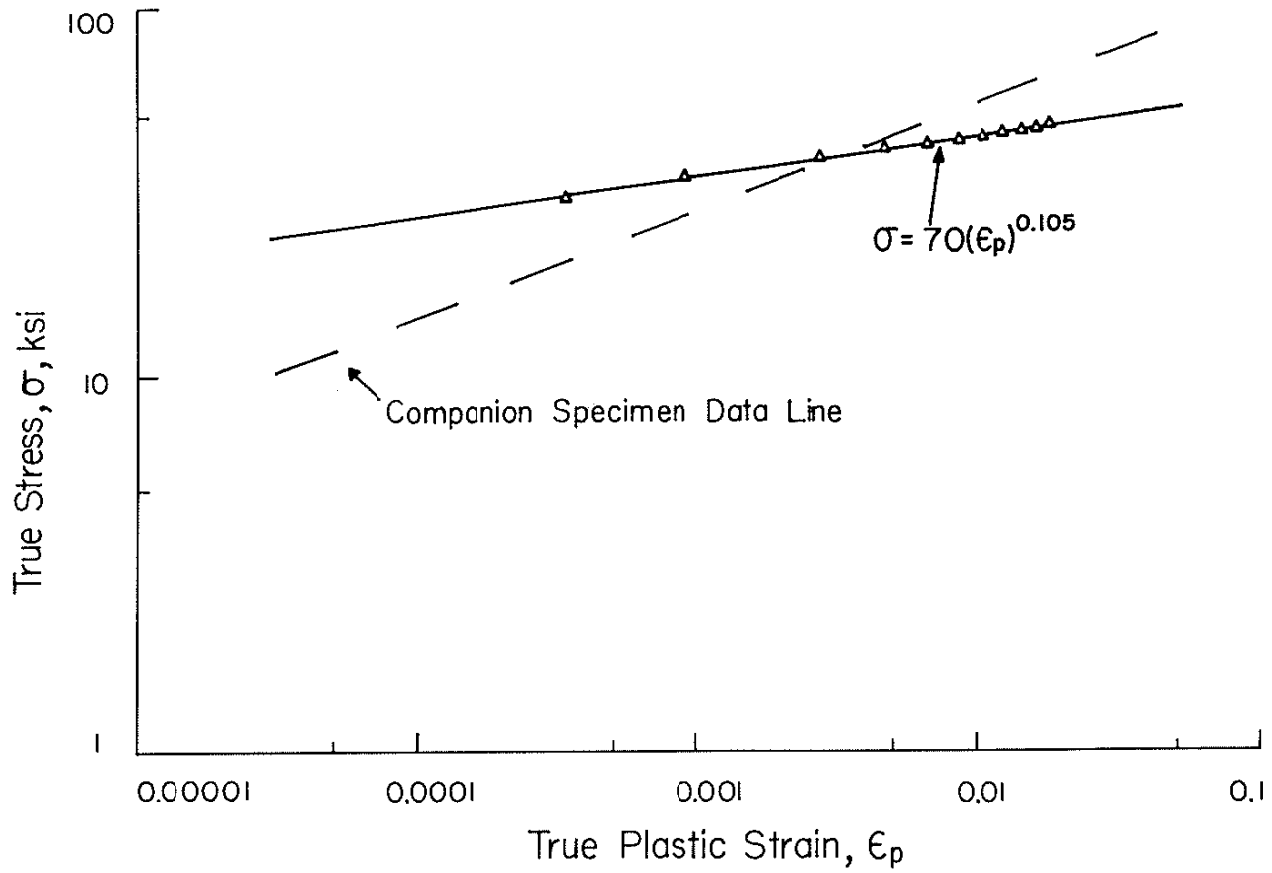

Fig. 56 Stress–Plastic Strain Data for Monotonic Tension after Incremental Step Straining of the Sheet Steel

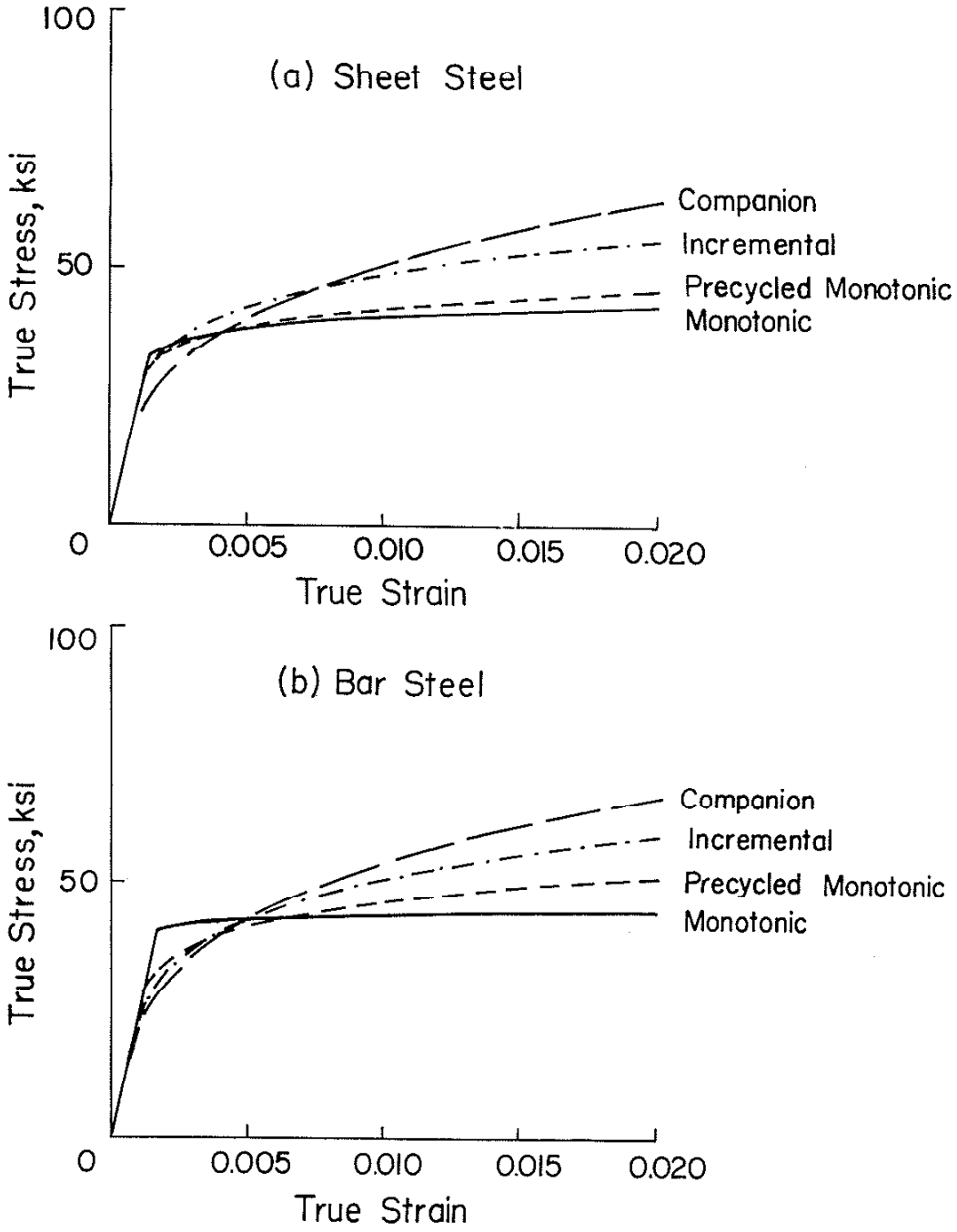

Fig. 57 Monotonic and Cyclic Stress-Strain Curves

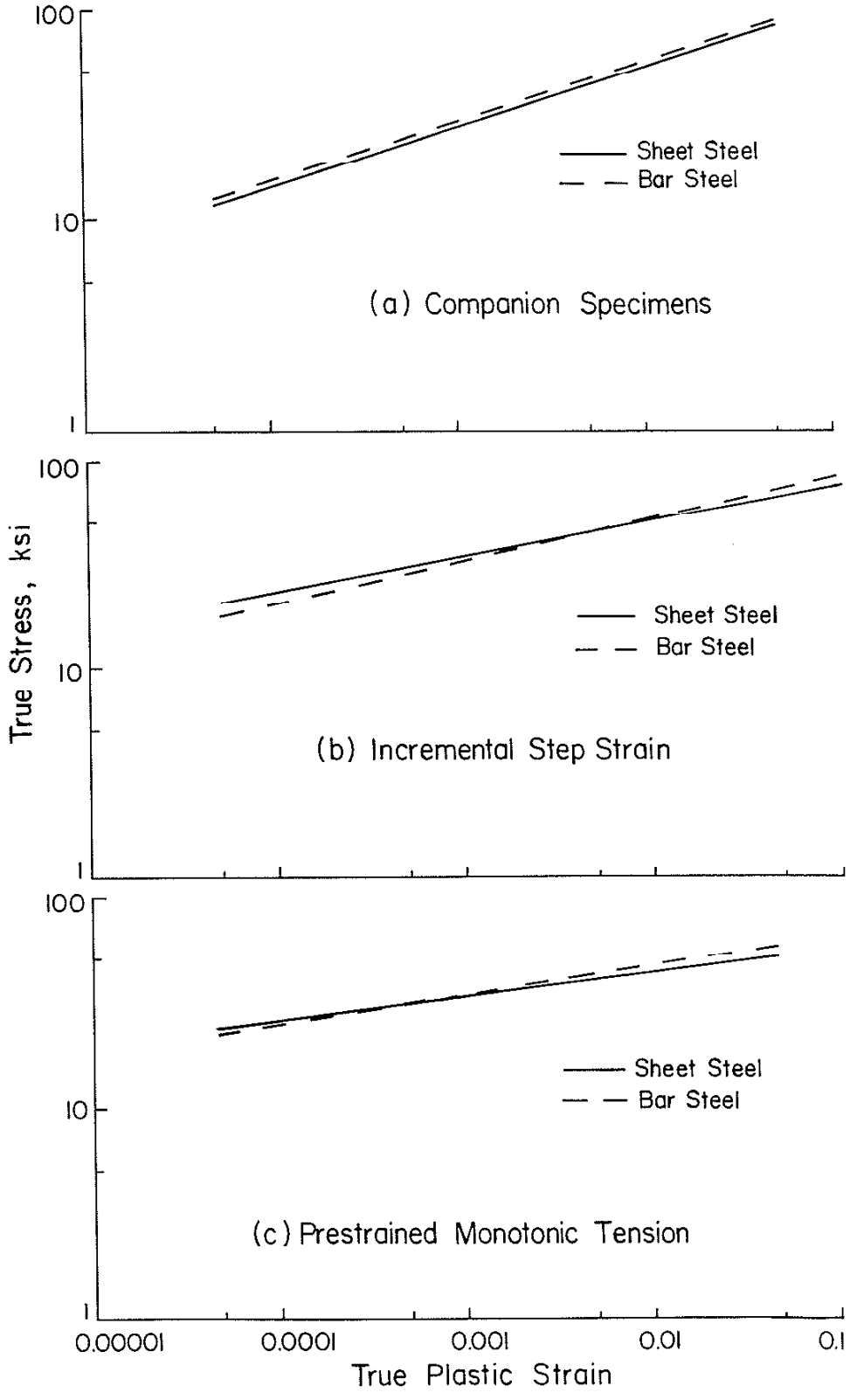

Fig. 58 Comparison of Least Squares Approximation of Cyclic Stress-Plastic Strain Curves for Both Steel

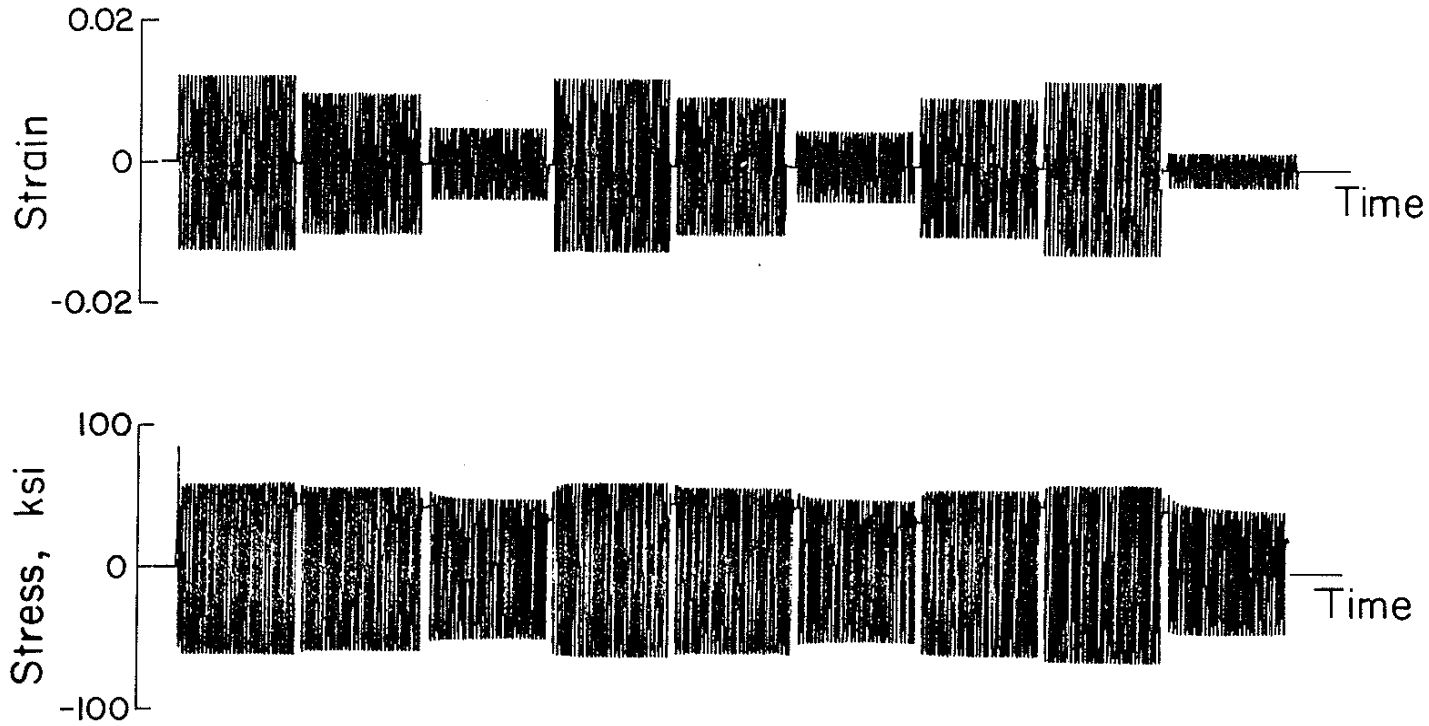

Fig. 59 Strain Control Block Test Results of Bar Steel

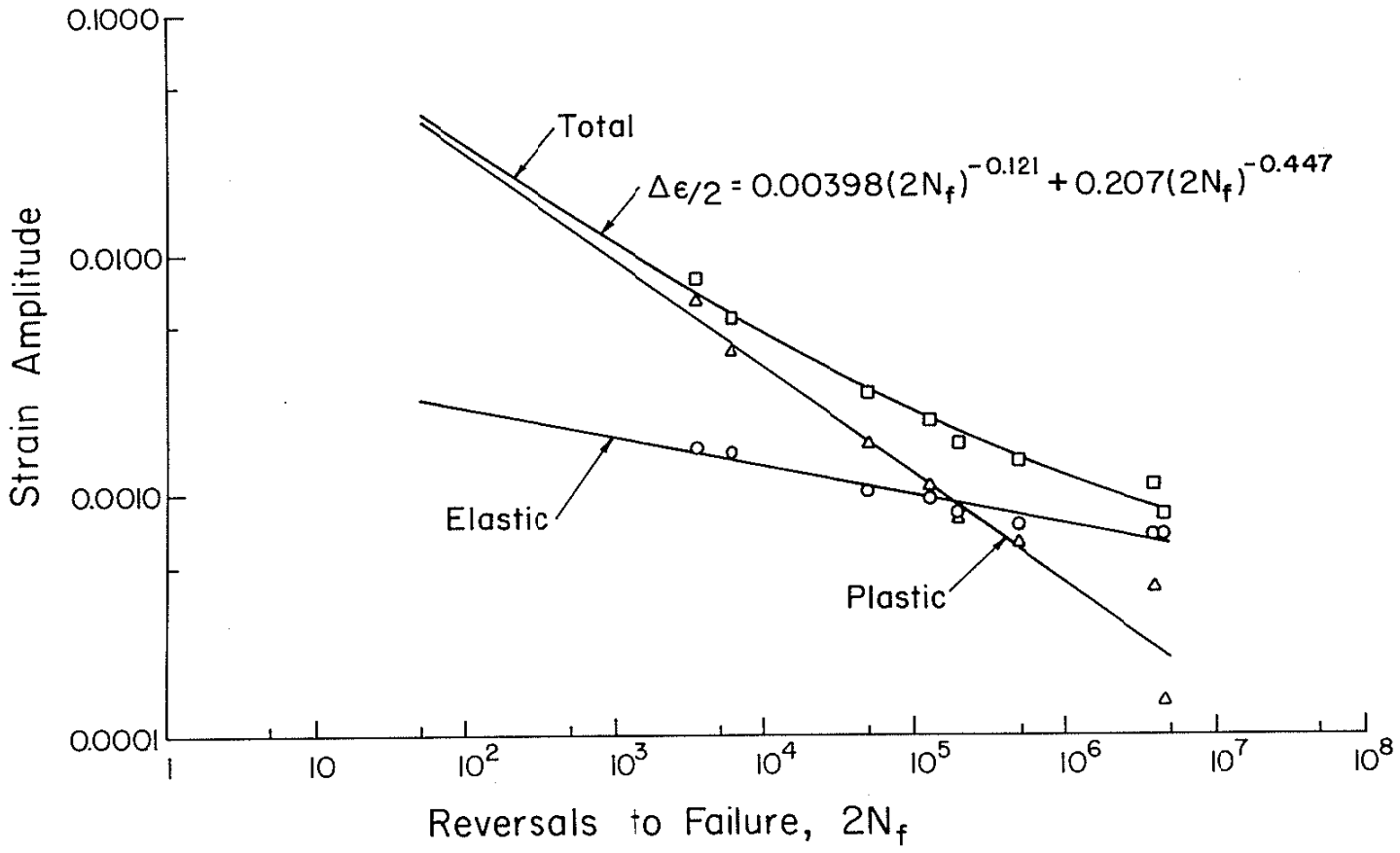

Fig. 60 Strain-Reversals to Failure Data for Sheet Steel

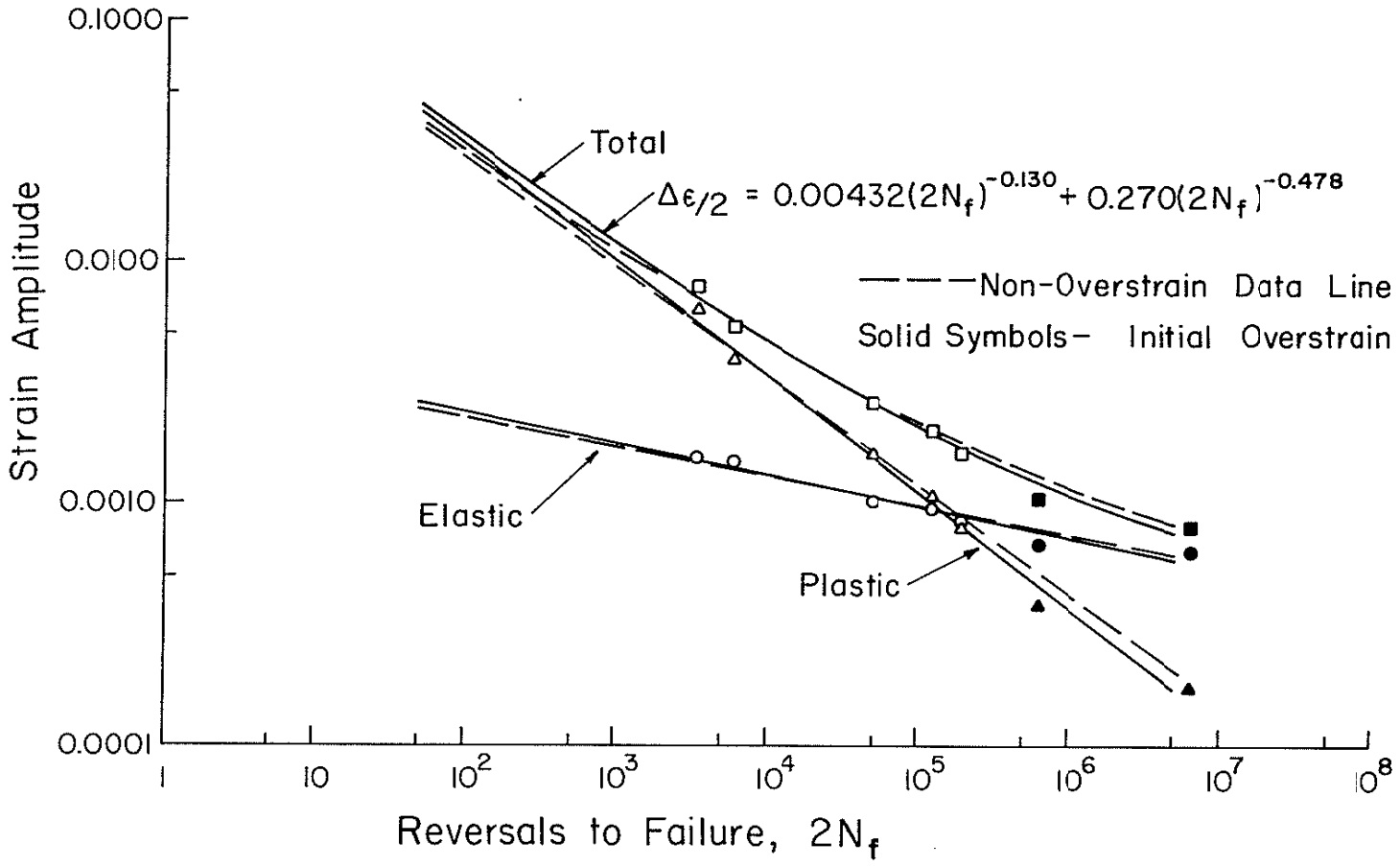

Fig. 61 Strain-Reversals to Failure Data for Sheet Steel Subjected to Initial Overstrains

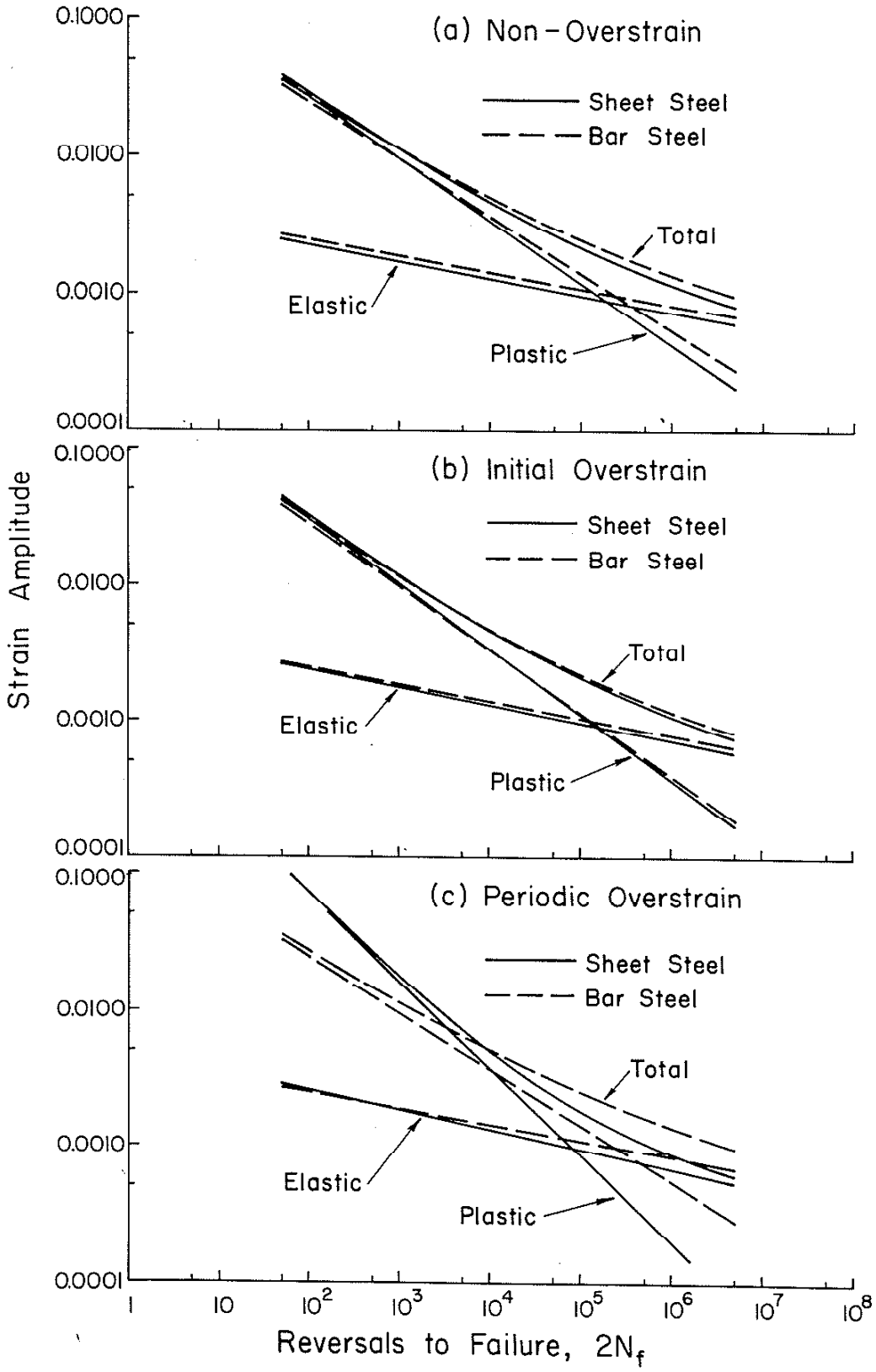

Fig. 62 Comparison of the Strain-Life Data for the Sheet and Bar Steels

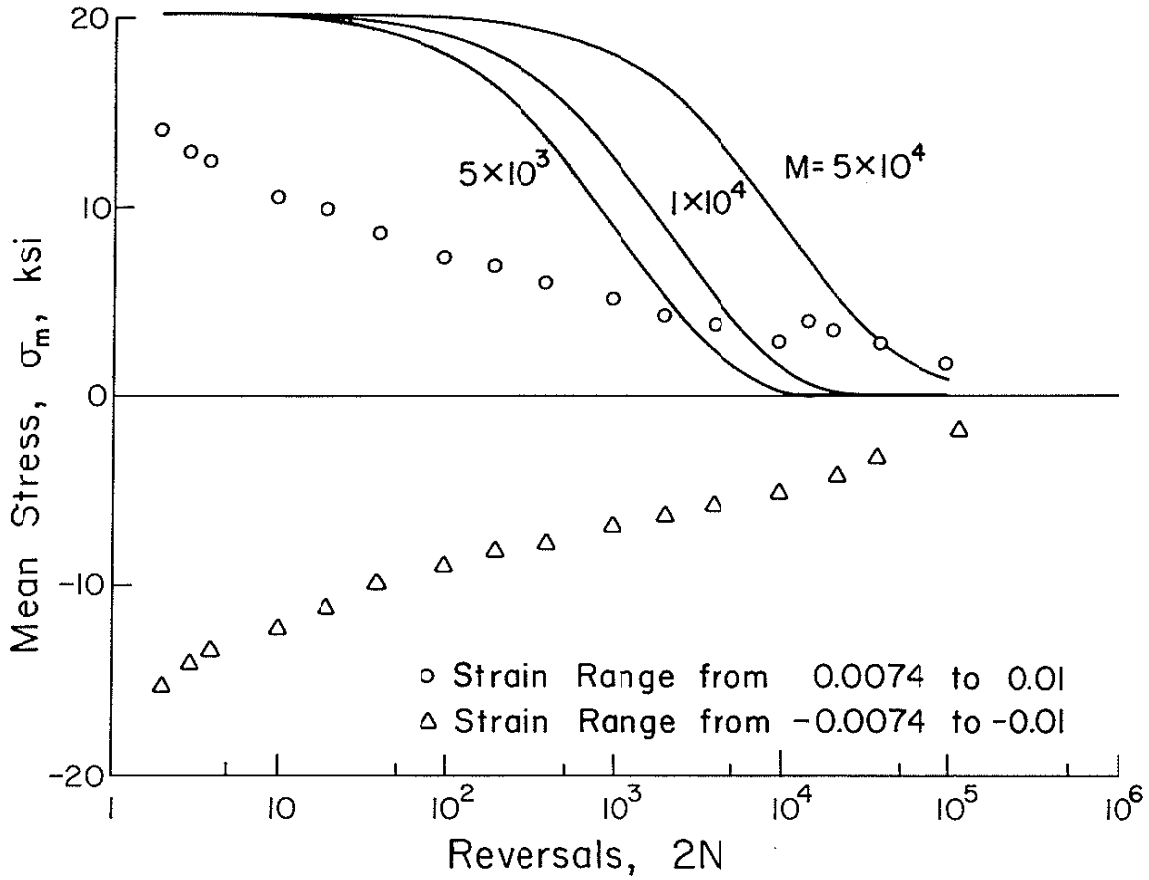

Fig. 63 Cyclic Relaxation Data for the Sheet Steel

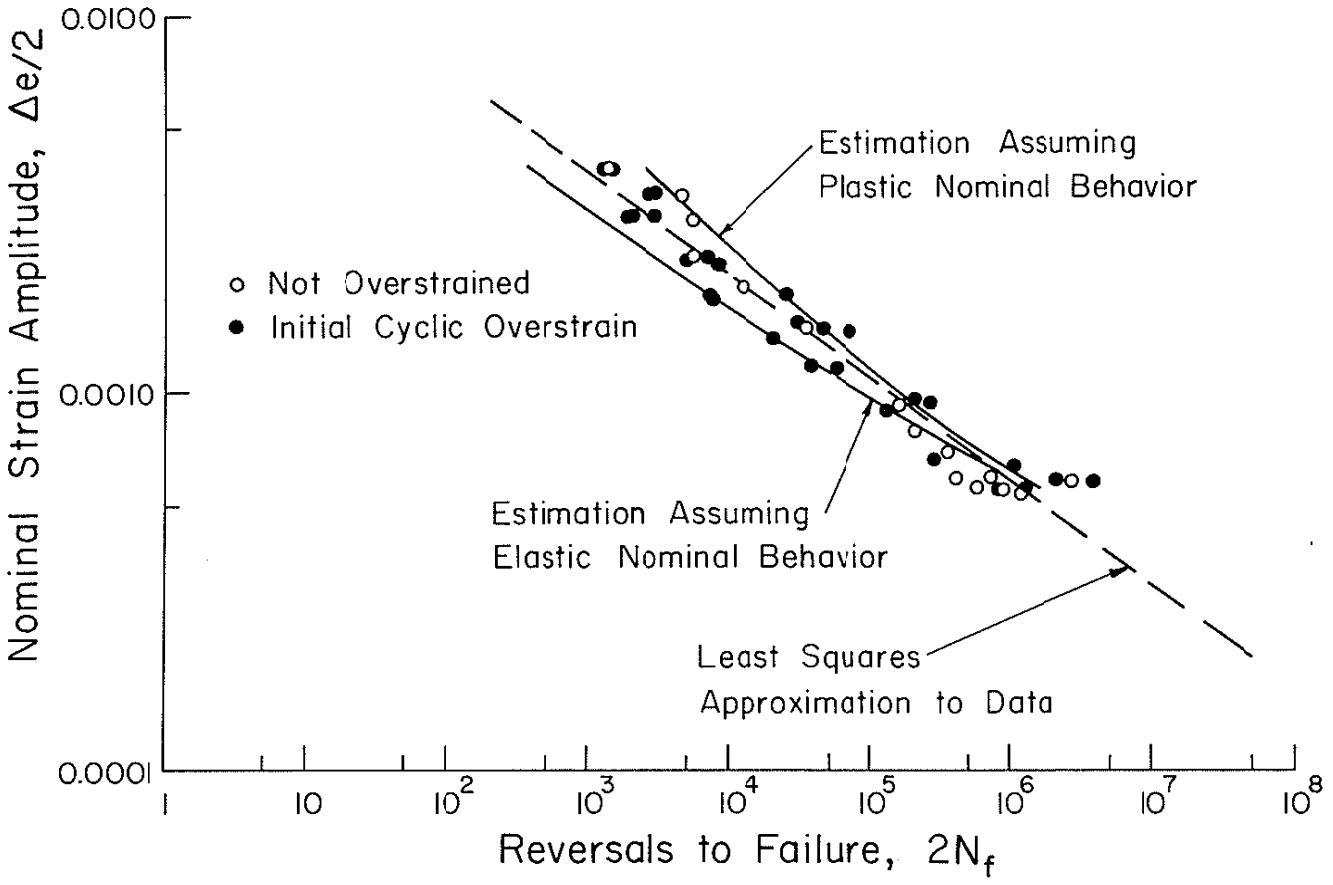

Fig. 64 Fatigue Results for Constant Amplitude Straining of the Fan Blades

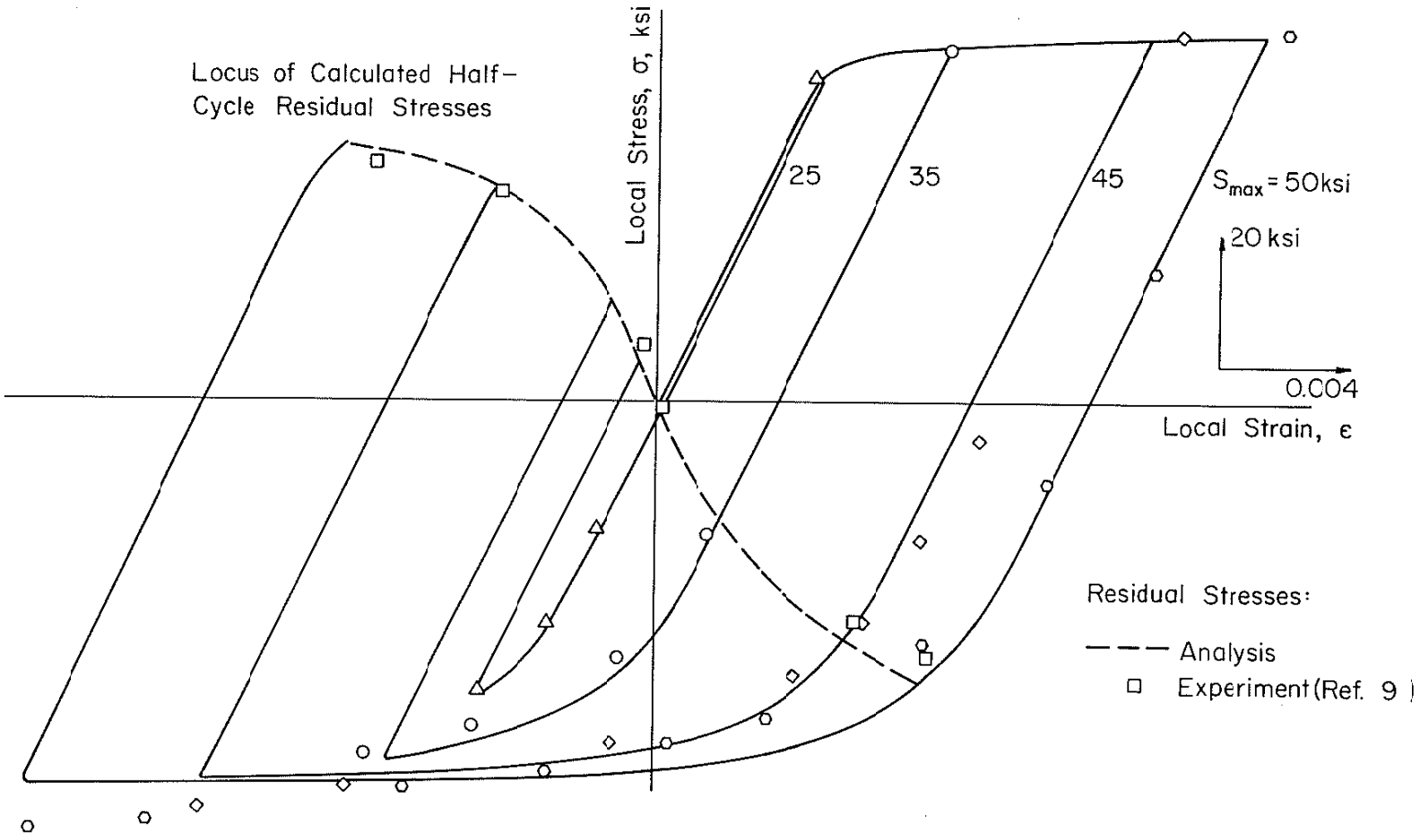

Fig. 65 Experimental and Finite Element Results for the Stress-Strain Response at the Root of an Edge-Notched Plate Subjected to One Cycle of Reversed Loading (Ref. 64)

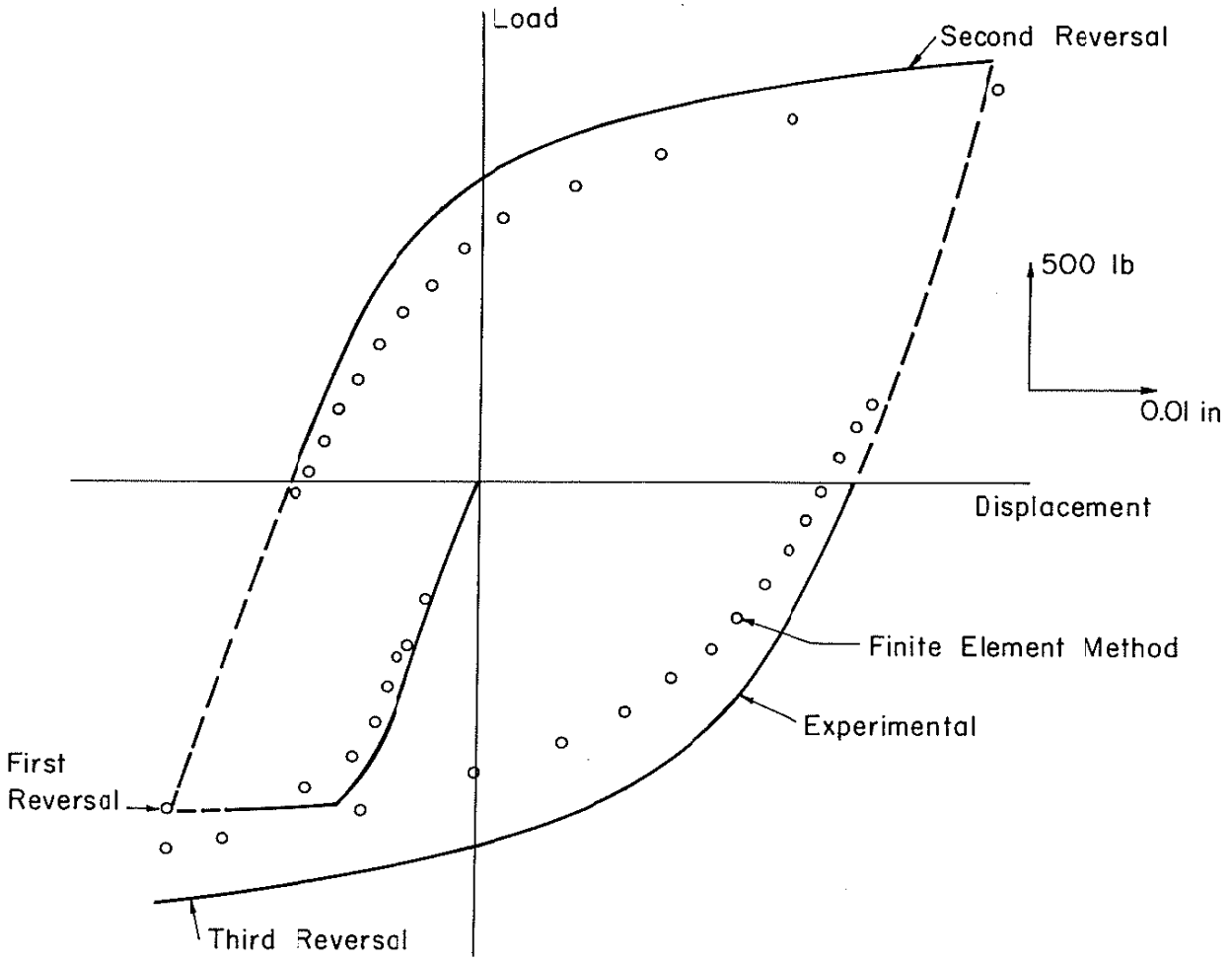

Fig. 66 Experimental and Finite Element Results for the Load-Deflection Response of a Beam Subjected to Three Point Cyclic Bending (Ref. 38)

APPENDIX A

CYCLIC STRESS-STRAIN AND FATIGUE DAMAGE PROCEDURE

Appendix A presents the details for determining the stress-strain response at the highly strained region and for the cumulative damage procedure. Figure 29 shows the general flow chart of the analysis. Sections of this flow chart will be expanded for further detail.

The basic procedure can be divided into three sections:

(1) determination of the nominal stress-strain response,

(2) determination of the control condition for the local response, and

(3) simulating the local stress-strain behavior and summing damage along each increment of the local stress-strain curve.

The procedure for simulating the local and nominal stress-strain response are identical except for the control limits. Local behavior is closely associated with the cumulative damage procedure.

Determination of the Stress-Strain Model Constants

Element yield stresses, $\bar{\sigma}_i$, and element moduli constants, E_i, are chosen to approximate the smooth stress-strain curve described by Eq. 10, Fig. 14. The number of elements, N, is chosen large enough to construct a hysteresis loop for any loading that might be encountered during the analysis. The smooth curve, which the model approximates, represents a stress-strain response for a particular degree of hardness. Hardening or softening is accomplished by determining a new stress-strain curve and adjusting the constants, E_i and $\bar{\sigma}_i$, to approximate it. Figure 46 shows a flow chart of the procedure that is explained in this section.

For this analysis, the yield stresses were first chosen and the element moduli calculated to approximate the appropriate curve. The yield stress of element 2, $\bar{\sigma}_2$, is determined from an initial plastic strain, $\bar{\epsilon}_1$. Equation 26 determines $\bar{\sigma}_2$.

$$\bar{\sigma}_2 = K^*(\bar{\epsilon}_1)^{n^*} \tag{26}$$

All subsequent yield stresses are increased by a constant increment, C.

$$\bar{\sigma}_i = \bar{\sigma}_{i-1} + C \qquad (i = 3, 4, \ldots) \tag{27}$$

Smaller values of $\bar{\epsilon}_1$ and C produce more accurate modeling of the smooth curve.

With the values of all $\bar{\sigma}_i$ determined, the element moduli constants, E_i, are calculated to approximate the smooth stress-strain curve. For each linearly approximated segment of the curve, the slope of that segment can be calculated from the following set of equations. For the first segment:

$$\delta\sigma_1^* = \bar{\sigma}_2 \tag{28}$$

$$\delta\epsilon_1^* = \frac{\bar{\sigma}_2}{E} + \bar{\epsilon}_1 \tag{29}$$

For all other segments:

$$\delta\sigma_i^* = \bar{\sigma}_{i+1} - \bar{\sigma}_i = C \tag{30}$$

$$\delta\epsilon_i^* = \frac{\delta\sigma_i^*}{E} + \left(\frac{\bar{\sigma}_{i+1}}{K^*}\right)^{1/n^*} - \left(\frac{\bar{\sigma}_i}{K^*}\right)^{1/n^*} \tag{31}$$

The slope of any element can then be determined from Eq. 32.

$$E_i^* = \frac{\delta\sigma_i^*}{\delta\epsilon_i^*} \tag{32}$$

The (*) refers to the segments of the curve. End stress and strain values of each segment are given by σ_i^* and ϵ_i^*. Increments of stress and strain along the curve are $\delta\sigma_i^*$ and $\delta\epsilon_i^*$. By this notation the number designating each segment corresponds to the number assigned to the element that is activated to form the segment, Fig. 14.

From the slopes of the linear segments, the element moduli constants are calculated. The reciprocal of the slope of the i^{th} linear segment is the sum of the reciprocals of the moduli of the elements that have been activated. For segment 1:

$$\frac{1}{E_1} = \frac{1}{E_1^*} \tag{33}$$

Equation 8 relates the slope of a segment to the element moduli of the model. The computational effort of the sum from $1/E_2$ to $1/E_i$ can be reduced by assigning a single value to the sum, $\Sigma(1/E_i)$. Equation 8 can be rewritten to compute $\Sigma(1/E_i)$ for each segment.

$$\Sigma\left(\frac{1}{E_i}\right) = \left[\frac{1}{E_i^*} - \frac{1}{E_1}\right] f(|\sigma|) \tag{34}$$

With the constants $\bar{\sigma}_i$ and $\Sigma(1/E_i)$ set for a particular relaxing constant M, the stress-strain behavior originally described by Eq. 11 can be simulated by the model. The model constants are a function of the relaxing constant M. For any choice of M, completely reversed response will be accurately simulated. The relaxation constant is determined by trial and error to fit test results that have cyclic relaxation.

Determination of Model Fatigue Damage Constants

To continuously sum damage for each increment of the modeled stress-strain curve, additional constants relating to fatigue damage are determined. Damage is summed by adding the damage that is produced by the additional plastic strain for a particular increment. Two additional constants for each increment are calculated. The total sum of plastic strain, $\bar{\epsilon}_i$, accumulated for activation of the i^{th} element and the damage D_i associated with that plastic strain are calculated. For the first segment,

$$D_1 = \left(\frac{\bar{\sigma}_2}{\sigma_f'}\right)^{-1/b} \tag{35}$$

For all other segments,

$$\bar{\epsilon}_i = \bar{\epsilon}_{i-1} + \delta\epsilon_i^* - \frac{\delta\sigma_i^*}{E} \tag{36}$$

$$D_i = \left(\frac{\bar{\epsilon}_i}{\epsilon_f}\right)^{-1/c} \tag{37}$$

The values of $\bar{\epsilon}_i$ and D_i represent the plastic strain amplitude and associated damage for a complete hysteresis loop. With this information, continuous damage summation is performed on each segment of the stress-strain curve.

Model Simulation of History and Cyclic Relaxation

Once the element constants $\Sigma(1/E_i)$, $\bar{\sigma}_i$, $\bar{\epsilon}_i$, D_i and M have been determined, the model can simulate cyclic stress-strain behavior including memory and cyclic relaxation of mean stress. To simulate cyclic hardening or softening, the constants $\Sigma(1/E_i)$ or $\bar{\sigma}_i$ or both are re-evaluated for the forthcoming reversal. This also necessitates changing $\bar{\epsilon}_i$ and D_i. The model constructs each segment of a hysteresis loop by determining the stress, σ_i^*, at which the next element will be activated and calculating the slope of the segment from the moduli of the elements that are activated. Elements are activated in ascending order.

At the beginning of each reversal, the last point of stress and strain from the previous reversal is set as σ_0^* and ϵ_0^*. Initially, these have a value of zero. The signs of the yield stresses are initially positive and are reversed at the end of each reversal. The values of the residual stresses, σ_i, which were set by all previous reversals, are known. Initially these are also zero.

Starting with subscript 2, the stresses for each increment are calculated from

$$\sigma_i^* = \bar{\sigma}_{i+1} + \sigma_{i+1} \tag{38}$$

The following sequence of equations determine the corresponding values of strain, ϵ_i^*.

$$\delta\sigma_i^* = \sigma_i^* - \sigma_i^{*-1} \tag{39}$$

$$\frac{1}{E_i^*} = \frac{1}{E_1} + \Sigma \frac{1}{E_i}\left(\frac{1}{f(|\sigma|)}\right) \tag{40}$$

$$\delta\epsilon_i = \frac{\delta\sigma_i^*}{E_i^*} \tag{41}$$

$$\epsilon_i^* = \epsilon_i^{*-1} + \delta\epsilon_i^* \tag{42}$$

Thus, the model constructs the stress-strain curve, including the effects of memory and cyclic relaxation, by linear approximations.

For each linear segment, a check is performed to determine if the simulation control limits have been exceeded. A linear extrapolation is then made. Equation 43 must be satisfied for the extrapolation.

$$(\sigma_f^* - \sigma_i^{*-1}) = E_i^* (\epsilon_f^* - \epsilon_i^{*-1}) \tag{43}$$

For simulation of a uniaxial specimen or the nominal region of a structure, Eq. 43 completely determines the final stress and strain state given a limit of either stress or strain. For the local region of a structure which must obey Eq. 3, the extrapolation is more complicated. Upon completion of each increment, the produce of the local stress and strain ranges is compared to the value of K_f^2 (ΔS Δe). To determine the final stress, σ_f^*, and strain, ϵ_f^*, state, Eq. 44 must also be satisfied.

$$(\sigma_f^* - \sigma_0^*)(\epsilon_f^* - \epsilon_0^*) = K_f^2 (\Delta S\ \Delta e) \tag{44}$$

Solving Eqs. 43 and 44 results in a quadratic equation.

$$\sigma_f^* = \frac{-A \pm \sqrt{A^2 - 4B}}{2} \tag{45}$$

where:

$$A = E_i^*(\epsilon_i^{*}{}_{-1} - \epsilon_1^*) - (\sigma_i^{*}{}_{-1} + \sigma_i^*)$$

$$B = \sigma_1^*(\sigma_i^{*}{}_{-1}) - \sigma_0^*(E_i^*)(\epsilon_i^{*}{}_{-1} - \epsilon_0^*) - K_f^2(\Delta S\ \Delta c)(E_i^*)$$

The sign of the radical is initially positive for the first reversal and changes every reversal. Knowing σ_f^*, the corresponding value of ϵ_f^* can be calculated by Eq. 44.

Upon completion of a reversal the sign of the yield stresses are changed, Eq. 46, and the residual stresses calculated, Eq. 47.

$$\bar{\sigma}_i = -\bar{\sigma}_i \qquad (i = 2,3,\ldots,N) \tag{46}$$

$$\sigma_j = \sigma_f^* - \bar{\sigma}_j \qquad (j = 2,3,\ldots,i) \tag{47}$$

If cyclic hardening or softening occurs, the residual stresses will retain their values. However, the yield stress values might change due to the transient behavior.

Figure 47 is a flow chart of the model simulation. Also indicated are the insertions for the incremental damage procedure.

Incremental Damage Summation

For each increment of stress and strain a damage summation is made. For the first segment, Eq. 15 calculates the damage for the stress increment. In terms of the stress range, $\delta\sigma_1^*$, the damage for the increment, $(1/2\ N_f)_1$ is calculated from Eq. 48.

$$\frac{1}{2N_f} = \left(\frac{\delta\sigma_1^*/2}{\sigma_f'}\right)^{-1/b} \tag{48}$$

For all consecutive increments involving plastic strain, the total plastic strain, $\bar{\epsilon}_i^*$, associated with a completely reversed closed loop is calculated, Fig. 48a.

$$\bar{\epsilon}_i^* = \frac{\delta\epsilon_i^*}{2} - \frac{\left(\delta\sigma_i^*/2\right)}{E} + \bar{\epsilon}_{i-1} \tag{49}$$

The damage for that increment is

$$\left(\frac{1}{2N_f}\right)_i = \left(\frac{\bar{\epsilon}_i^*}{\epsilon_f'}\right)^{-1/c} - D_{i-1} \tag{50}$$

The incremental damage is calculated for each element of loading and added to the total damage.

For the example shown in Fig. 48a, D_{i-1} is the damage associated with the segment ABC of the curve. The value of $\bar{\epsilon}_i^*$ is the plastic strain for ABCE, although the last reversal was DCE.

Upon activation of an element with no increase in stress and at the end of a reversal, a mean stress correction as expressed by Eq. 25 is added to the total damage summation. The first correction is based on the total stress range from the initiation of the reversal to the stress at the point where the correction is made. Figure 48b illustrates both types of damage summation for the reversal ABCDE. Upon activating element 3 at point C, no increase in stress occurs until element 4 is activated. The correction for mean stress is performed with the stress range, $\Delta\sigma$, from A to C. Point E is the end of the reversal. Since a mean stress correction has been performed for this reversal, the correction is calculated for the stress from A' to E and the correction from A' to C is subtracted from the first calculation. This is similar to the plastic strain damage increment. The total stress amplitude, $\Delta\sigma_2/2$, for the complete loop, which is from A' to E, is remembered by the model and can be expressed as Eq. 51.

$$\frac{\Delta\sigma_2}{2} = \frac{\delta\sigma_i^*}{2} + \bar{\sigma}_i \tag{51}$$

The smaller stress amplitude, $\Delta\sigma_1/2$, is the value of $\Delta\sigma_2/2$ minus the last stress amplitude from the previous mean stress damage correction. If the stress at the last correction is σ_o then

$$\frac{\Delta\sigma_1}{2} = \frac{\Delta\sigma_2}{2} - \frac{\sigma_f^* - \sigma_o}{2} \tag{52}$$

The mean stress, σ_m, for any segment is given by

$$\sigma_m = \sigma_i^* - 1 + 2C - \bar{\sigma}_{i+1} \tag{53}$$

where C is the stress increment for original construction of the model constants.

APPENDIX B

FATIGUE DAMAGE ANALYSIS OF A BOX-BEAM STRUCTURE

Appendix B presents a more detailed analysis of the box-beam structure, Fig. 31. Constant amplitude and block loading data are shown in Figs. 32 through 36. Analysis of this structure consisted of obtaining: (1) the fatigue notch factor, K_f, (2) monotonic and cyclic stress-strain properties, (3) fatigue properties that include the effect of an initial cyclic overstrain and periodic cyclic overstrains.

Fatigue Notch Factor

The fatigue notch factor can be determined by comparing the stress-life data for the beams and smooth specimens. This comparison is usually done at long life values and necessitates construction and testing of the structure. For this problem, K_f is determined by photoelastic and analytical means. By this technique, it would not have been necessary to fabricate and test the beam to determine K_f.

Reference 53 reported values of the theoretical stress concentration factor, K_t, for flat plates with various arrangements of circular holes. Figure 49 shows the portion of the box-beam under consideration. The b/a ratio for the photoelastic model was 0.63 as compared to 0.66 for the box-beam. For a d/b ratio of 0.19, Ref. 53 reported a K_t of 2.9.

The fatigue notch factor, K_f, was determined by a highly stressed volume approach discussed in Ref. 12. For most metals, Eq. 54 was found to be accurate.

$$K_f = K_t \left(\frac{V_n}{V_u} \right)^{0.034} \tag{54}$$

where V_n and V_u are the highly stressed volumes of the notched and unnotched specimens, respectively. Figure 50a shows the unnotched specimen design. For axially loaded plates with shallow notches,

$$V_n \approx 0.018\, tr\sqrt{rb_n} \tag{55}$$

Here, t is the thickness, r the notch radius, and b_n the notched minimum width. The notched minimum width for the box-beam was taken to be the width of the shaded area shown in Fig. 49 and the unnotched specimen volume was for a cylindrical $\frac{1}{4}$ inch diameter specimen with a straight section of 0.66 inch. From this information the approximate value of K_f was calculated to be 2.4, which is an intermediate value of the various estimations reported in Ref. 50.

Stress-Strain Properties

Reference 55 reports monotonic and cyclic stress-strain and fatigue properties for 7075-T6 aluminum. However, the majority of the data were for large to intermediate strain amplitudes. It was estimated that most of the strain amplitudes experienced at the rivet hole would be below this range. Therefore, additional data were obtained.

Monotonic and stable cyclic stress-strain data were obtained from a single specimen, which was also used to generate data for determining the relaxing constant for the simulation model. Some monotonic tension properties were obtained from the first reversal of the incremental step strain spectrum. This only produced data up to a total strain of 0.015. None of the fracture properties were determined. After three blocks of incremental straining, data were taken on the decreasing portion of the block for determining the stable cyclic stress-strain curve. Both monotonic and cyclic data are presented in Fig. 51.

At the end of three blocks of incremental strain cycling, which brought the specimen to a state of zero stress and strain, strain control limits from 0.0 to -0.0155 were imposed until final fracture. This control condition produced an initial mean stress that relaxed with cyclic straining. Figure 52 shows the data obtained

during cycling at these limits. Also included are the simulation results for two values of the relaxing constant, M. Although a value of 1×10^4 ksi results in the simulation fitting the test data after 10^3 reversals, this value does not produce the correct rate of relaxation. Cyclic hardening and relaxation occur simultaneously, which complicates the process of obtaining a value for M. Figure 53 shows only the mean stress versus reversals data and the simulation results for three values of M. The final choice of the relaxing constant was 3×10^3.

No attempt was made to determine a hardening function for this analysis. Only stable cyclic properties were used. Reference 49 reports a tensile yield stress of 82 ksi for the cover plate metal. The data presented in Fig. 51 indicates a 0.002 plastic strain offset yield of 71 ksi for the monotonic curve and 79 ksi for the cyclic. A monotonic yield of 71 corresponds to handbook values for this aluminum. The results reported in Ref. 49 were from specimens that were machined from the top plates of the box-beam that were made from extruded sheets. Consequently, the plates had already been strained and were behaving more as a cyclically hardened specimen.

Fatigue Properties

Figure 54 shows the strain-life data for the aluminum and Tables 9 and 10 list the data. Since the highly strained region is most likely overstrained during manufacture, initial overstrain data was generated. Both sets of data are shown. The least squares approximation is for the overstrained data and non-overstrained data with strains exceeding 0.0043.

Since the flight spectra A, B and C produce periodic overloads, the effect of this type of loading was also investigated for the aluminum. Periodic overstraining produced data that were similar to that generated with an initial overstrain. These data are not shown in Fig. 54 but are listed in Table 11. Since the periodically overstrained data would not appreciably change the least squares approximation shown in Fig. 54, only the initial overstrain data line was used for this analysis.

Additional Flight Spectrum Data

In an attempt to determine if the block size effect shown in Fig. 36 is only a characteristic of the box-beam, the same stresses that were applied to the beam for flight spectrum B with a 0.0% margin of safety were also applied to plates with circular center notches. Details of the plate, for which K_f is 1.95, are given in Ref. 15. Figure 55 shows the test results. A block size effect is shown, however it resembles that for the 11% margin of safety. Since K_f for the notched plate is approximately 19% smaller than for the box-beam, the data for Fig. 55 might in reality more closely resemble that of 11% margin of safety.

APPENDIX C

FATIGUE ANALYSIS OF AN AUTOMOTIVE FAN BLADE

Appendix C presents details of the analysis for the automotive fan blade. Stress-strain and fatigue properties of the fan blade material are determined. Behavior of another structural steel, supplied in round bars, was compared with the sheet steel. The bar steel is a common type, the properties for which might exist in a "data bank."

Reference 56 gives more detail on the stress-strain and fatigue properties of both the sheet and bar steels. This appendix presents the data pertinent for the fatigue analysis of the fan blade. Specimen configurations are shown in Fig. 50. For the transverse specimen, transverse strains were measured across the thickness of the specimen and converted to axial strains with an analog computer programmed for Eq. 56.

$$\epsilon = \frac{\sigma}{E} - \left[2\,\epsilon_{tr} + 2\,\mu_e\,\frac{\sigma}{E}\right] \tag{56}$$

For Eq. 56, a plastic Poisson's ratio of 1/2 was assumed and the value of the elastic Poisson's ratio, μ_e, adjusted to produce zero output from the plastic strain relation $\left[2\,\epsilon_{tr} + 2\,\mu_e\,\frac{\sigma}{E}\right]$ for small strains.

Stress-Strain Properties

Figure 17 shows the monotonic tension test results for a specimen, Fig. 50b, of the sheet steel. Monotonic tension properties for both the sheet and bar steels are reported in Table 12. These properties indicate the sheet steel to be more ductile than the bar steel. Most of the properties differ by approximately 10%.

Several experimental techniques for determining the stable cyclic stress-strain curve (37) were applied to the bar and sheet steels: (1) companion specimen, (2) incremental step strain, and (3) precycled monotonic tension. Figure 18 and

Table 13 present the companion specimen test results. The stress-strain response shown in Fig. 19b was obtained from the decreasing portion to the second block of the incremental strain spectrum, Fig. 19a. Figure 20 shows the data from this test. After $1\frac{1}{2}$ blocks of incremental straining, the same specimen that generated data shown in Figs. 19 and 20 was pulled in monotonic tension to fracture, Fig. 56. Figures 20 and 56 include the companion specimen data line. Significantly different results are obtained by each procedure.

Figure 57 illustrates the different stress-strain curves produced by each set of data for both steels. Such large discrepancies between the data for the different methods was not observed for the higher strength metals cited in Ref. 37. For each technique, a close similarity exists between the two steels, Fig. 58. Cyclic properties, as determined by all the methods, are listed in Table 14.

For both the bar and sheet steels, a stable condition only exists for a constant strain amplitude. Figure 59 shows the stress response of the bar steel subjected to a block strain spectrum. The first level consisted of 60 reversals of ± 0.0125 strain, at the end of which the stress-strain behavior appeared stable. For each new strain amplitude, a transient period existed during which cyclic hardening or softening occurred. Since the companion specimen test results represented the most stable condition, these data were employed for the fatigue analysis.

Fatigue Properties

Strain-life data were generated for the bar and sheet steels. Since some of the load histories involved overloads, initial and periodic overstrain test results were obtained. Table 13 lists the constant amplitude data that were not overstrained and Tables 15 and 16 the initial and periodic overstrain data. Figure 60 shows the data that were not overstrained. An initial cyclic overstrain did not appreciably reduce the fatigue life of the sheet steel, Fig. 61. With continued periodic overstraining every 2×10^5 reversals, a significant reduction in life was observed, Fig. 28.

A different situation existed for the bar steel. The fatigue life of this steel was affected by an initial cyclic overstrain but was not further affected by continued periodic overstrains. Figure 62 compares the data for both steels. Close similarity exists for the initial overstrain data. A correct assumption would have been made by assuming the initial overstrain data for the bar steel to be an appropriate substitute for either the non-overstrained or overstrained data for the sheet steel. Serious error would occur substituting the periodic overstrain data of the bar steel for the sheet steel.

Cyclic Relaxation of Mean Stress

Mean stress relaxation test results from four specimens determined the relaxation constant, M, for the sheet steel. Results from two of these specimens are shown in Fig. 63. All the specimens used to determined M were initially subjected to $1\frac{1}{2}$ blocks of incremental step straining, Fig. 19a. To initiate a tensile mean stress, strain limits of 0.01 and 0.0074 were controlled. As a comparison, the mirror image of these strain limits were controlled on another specimen (-0.010 to -0.0074). These results are also shown in Fig. 63, demonstrating the similarity in the rate of cyclic relaxation for tension or compression.

Also shown in Fig. 63 are the simulation results for three values of M. A value of 5×10^4 was chosen based on all the relaxation data. This value of M produced the same change in the mean stress for 10^5 reversals as was observed. The error in calculating the initial mean stress is due to the difficulty of the model to simulate transient behavior. For the strain limits used for the relaxation tests, if relaxation was not included in the model large errors would exist in fatigue predictions by including a large mean stress that actually relaxed.

Additional Fatigue Analysis Results

Since completely reversed constant amplitude data for the fan blade were available, an expression for total nominal strain amplitude and reversals to failure was

obtained. Figure 64 shows the constant amplitude, both non-overstrained and overstrained, data on log-log coordinates. A least squares fit to these data is to be made. This expression was employed for each reversal of loading to make life predictions for SAE load histories. Tables 7 and 8 also include life estimations based on nominal strains. Also of interest is the effect of simplifying the analysis by assuming the nominal stresses to be elastic. Life estimations based on elastic nominal strains are given in Table 6 and Fig. 64. All nominal strain based life estimations resulted in large errors. Assuming elastic nominal behavior, more conservative predictions are made.

APPENDIX D

FINITE ELEMENT METHOD FOR DETERMINING THE LOCAL STRESSES AND STRAINS

The analysis of the box-beam structure and the fan blade necessitated experimental determination of the nominal stresses or strains. Alternative approaches might consist in determining the local stresses and strains knowing only the applied loads and constraints. To be of consequence for a fatigue analysis, the approach must account for plastic strains and cyclic loading. The finite element method is useful for elastic analyses and has recently been expanded to include plastic strains (57-63). Relatively little work has been done for the complex type of cyclic loading encountered in a fatigue environment.

Several finite element procedures (38, 64, 65) have been developed that might be used for fatigue problems. Isakson et al. (64) determined the stresses and strains for three structures that were cyclically loaded: a notched plate, a shear lag specimen and a swept wing. Good correlation was obtained for analytical and experimental results for the stresses and strains at the root of the edge-notched plate subjected to cyclic loads that produced plastic strains. Reference 9 reported experimentally measured strains and stresses that were computed from the stress-strain curve of the metal. Figure 65 shows the calculated and test results for plates that were loaded to prescribed loads in tension and then the load released. For each specimen a different maximum load was obtained. The stress-strain properties for this aluminum were different in tension and compression since the plate had been strained before the plate was made. This was also accounted for in the analysis. Agreement is good with respect to predicting the stress-strain curve during loading and unloading and for estimating the residual stresses after unloading.

Plummer (38) also expanded the finite element to include plastic strains and cyclic loading. Prager's kinematic hardening model and an effective stress-strain relation were employed to extrapolate from the uniaxial model response to multi-axial behavior. The uniaxial model was that used to simulate the behavior shown in Figs. 23 and 24. Isoparametric, plane stress elements were used to model a short beam under three point bending. Figure 66 shows the experimental and analytical results fro three reversals of load. The uniaxial model was initially set to simulate flat top yielding and for each consecutive reversal hardening occurred. Considering the extensive change in the materials properties, the calculated results are in good agreement with the experimental data.

Based on the results shown in Figs. 65 and 66, the finite element method shows promise for eliminating the necessity for experimentally determining the nominal stresses and strains and the fatigue notch factor, K_f. However, an analysis of either the automotive fan blade or the box-beam structure is not practical at this time.